UNIVERSITY OF CALIFORNIA,

IRVINE

Large Area Magnetic Micropallet Arrays with Ferromagnetic Cores for High Throughput Cell Colony Sorting

DISSERTATION

submitted in partial satisfaction in requirement
for the degree of

DOCTOR OF PHILOSOPHY

in Biomedical Engineering

by

Wesley Akira Cox-Muranami

Dissertation Committee:
Professor Guann-Pyng Li, Chair
Dr. Edward Nelson
Professor Jered Haun
Professor Mark Bachman

2015

DEDICATION

For my wife, my family, and my pets.

TABLE OF CONTENTS

LIST OF FIGURES

ACKNOWLEDGEMENTS

I would like to first thank my primary advisor Dr. Mark Bachman for allowing me to be a part of his great lab for the past 5 years. I entered the University of California, Irvine with the hopes of working on microfabricated devices for the biomedical field and I could not have asked for a more intelligent, creative, and helpful mentor. Never without a great idea looming near the surface of his mind, Dr. Bachman was always ready and willing to discuss project issues and new potential endeavors. He not only guided me through issues, but also challenged me to come up with my own solutions. I will look fondly back at our long conversations regarding new inventions and the politics of academia while drinking coffee at the local cafe.

I would also like to thank Dr. Edward Nelson for being the first collaborator to actually call me out on my presentation style and help me improve as a technical speaker. His words incited some introspection which allowed me to rethink the way that I expressed my data and other scientific information to varied audiences. He was also my primary conduit into partaking in conversations relating to biological processes that I would otherwise not have had access to and I am very thankful for the experience.

Dr. Li, my third advisor, was a great insightful third party at every meeting. While he was not directly in charge of advising my projects, he was always there to offer new information regarding the happenings of the industry and the types of inventions that would be of interest to outsiders as well as how to tune certain work for better relevance to the field. I am especially grateful for the advise that he gave me in planning my first journal submission as well as how to best present novel work to the academic world.

Aside from my primary group of research advisors, I would also like to acknowledge a couple other professors at the University of California, Irvine for their contribution to my success at this institution. Dr. Jered Haun was a great professor to work with as a teaching assistant on multiple occasions. I appreciated the value that he gave to the opinions of his TA's. Dr. Haun's willingness to allow me to teach a lesson to his class reassured my confidence in public speaking and discussing complicated subjects to large audiences while also being able to answer their on-the-spot questions. Dr. Hung Fan helped kick off chapter 3 of this dissertation thanks to his support of the large area magnetic micropallet arrays. Dr. Fan allowed me to test the technology with his line of cells infected with Jaasiegte sheep retro virus and the use of these cells led to many outstanding results. I greatly appreciated him sharing his unique cells with me and his belief in the devices.

Other people who have aided the work presented in this paper include: Trisha Westerhoff, my great biology collaborator from Dr. Nelson's lab. Dr. Koutoku Inoue and Takahiro Kagami, my collaborators from Koto Electric Co. and Kanto Gakuin University in Japan who taught me the ins and outs of metal plating. Dr. Jason Luo, fellow lab grunt and the man who gave me a chance to work with him when I first joined the lab; also all around fun guy. Dr. Michael Klopfer, another lab mate with an undying sense of creativity which was definitely contagious. Dr. Lily Wu, an early lab manager and the only person who seemed to know what was going on with the lab at all times. Finally Dr. Nick Gunn for laying a great foundation in micropallet research for me to draw inspiration from.

While this next section may get a little sappier, I would like to extend my deepest sense of appreciation for my mother and father. Thank you both for igniting my lifelong goal of working to better the lives of those afflicted with serious illnesses with my work. Whether they knew it at the time or not,

the conversations regarding the treatment and outcome of cancer patients that I would overhear between my mother, who is a nurse practitioner, and my father, an engineer, while growing up seeded me with an unending desire to try to help the human civilization rid the world of cancer and other life altering diseases. Thank you for your unending support and always being available to discuss personal matters as well as the current state of the medical field whenever we have a chance to catch up.

Finally, I would like to give a huge thanks to my best friend and wife, Karlene. You've always been here for me to support me and whip me back into shape whenever I have slouches in productivity. Also, thanks for listening to my incessant rambling regarding anything from electromagnetism to microbiology and whatever other subjects that occupy my mind at all times. We've come a long way since I first met you in 7th grade. Thank you for all of your patience that you maintained as I undertook this endeavor. It was worth it. I wouldn't be the person that I am today if I hadn't met you so long ago. Thank you for everything. Love you lots K.K. Also, thanks Shelly, for sitting next to me for about 95% of the writing of this dissertation.

The work described in this paper was supported by the National Science Foundation's Integrative Graduate Education and Research Traineeship program (NSF-IGERT) "LifeChips" Award DGE-0549479. The work was made possible, in part, through access to the Optical Biology Core facility of the Developmental Biology Center, a Shared Resource supported in part by the Cancer Center Support Grant (CA-62203) and Center for Complex Biological Systems Support Grant (GM-076516) at the University of California, Irvine. Work was also funded in part by NSF I/UCRC: Center for Advanced Design and Manufacturing of Integrated Microfuidics (CADMIM) award #IIP-1362165. The content of this dissertation is solely the responsibility of the author and does not represent the official views of the funding agencies.

Figures used in Chapter 2 of this dissertation are presented here with the express consent of the Royal Society of Chemistry, Lab on a Chip publication. The corresponding journal article title is "Large Area Magnetic Micropallet Arrays for Cell Colony Sorting." Permission to include the images were obtained through Copyright Clearance Center's Rightslink service (License number: 3755550203969)

CURRICULUM VITAE

Wesley Akira Cox-Muranami
Department of Biomedical Engineering
University of California, Irvine
Irvine, CA 92617

Education

University of California, Irvine, Irvine, CA

Ph.D. Biomedical Engineering 2016

M.S. Biomedical Engineering 2013

B.S. Biomedical Engineering 2011
- Specialization in Biophotonics

Research

University of California, Irvine, Irvine, CA

Patterned Gold Plating on 3D objects by Use of a Highly Focused Laser 2015
- Laser selection and optical system set-up for high precision laser patterning of metal traces

Large Area Magnetic Micropallet Arrays for Cell Colony Sorting 2014-2015
- Design and fabrication of biocompatible cellular sorting arrays
- Photolithography, electroplating, cellular biology, confocal microscopy

Electronic Release System for Micropallet Arrays 2013
- Micro metal trace patterning

Metal Side Coating of Micropallet Arrays for Enhanced Imaging 2012
- Light ray trace simulation
- Fluorescence microscopy and automated image analysis design

Fabrication of High Surface Area Microstructures through the Growth of Filamentous Fungi 2011

Awards

University of California, Irvine, Irvine, CA

Undergraduate Research Fellowship 2011

Teaching Experience

University of California, Irvine, Irvine, CA

BME 180C: Biomedical Engineering Design	2015
BME 50B: Cell Molecular Engineering	2014
BME 121: Organ Transport Systems	2013, 2014
BME 120: Sensory Motor Systems	2012, 2013

Internships

Illumina, Inc.
iAspire Intern - Microfluidics 2014-2015

- Digital microfluidic control design
- Material analysis and testing
- Microfluidic system design

Flint Rehabilitation Devices, LLC 2013-2014
Part time intern

- Small scale device fabrication
- Soldering, fabrication process optimization

Publications and Presentations

Cox-Muranami, Wesley, et al. Bottom-up Manufacturing of Complex Functional Microstructures Through the Growth and Modification of Mold Hyphae. MF3 IAB Meeting. Irvine, CA, USA. May 9, 2012 (Poster)
Cox-Muranami, Wesley, et al. The Micropallet Array: Novel Nanotechnology for Identification, Collection, and Analysis of Rare Breast Tumor Cells. CADMIM IAB Meeting. Irvine, CA, USA. May 7-8, 2013 (Poster)
Babikian, Sarkis, Cox-Muranami, Wesley et al. Ethylene-Vinyl Acetate as a low cost encapsulant for hybrid electronic and fluidic circuits. ECTC. May 28, 2013. (Conference Paper)
Cox-Muranami, Wesley, et al. The Micropallet Array: Novel Nanotechnology for Identification, Collection, and Analysis of Rare Breast Tumor Cells. CADMIM IAB Meeting. Irvine, CA, USA. April 10-11 2014 (Poster)
Cox-Muranami, Wesley, et al. Magnetic Microarrays for Cell Colony Sorting. Irvine, CA, USA. CADMIM IAB Meeting. March 3-4, 2015 (Poster)
Cox-Muranami, Wesley, et al. Magnetic Microarrays for Cell Colony Sorting. Irvine, CA, USA. UCI Biomedical Engineering Seminar Series. May 22, 2015 (Talk)
Cox-Muranami, Wesley, et al. Large Area Magnetic Micropallet Arrays for Cell Colony Sorting. Lab on a Chip. November 19, 2015 (Journal Paper)
Cox-Muranami, Wesley, et al. Highly Efficient Cell Purification on Magnetic Ferrocore Micropallet Arrays. December, 2015 (In Preparation)

ABSTRACT OF THE DISSERTATION

Large Area Magnetic Micropallet Arrays with Ferromagnetic Cores

for High Throughput Cell Colony Sorting

By

Wesley Akira Cox-Muranami

Doctor of Philosophy in Biomedical Engineering

University of California, Irvine 2015

Professor Mark Bachman, Co-Chair

Professor G.P. Li, Co-Chair

Eukaryotic cell sorting is a ubiquitous technique used for biological applications ranging from pharmaceutical drug discovery to cancer research. Evaluating and differentiating cells based on their features, whether they be intracellular or extracellular, has revealed that cellular systems are highly complex, possessing varying behavior even among cells typically classified within the same groups. While there have been massive improvements in characterization capabilities for single cells achieved through use of inventions such as the fluorescence activated cell sorter, there has yet to be an equally impactful technology developed for analyzing clonally expanded cell colonies. Being able to analyze and isolate cell colonies is necessary for cancer and stem cell research where the observed behavior of cells in colonies is just as important, if not more so than when they are in their single cell forms. There is currently a need for new analysis and sorting systems that enable researchers to conduct more in depth

studies of cell colonies as well as increase the throughput of colony collection protocols which are typically time consuming and manually intensive.

Micropallet arrays are a powerful technology specifically designed for high precision sorting of adherent mammalian cells. This technology, composed of thousands of photolithographically fabricated microscopic structures, has enabled researchers to study, identify, and collect individual cells from within vastly heterogeneous samples. Furthermore, micropallet arrays have been an ideal sorting technology for characterizing the natural morphology of single adherent cells preserved by enabling continuous cellular contact with the pallets throughout the entirety of analytical studies. In some cases, rare cells such as cancer stem cells with an occurrence rate as low as 0.01% have been successfully identified and collected from within heterogeneous cell samples prepared from breast cancer tumor biopsies and seeded to the arrays. While being a powerful sorting technology for single cells, micropallet array technology has just recently been expanded upon for meaningful cell colony research.

In this work, we describe a novel micropallet array design specifically created for efficient, high throughput cell colony sorting. A new approach for simple, consistent large scale micropallet ejection was achieved by utilizing an innovative pallet formation substrate consisting of ultra-thin gold coated microscope slides. These semi-transparent slides maintained the optical clarity necessary for in depth cellular analysis on the pallet surfaces while also acting as laser absorption layers for the creation of heat generated vapor microbubbles. The formation of the bubbles generated sufficient force to lift off targeted pallets with little to no damage to the cell colonies adhered to the pallet surfaces, a result previously shown to be difficult. In addition to enabling consistent pallet ejection, the conductive gold layers also acted as seed layers for the electroformation of ferromagnetic nickel structures integrated into the micropallet arrays. With creative pallet designs, the ferromagnetic structures were fabricated within every pallet, making individual pallet manipulation via magnetic probe possible. This complete system with simplified pallet ejection and collection was successfully utilized to perform highly efficient cell colony sorting studies at rates not possible with conventional methods.

Chapter 1: Introduction

1.1 Overview of Dissertation

The work described in this paper was conducted with the goal of creating an adherent cell colony sorting platform with simple usability and accessibility by expanding on an existing technology known as the micropallet array. Micropallet arrays, discussed in greater detail later in this chapter, are a microarray technology developed in order to enable researchers to analyze and sort cells while keeping them in contact with a biocompatible substrate. In this way, it has been possible to characterize adherent cells under highly favorable conditions when compared to more conventional sorting methods by better maintaining ideal culturing conditions. The goal of this work was to take this remarkable technology and expand it to be used with larger scale biological samples such as whole cell colonies and microorganisms without diminishing its simplicity. A further goal was to also increase the utility of micropallet arrays by adding greater functionality as well as usability by designing micropallet arrays better suited for automated control and characterization.

Chapter 1 (this chapter) introduces the concept of cell sorting and the ways that it is used in biological research. Modern cell sorting technology is discussed including an in depth analysis of micropallet arrays and the advances that have been made with the technology since its first invention. A comparisons between conventional cell sorting methodologies and micropallet arrays is made as well.

Chapter 2 describes a new micropallet array platform developed to enable large area micropallets to be consistently released from the arrays by a 2-photon laser mounted to a common biological imaging system with the aid of an absorptive gold layer. The new array design also enabled simplified pallet collection and further manipulation of cell colony samples by integrating ferromagnetic cores within every pallet. Included in this chapter is the first instance of the use of electroplating techniques as a part of micropallet array fabrication for enhanced device functionality. These large area magnetic micropallet arrays were shown to be biocompatible and capable of high throughput cell colony sorting and collection.

This chapter was focused on detailing and analyzing the physical properties of the newly designed arrays and discussing their potential to be used for impactful cellular work.

Chapter 3 continues the discussion regarding the large area magnetic micropallet arrays, henceforth referred to as Ferrocore micropallet arrays to distinguish them from previously published micropallets with ingrained ferromagnetic nano and micro particles. The focus of this chapter shifts from the Ferrocore arrays themselves to describing biological research that was conducted and improved upon by using the technology. Two distinctive cell sorting procedures for transfected cell purification were performed on the arrays with the goal of discovering benefits of using this technology over standard cell sorting methods. It was found that cell purification was not only faster on Ferrocore micropallet arrays, but that the technology also enabled a much more in depth look at cells during sorting allowing for even finer tuned cell selection capabilities.

Chapter 4 discusses the exploration of applying a new type of electroless plating technique to the micropallet arrays. It was found that by using a novel short wavelength UV surface activation process it was possible to plate opaque, reflective nickel sidewalls onto standard micropallets. This brand new micropallet array innovation was found to benefit the arrays by improving optical features for automated visualization and analysis. The metal sidewalls were also shown to have strong enough magnetic response to allow for the recovery of released micropallets by magnetic probe.

Chapter 5 concludes this paper with a description of a foray into a completely new type of micropallet array system aimed at eliminating the need for lasers for ejecting micropallets by creating an electronically controlled pallet release substrate. Many different potential options exist for electric release, but this chapter focuses on the development of a system designed specifically for ejecting pallets with the force generated by the creation of gas bubbles by the electrolytic degradation of water into gas. Short wavelength surface alteration of cyclo olefin polymer for patterned electroless nickel deposition was utilized to fabricate a multilayered, transparent, two dimensional trace array designed for the electronic control of micropallet structure release.

1.2 Cell Sorting and Its Use in Biological Research

The ability to analyze and extract specific cells exhibiting desirable features from heterogeneous populations is an important facet of modern biological research. Cell sorting is the process in which a mixed group of cells are separated based on key, identifiable factors including extracellular features typically referred to as the morphology of cells and intracellular features which primarily result from gene expression within the cells. While early cell sorting techniques were only capable of differentiating cells into broad groups based on obvious, observable differences in physical characteristics, modern advances in cellular labeling and imaging have widened the scope of sorting capabilities by dramatically increasing the number of factors that can be included when identifying cells of interest.[1] The uses of cell sorting are so vast that it can be said that almost all facets of modern biological research have some inclusion of cell sorting protocols used to obtain impactful results. One of the most common uses of cell sorting is for the creation of populations of cloned cells which exhibit desired behaviors not readily available in wild type cells.[2-5] Practical application of cloned cell line creation are numerous and include the establishment of cells exhibiting a higher-than-normal production level of specific proteins for harvesting and subsequent use by researchers as well as the formation of populations of cells with immunofluorescent stains for cellular imaging purposes.[6-8] The uses of these types of cell lines include, but are not limited to advances in drug discovery, stem cell differentiation studies, and cancer research.[9-13] Impactful research in each of these fields greatly relies on the ability to specifically observe and identify individual types of cells and cellular behaviors within naturally heterogeneous cell populations and then cultivating unique cells of interest for further in depth analysis.

1.2.1 Single Cell sorting with FACS and MACS

Probably the most commonly utilized system for single cell sorting is fluorescence activated cell sorting (FACS). Since the invention of the fluorescence activated cell sorter near the end of the 1960's, the collective knowledge about cellular subsets and cell functionality has increased at an extremely rapid pace.[14,15] FACS is a procedure in which single cells are suspended in fluids which are flowed through

an optical system functioning much like a fluorescent microscope system. The cell filled fluid passes a laser emitted by the FACS sorter which causes two types of measureable phenomena when the laser interacts with the cells, scatter and fluorescence. Back and forward scattered light is collected by surrounding sensors and used to analyze the size and shape of the passing cells while the captured fluorescent signals identify intracellular features marked with fluorescent stains before running the cells through the devices.[16-18] The combination of the two optical analysis criteria built into a fast scanning system, boasting cell scanning rates between 5000 cells/sec to 50,000 cells/sec,[19,20] enables researchers to quickly differentiate and sort individual cells from sample sizes numbering in the millions. In addition to their analytical capabilities, FACS systems are also able to sort the scanned cells by applying a charge to the fluid carrying the cells and guiding the flow of cells by electrostatic deflection in different directions based on pre-defined user settings.[21] With the ability to analyze and sort millions of cells at quick speeds, fluorescent activated cell sorting has become a staple procedure for biological research.

Although FACS has become a standard method for single cell analysis and generation of pure cell lines, a need for even faster cell sorting spawned the invention of magnetic activated cell sorting (MACS).[22] The design of MACS systems emphasizes quickness over specificity for sorting and collecting target single cells. The standard MACS procedure utilizes antibody bound magnetic microparticles to mark cells of interest based on their extracellular characteristics, also referred to as cell surface markers.[23,24] Cells are mixed with the magnetic particles, incubated, and then washed to get rid of unbound magnets before being run through a fluidic system with the magnetically driven diversion of labeled and unlabeled cells. This quick separation method can either be used for purifying cells with desirable features or to sort out cells that are not wanted for experimentation.[25,26] MACS is typically better suited for cell sorting procedures requiring less specified behavioral differentiation of single cells than FACS. MACS has also been shown to maintain better cell viability of the collected samples due to less harsh sorting conditions. [27]

1.2.2 Other single cell sorting methods

Although FACS and MACS address the needs of most research requiring single cell analysis and sorting, the methods have some shortcomings that have been addressed by newer sorting methods. One of the most apparent limitations of classic FACS and MACS systems is that they are large scale devices that tend to require equally large scale sample sizes for adequate data acquisition. This constraint can limit the use of these sorting methods for cell types that are rare or don't readily multiply to massive numbers. The devices are also better tailored for sorting cellular samples that are already relatively well characterized so that their specific traits can be marked before sorting is initiated.[28] Furthermore, the necessity to pre-mark cellular samples before analysis hinder the capabilities of FACS and MACS to be used as point-of-care diagnostic devices for rare cell subset detection such as circulating tumor cell detection in patient blood samples. There are also instances where the final cell purity levels obtained by FACS and MACS are simply not enough and other sorting methods are required to obtain desirable purification results.[29]

Various new types of cell sorting techniques have been conceived since the invention of FACS and MACS which utilize newer methods of differentiating unique cells from one another. One type of cell sorting which addresses the need for label free cellular analysis for differentiating uncharacterized cells is the use of Raman spectroscopy for cell sorting. Raman spectroscopy generates a collection of "Raman bands" by more closely identifying light scatter generated by illuminating cells with a greater level of granularity than typical sorting methods. This technique negates the need for additional cell labeling components such as immunofluorescent stains by visualizing cells at a much more specific level than fluorescence imaging and even phase contrast microscopy.[30,31] Raman spectroscopy is also capable of *in vivo* cellular imaging and characterization which is not within the scope of more conventional sorting methods. Another interesting type of sorting criteria unrelated to standard methods is based on the behavioral differentiation of cells. One group showed that cell sorting could be conducted based on the motility of cells seeded to planar surfaces.[32] In a similar manner, another group sorted cells based on their ability to stick to a surface altered growth substrate.[33] These techniques are interesting due to their reliance on observable cell behavior under more normal culture conditions than if the cells were prepared

for use in FACS / MACS. Cell sorting without the use of laser optics has also been a popular topic to simplify cell separation protocols by use of size dependent filtration systems.[34,35]

A cellular collection technique that has made much headway since its inception is a method of using a laser to dissect and collect targeted regions of cell tissue samples known as laser capture microdissection (LCMD). LCMD is a technique which achieves targeted cell collection from heterogeneous tissues by irradiating the samples with a highly focused laser beam following a user drawn region. While it may seem that direct laser exposure to cells would be detrimental to their viability, much work has focused on the live collection and growth of cells retrieved in this manner.[36-38] One of the most useful aspects of LCMD cell sorting is the ability to observe target cells in real time during collection while the laser target region is being drawn by the user.

One of the most popular trends in biological research device design in the last decade has been the miniaturization of cellular analysis systems.[39] Often referred to as lab-on-a-chip systems, what were once sorting procedures requiring liters of chemical reagents and millions of cells now can be accomplished with less than a milliliter of fluid and tens of cells, with some caveats, of course. Microfluidic device designs aimed at reducing the overall cost and consumption of disposables and reagents have sought to recreate and even improve on older, larger scale systems for cellular biology.[40-43] These systems also possess a greater potential for point-of-care utilization due to their small scale footprints and low cost of manufacturing. Smaller systems typically boast faster data acquisition as well. Microfluidic device designs allow for more gentle methods of cell sample transport and also enable weaker force utilization for cell separation when compared to larger scale FACS / MACS systems. Some of the most common separation techniques include the use of magnetic deflection, optical force generation for sorting, and dielectrophoretic cell separation.[44-46] While the first method is obvious by its name, the latter two are newer methods enabled by microfluidic device fluid dynamics. Optical force separation refers to the use of lasers energy as a physical deflecting force to separate cells flowing through a microfluidic channel. Optical systems are capable of producing very precise and tunable electromagnetic force generation and are ideal for intricate microsystem use.[47,48] Dielectrophoresis is a

newly developed cell separation technique capable of cellular sorting based on deflection and attraction events generated by the application of non-uniform electric fields on particle samples. Although the mechanism of sorting is not completely understood, it has been shown that different cells can be diverted to different flow paths and separated from one another using this method. Dielectrophoresis is ideal for microfluidic sorting and point of care systems because it is capable of unlabeled cell sorting without the need for large scale force generation systems; electronic components designed to generate an electric field can be readily produced at microscopic scales.[49-51]

Continuing with the theme of electronic control of cell sorting on chips, there has been a recent surge in the utilization of a newer type of microfluidic liquid manipulation known as digital microfluidics (DF).[52,53] Briefly, DF technology utilizes surface charge differences generated on dielectric materials in order to move liquid droplets. By creating vast grids of electrodes beneath dielectric films, it is possible to move droplets in a stepping manner, resembling an inch-worm moving across a branch, without the need for moving pieces or external force generated machinery such as fluidic pumps. DF systems are especially interesting because of the proven ability to contain biological cell samples within these droplets in order to perform highly customizable assays.[54]

Microfabricated systems for cellular sorting provide a more cost effective means of biological analysis that allow for the utilization of forces and techniques otherwise irreproducible on larger, classic systems. These lab-on-a-chip devices have the potential to be utilized as point-of-care diagnostic tools and could see expanded use in hospital settings as well as parts of the world where expensive biological research tools are not readily available or entirely useful. As advancements in microfabrication techniques are made, so too will the ability to better characterize individual cells with limited sample sizes.

1.2.3 Modern cell colony sorting techniques

The vast analysis of modern sorting methods for single cell suspensions in the previous section was written in order to provide a juxtaposition to the comparatively lacking field of both macro and micro scale cellular colony sorting technique development. Cell colony research involves the observation of

cells expanded in culture and often requires the isolation of pure populations from heterogeneous mixtures that are intrinsic to bulk cell culture techniques. Stem cell research in particular is greatly reliant on single cell colony observations in order to select differentiated cells from their undifferentiated counterparts in culture.[55-57] Clonal growth of cancer cells also reveals important information about tumor behavior and progression.[58-61]

Due to its importance in science, cell colony sorting has been discussed by multiple groups in an effort to optimize colony selection and growth strategies. The most common type of colony analysis is the use of clonal formation assays typically conducted after the retrieval of target cell types to test for cell viability.[62-64] These procedures have also been further adapted to include cellular analysis steps to confirm that the cells of interest were properly collected from mixed samples in order to detect whether further purification of cells is necessary. A similar procedure known as the focus forming assay differentiates cancerous cells from healthy cells within heterogeneous samples by identifying undeterred colony growth in otherwise confluent cell cultures which normally induce contact inhibition.[65,66] Although these two methods have worked for researchers up to this point, they are both slow and cumbersome, requiring many manually intensive and repeated cell seeding or passage protocols. The shared growth substrates used for these studies can also cause unwanted extraction of unimportant cells growing alongside cells of interest leading to loss in purity and the necessity of further repeating the process. Some newer methods of cell colony extraction have been developed such as automated detection and retrieval of cells, but they too are hindered by difficulty in collected pure cell samples.[67-71] There is currently a need for improved cell colony sorting platforms to achieve higher purity, shortened time frame for the process, as well as better automated systems to increase the throughput.

1.3 The Micropallet Array as a Cell Sorting System

The micropallet array is a novel microfabricated chip based cell sorting system designed to enable the capture of single cells and cell colonies on individual biocompatible growth substrates aligned in arrays.[72-75] As a new approach to cell sorting the micropallet arrays allowed adherent cells to be

maintained in contact with a substrate during observation and growth, which is the case in their natural environments and which aids in their ex vivo culture. Micropallets with cells of interest could be easily identified by microscopy and then collected via laser catapult.[76,77] Cells seeded to micropallet arrays benefit from being able to maintain contact with their own individual pallets through the entire sorting process, negating the need for harsh chemical digestion of cells in order to form single cell solutions as is required by the conventional sorting methods described in section 1.2.1. In addition to single cell sorting, cell colony sorting can also be performed on the arrays simply by fabricating micropallets consisting of larger pallets and growing cells on the arrays over a longer, predefined length of time.

The fabrication of micropallet arrays consists of the photolithographic patterning of microstructure arrays onto the surface of glass microscope slides. The arrays are made to consist of thousands of individual pallets structures fabricated from transparent, biocompatible photoresists such as 1002F.[78,79] Pallets can be designed to be a variety of shapes and sizes depending on the specific needs of the maker with limitations only coming from the properties of the materials used to make the structures and the cleanroom tools available. After the formation of the pallets, chemical enhancements are made to the array surfaces in order to make them hydrophobic to enable the sequestering of cells to pallet surfaces due to the formation of "virtual air walls" between adjacent pallets.[80] Efforts have also been made to form physical barriers between pallets to circumvent the need for chemical alteration of the arrays, but up to this point virtual air walls have won out as the standard barrier forming method.[81] Figure 1.3.1 Shows a completed micropallet array ready for cell seeding.

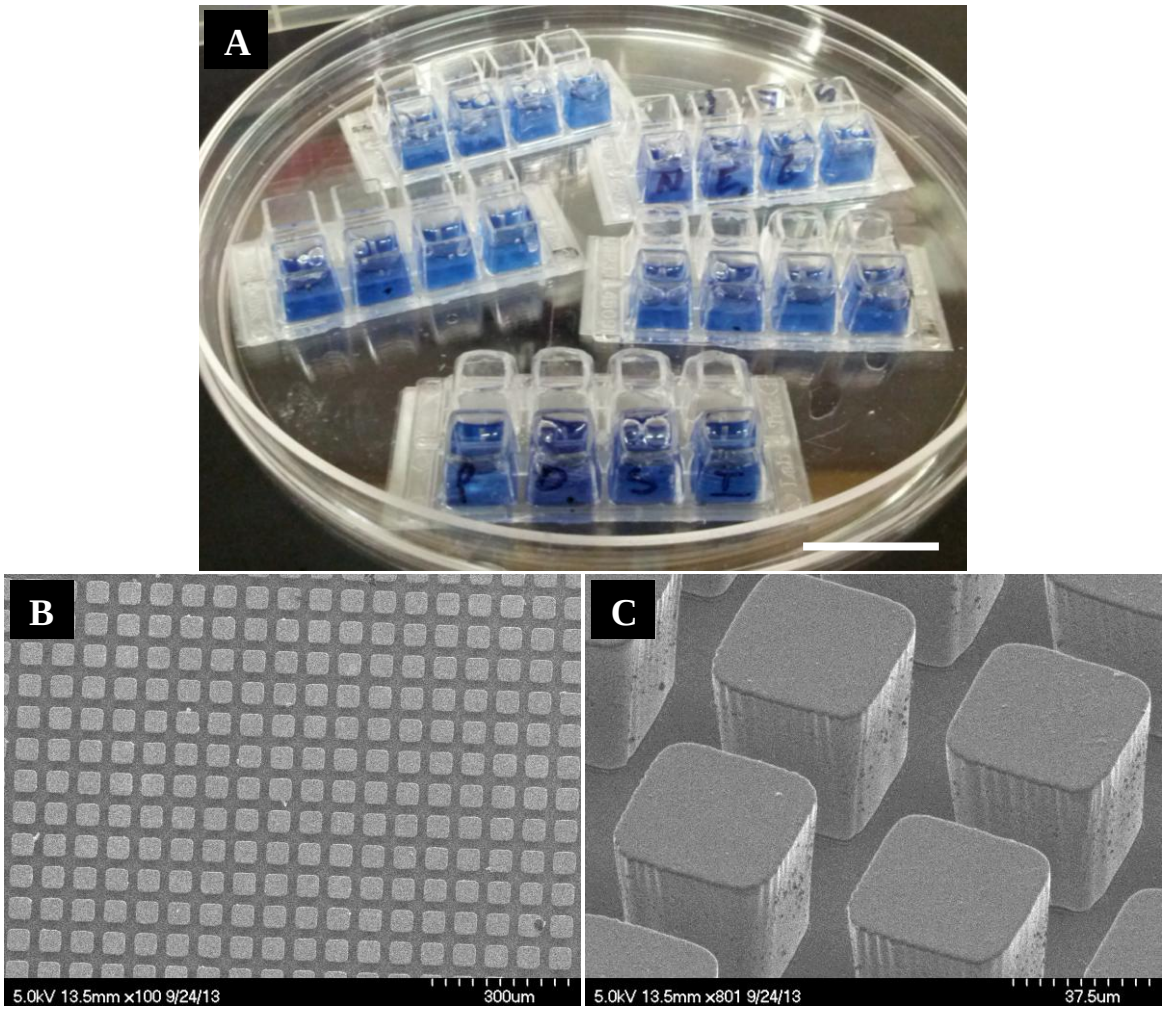

Figure 1.3.1 The micropallet array
A) Five micropallet array slides fitted with 8-well culture chambers. Four of the eight wells of each chamber slide are filled with a blue solution. Micropallet arrays consist of thousands of microscopic pallet structures fabricated from transparent, biocompatible photoresist onto the surface of glass microscope slides. The scale bar is 21.6 mm. B) Scanning electron microscope (SEM) image of top view of a micropallet array. Each pallet is a 40 µm by 40 µm square with 50 µm height. The gaps between the pallets are 30 µm wide. C) Isometric SEM image of micropallets.

In order to be used for cell cultures requiring liquid environments, micropallet arrays must be fitted with vertical chambers in order to hold the liquid above the arrays, but this step in fabrication is flexible and many different forms of chambers have been utilized for this purpose. While cells will adhere to and grow on micropallets made of 1002F photoresist, it has been shown that coating the arrays with extracellular matrix proteins and antibodies can dramatically increase cellular adhesion strength and viability which are both key factors in successfully utilizing the technology.[82, 83] Once coated, the

micropallet arrays are ready to be used for adherent cell sorting procedures ranging from the optical analysis of heterogeneous single cell populations seeded to the arrays to cell colony differentiation and collection.

Seeding cells to the micropallet arrays is a straight forward procedure which is achieved by creating low concentration single cell suspensions in culture media and pipetting the solution in the culture chambers mounted to the surface of the arrays. Once pipetted, the cells become randomly distributed over the micropallets and the number of cells that seed to the arrays follows the Poisson law of small numbers while the total number of cells per pallet follows a Poisson distribution. Using this law, it was previously shown that in order to create the best chances of achieving single cell seeding to individual micropallets the total number of single cells introduced to the arrays should not exceed one third the total number of pallets available in a culture. For example, if there are 1000 pallets contained within a chamber, then to best achieve single cell adherence to pallets the number of cells seeded should not exceed 333 cells. It has been empirically found that in order to better achieve a uniform distribution of cells over the entirety of an array, as opposed to local masses of cells, cell media and micropallet array temperatures should be matched. It is thought that differences in temperature of the arrays and seeding media can lead to convective currents which cause cells to amass around the edges of culture wells. Although this worry has not been thoroughly studied to this point, all cellular experimentation described in this paper used matching micropallet array and media temperature. Figure 1.3.2 includes a visualization of proteins coated onto a micropallet array as well as seeded adherent cells.

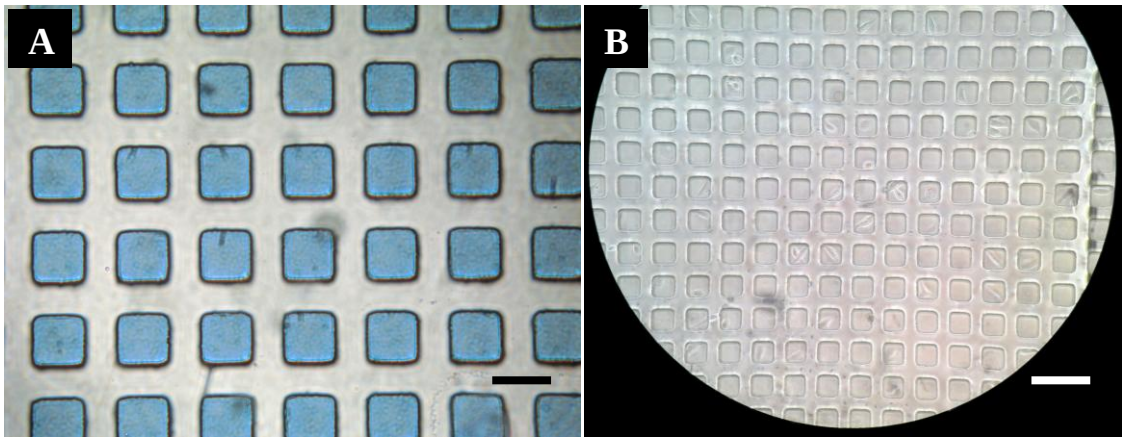

Figure 1.3.2: Protein and cells seeded to micropallet arrays
A) Human fibronectin proteins seeded to micropallet arrays visualized with TrueBlue Peroxidase. Protein seeded to the array surfaces was visualized with a blue stain and can be seen sequestered to just the tops of the pallets due to virtual air walls preventing gap filling. The scale bar is 40 µm. B) Cells seeded to a micropallet array. NIH/3T3 cells were seeded to a micropallet array and allowed to adhere for 3 hours. The scale bar is 100 µm.

1.3.1 Advances in micropallet array technology

Major improvements to the functionality of micropallet arrays have been achieved through fundamentally altering the fabrication process for the technology. The standard fabrication of micropallet arrays, as described above, involves the photopatterning of a single layer of transparent resist directly onto the surface of cleaned glass slides to form thousands of cubic structures. Some subtle changes have been made to this process over time, such as using thinner glass slides for better imaging characteristics, but in general micropallet fabrication has been held standard. Recent advances made to the technology have altered this fabrication scheme with the goal of crafting more user friendly micropallets as well as expanding their potential uses for varied biological samples.

Improvements to micropallet arrays have targeted three primary aspects of the technology. They include changes to the material used to make micropallets, the shape of fabricated micropallets, and finally the way in which micropallets are ejected from the glass slide substrates for collection. The 1002F photoresist typically used to make micropallets is a great material for creating pallets with great biocompatibility and imaging characteristics,[78] but they are a passive material with limited utility beyond pallet growth. Recently there has been an effort to enhance the functionality of the pallets of the

arrays by altering the material from which they are made. In an important study, magnetically responsive micropallet arrays were created by mixing ferromagnetic iron nanoparticles into 1002F photoresist. Pending arduous iron particle concentration optimization, the resulting magnetically responsive pallets were shown to be biocompatible and to be transparent enough to allow fluorescent microscopy with only slight losses to imaging clarity.[84] There were slightly more dramatic losses to phase contrast imaging qualities, however, and so subtle, unstained cellular characteristics were harder to observe on the arrays. A novel magnetic probe was also designed during this study which enabled the direct collection of ejected pallets, eliminating the cumbersome array flipping technique previously held standard for pallet collection. Magnetic control of pallets was a breakthrough as it had the potential to enable directed cellular analysis procedures to be performed on single collected cells through the highly specific manipulation of the magnetic probe with an attracted pallet. Another group has since improved on the optical clarity of magnetic photoresists for micropallet fabrication, further enhancing the utility of the technology.[85]

Changing the shape of the pallets forming the arrays has also been a target of much innovation. An issue that has previously limited the expansion of micropallet use to cell colony sorting, instead of just single cell sorting, had been that the laser ejection method typically used for single cell sized pallets did not translate well to colony sized pallet structures.[76] When pallets were made large, the laser energy required to eject pallets of interest was too great to retain adequate cell viability on the surfaces of the pallets. As a creative approach to circumventing this issue, table-top style micropallet arrays were designed and tested for cell colony sorting purposes.[86] By utilizing a dual layer photoresist fabrication system integrating the patterning of SU8 and 1002F together, table top shaped arrays with standard micropallet sized "table leg" structures with larger colony pallet sized "table top" structures were formed and successfully tested for cell colony sequestering and collection. The creation of smaller leg structures for laser targeting allowed standard laser energy use applied to each of the legs in order to eject the larger top. While the ejection of table top pallets required multiple laser targeting steps to release each of the four legs, the overall energy required for release was still much lower than for a large standard shaped

pallet without legs. In another interesting approach to changing the shape of micropallet arrays, the ability to use thin, vertical structures in tandem with standard micropallets in order to split expansive cellular colonies has been shown.[87, 88] This approach too avoided the use of large area micropallets while still allowing for cell colony analysis by relying on the capability for adherent cells to reach over gaps to grow over closely spaced structures. Pairs of normal scale pallets were fabricated with individual smaller, thinner structures in between them. The gaps between the pallets and the small structure were close enough for cells to grow across the group and form a large colony. When cell colonies were grown over the expanses, the smaller structures could be ejected, collected portions of the colonies, and collected to perform cell-lethal assays which would then reveal intracellular characteristics of the rest of the corresponding cell colonies. Portions of the cell colonies remaining on the standard pallets could then be collected once a target colony type was identified by the cell lethal assays.

A new and emerging improvement being made to micropallet function has been an effort to change the means in which individual pallets are released from the arrays. As mentioned above, laser energy requirements for large, cell colony sized micropallets are too high to retain adequate sample viability post-ejection. While changes to pallet shape adequately solved this issue for certain types of cell colony growth studies on pallets, there was still a need to be able to eject large, solid pallets for proper cell colony sequestering on individual growth substrates. One very interesting method that was able to accomplish this task was the replacement of the laser ejection system with an ultrasonic wave generator.[89] By pairing micropallet arrays to an ultrasonic transducer, it was possible to eject extra large pallets with a width and length of 500 μm with a 300 μm height. Although this pallet size was not typical of micropallet arrays, cellular viability was retained and the core function of cell sequestering was maintained as well, making this innovation relevant and interesting. Efforts to expand the potential user base of the arrays to those without sophisticated laser ejection systems is an important improvement and similar changes should be considered for all micropallet work moving forwards.

1.3.2 The future of micropallet arrays

Advances to micropallet array technology should continue to improve on the usability of the arrays as well as improve on larger, more complicated micro system integration. In their current form, micropallet arrays are great for direct cell analysis to sorting applications, but are limited by the need for hands on control of each usage step. Cellular analysis is currently conducted by eye using fluorescent and phase contrast microscopy to locate target cells seeded to the arrays. This process is slow and cumbersome due to the small fields of view provided by high resolution imaging systems. User scanning of the arrays can be prone to error due to the identical look of adjacent micropallets making specific location tracking difficult. The cell seeding process is also random as discussed in section 1.2 and can cause non-ideal cellular distributions within a well.

Micropallet array innovations must focus on the usability and throughput of the technology. A primary way in which this can be accomplished is by enabling the automated analysis and collection of cells seeded to the pallets. Solving the slow process of manually inspecting pallets and transferring them to other cultures would greatly reduce the amount of hands-on time in front of microscopes as well as increase cell sample viability by finishing analysis faster and returning the cells to ideal culture conditions. To keep micropallet arrays relevant, more efforts must be made towards better optimizing the technology for cell colony sorting to allow tumor and stem cell studies to be conducted. These two cell types are of particular interest to the medical industry. Finally, with the entire industry pushing for lab function miniaturization, the arrays should designed to be better ready for deeper device integration. As they are now, micropallet arrays are contained systems with no real device interfacing opportunity.

Chapter 2: Magnetic Micropallet Arrays for Cell Colony Sorting

2.1 Overview

This chapter discusses the development of a large area magnetic micropallet arrays with a novel approach to pallet release and collection. At the time that this work was started, there were a small number of published articles reporting on micropallet arrays specifically designed for cell colony sorting. There was, however, a common issue discussed within those limited works relating to the difficulty to consistently release large micropallets. Adapting the laser release methodology developed for standard micropallet ejection did not translate well with larger pallets because the greater energy required to eject the pallets resulted in unwanted cell damage. In order to solve this issue, a novel method of patterning a laser absorptive gold thin film below the large micropallets was developed. This method relied on the creation of heat generated vapor bubbles on the gold film surface expanding below the pallets and causing release. Gold, being a great conductor, acted as a seed layer for the formation of ferromagnetic nickel structures that were cleverly integrated within every individual micropallet to enable magnetic manipulation of released pallets. The nickel elements were then gold coated and the completed arrays were shown to be biocompatible and capable of cell colony growth over many days. The work described in this section includes various microfabrication techniques including electron beam vapor deposition, photolithography, and micro electroplating. Standard cell culture procedures were utilized as well as confocal microscopy for immunofluorescent imaging and pallet analysis. This chapter is adapted from a paper published in Lab on a Chip, a publication from The Royal Society of Chemistry. (DOI: 10.1039/C5LC01131K)

2.2 Introduction

The progression of micropallet array technology was described in detail in chapter 1. Although several innovations have been made to micropallets, there has been a stagnation in the technology in terms of making dramatic changes to the fabrication process and usage of the devices. The standard

micropallet array consists of glass slides coated with a transparent photoresist, typically 1002F or SU8 resists, which is photolithographically patterned to form thousands of cell sized pallets for improved culture conditions during adherent single cell sorting. Some advances in fabrication processes for enhanced micropallet functionality have been made, but they primarily retain the use of just glass slides coated in photoresist with the changes made to the design of the pallet shapes.[86-88]

The most dramatic change that has been made to micropallets was work involving the inclusion of magnetic microparticles within patterned resists to form micropallet arrays with magnetically retrievable pallets.[84,85] This fundamental change to pallet fabrication resulted in solving issues associated with the otherwise very work intensive collection protocols previously utilized for ejected micropallets. Classic micropallet collection required the complete inversion of micropallet arrays over collection wells in order to transfer ejected pallets from the arrays to separate culture wells. This procedure greatly limited the downstream control of collected cellular samples and also had the possibility of collecting unwanted cells with the ejected micropallets in cases where cells seeded to the arrays had very weak adherence characteristics and became disconnected from pallets during collection. The ability to transfer micropallets using an external magnetic probe allowed for a much more straight forward collection procedure and also gave the researcher more control over where the collected pallet finally ended up. The alteration of pallets in order to enable magnetic collection highlighted the fact that micropallet arrays, although significantly useful, had the potential to have even greater utility with the right additions to pallet fabrication.

Although micropallet arrays were originally conceived with the intent for both single cell and cell colony sorting protocols,[73] much of the early work was focused on single cell analysis. More recent work has had a greater focus on cell colony sorting which has revealed that the micropallet array technology as it stood was not optimized for large pallet collection. Using the laser ejection protocol utilized for standard micropallets did not translate well to the larger pallet areas required for cell colony growth and analysis due to the higher laser energy application necessary for ejection of the cells. More laser energy meant either more damage to the micropallets during ejection or worse damage to the

collected cell colonies. Work focused on simplifying and improving on the consistency of large pallet release have been published,[86,89] and although successful, relied on methods closely related to those that were long established.

The work described in this chapter came about as an attempt to solve the issues with large area pallet release and manipulation by applying engineering techniques yet to be explored with micropallet arrays. The very first idea that was seriously considered was to use sacrificial layers to facilitate large pallet ejection by creating additional ejection forces upon excitation by laser. Another idea was to use patterned adhesives placed in strategic locations below micropallets which could in some way be destroyed to release pallets that otherwise were not adhered to a substrate. A simple flowchart which was presented at the onset of this project is included in Appendix A, figure 6.1.1.

2.2.1 Concept of magnetic micropallet arrays for cell colony sorting project

The research direction that was ultimately pursued for having the greatest potential was an idea that was inspired by a new type of biological transfer system known as laser induced forward transfer (LIFT).[90-92] LIFT is a process in which a thin layer of silver is layered onto a quartz slide and biological materials are seeded over the surface of the silver. A laser pulse is directed underneath an area of interest and the target section is ejected from the slide carrying the biological sample on top. The sample is then transferred to a nearby capture surface. The reason that this technique was of interest was that the only major shortcoming with the process had to do with some loss in sample viability following transfer. It seemed as though the silver surface was not thick enough to protect cells from direct damage caused by the laser and so it was thought that the addition of carrier structures, such as micropallet arrays, would greatly benefit the procedure by providing a protective surface for the biological samples. The area sizes that were successfully translated by the LIFT procedure were also close to the area that was required for cell colony sized pallet ejection. After some discussion, it was decided that this concept made sense and so the LIFT procedure was adapted for use with micropallet arrays.

Some major changes were applied to the LIFT concept to be adapted towards micropallet use. First, instead of silver, gold was selected as a better choice as the material had better biocompatibility than silver. Second, the silver layers used for LIFT were opaque due to their thickness and would not have worked for specified cellular imaging on their surfaces. The gold layers for this project were intentionally plated at super thin levels so that while a uniform gold layer was present, it was thin enough to be visually semi-transparent so that cell features would still be visible through them. Interestingly enough, this was actually similar to a technique used for the fabrication of visors designed to protect astronauts in space from ultraviolet light.[93] There were two primary outcomes that were thought to be possible with laser ejection. First, much like with LIFT, it was thought that it was possible to completely remove the gold film below a corresponding micropallet by laser irradiation which would then release the pallet from the glass slide below. Even though this would not generate any upward force below the pallet, releasing the gold substrate would theoretically be enough to allow freed pallet collection. Second, it was known that heating gold could result in the formation of microbubbles on the gold surface.[94,95] If the bubbles generated enough force below the pallets, they would cause the targeted pallets to release upward from the array for collection. It ultimately turned out that the latter release modality was what was reproducible by using a multiphoton laser system paired to a confocal microscope commonly used for pallet imaging.

Finally, the conductivity of the gold layer was of great interest as it had the potential to be used as a seed layer for electroplating procedures to be performed on the micropallet arrays, which was something that had yet to be explored before this work. An interesting idea was inspired by recent work involving the electroformation of interposers in 1002F scaffolds completed in Dr. Bachman's lab. Small nickel interposer structures were successfully electroformed within via holes that were patterned into a 50 μm thick layer of 1002F over a conductive copper layer. This process was readily transferrable to micropallet arrays fabricated over semi-transparent, conductive gold thin films. Electroformed nickel structures were found to possess ferromagnetic properties through the work described in chapter 4 and were thus of great interest for use with the colony micropallet arrays. The interposer fabrication process was applied to micropallet arrays fabricated on thin gold films with the pallets all including small via holes to be filled

by nickel electroformation. The completed arrays consisted of individually releasable, large scale micropallet for cell colony sorting with ferromagnetic core structures formed into their via holes which allowed for magnetic retrieval of pallets. Furthermore, following electroplating, micropallet arrays viewed with phase contrast and confocal microscopy had stark contrast between the pallets and the gaps between them. The ferromagnetic core structures were also very dark compared to their 1002F surrounding and had the potential to be used as imaging fiducials for automated pallet location.

The concept of magnetic micropallet arrays for cell colony sorting fabricated by the electroformation of ferromagnetic structures within pallet via holes had much potential. The gold film assisted release of micropallets via vapor bubble formation worked consistently and was reproducible when using a low energy multiphoton laser which came included in the confocal microscope system that was already being used for other pallet related research. The ferromagnetic cores within the pallets allowed for magnetic retrieval of pallets which then opened up the potential for specified downstream cell colony analysis. Furthermore, being able to control the pallets by using an external magnetic had great implications towards allowing integration of micropallet arrays within larger systems that would otherwise not be possible if gravitational pallet collection was the only available option. Finally, the form factor of the electroplated micropallet arrays greatly eased the visual identification of pallets. Although not discussed in this paper, automated visualization could be greatly simplified when working with the micropallet array designs discussed in chapter 2 (this chapter) and chapter 3. All in all, large area magnetic micropallet arrays for cell colony sorting consisted of many different innovations which were brand new to the field of micropallet arrays and had a significant impact on what could be done with the technology in the future.

2.3 Materials and Methods

The fabrication of the magnetic micropallet arrays for colony sorting included various fabrication techniques that are commonly used in microfabrication. These techniques included: Electron beam vapor deposition, photolithography, and electroplating. Due to each technique being greatly explored and

understood in the world of microfabrication, the creation of the magnetic micropallet devices was a fairly straightforward, albeit time consuming, procedure. The following section details the specific methods used to create the devices.

2.3.1 Gold Thin Film Deposition

Thin films of gold were prepared on glass slides to form a seed layer for cell colony array fabrication. Standard microscope slides (VWR, Radnor, PA) were cleaned in piranha etchant solution (H_2SO_4 and NH_4OH at a 3:1 ratio) and washed in running deionized water (diH_2O). After the diH_2O wash the wet slides were dried with a stream of N_2 gas and then more thoroughly dehydrated in an oven at 135 ˚C for one hour. Dehydration of the slides was necessary as any leftover wetness on the glass slide surfaces could lead to poor gold layer adhesion. A titanium seed layer was evaporated to the cleaned glass slides using a Temescal CV-8 electron beam deposition tool (Vesco, Estero, FL) to a final thickness of 38 Å. The seed layer provided better adhesive strength between the glass slide and the gold layer to come. A thin, 200 Å layer of gold was evaporated onto the titanium seed layer using the same device. Although gold is typically thought of as an opaque metal when viewed in common, every day forms, the glass slides coated in such thin gold films were visually semi-transparent with objects being viewable through the slides themselves. Figure 2.3.1 displays glass slides coated in the thin gold film.

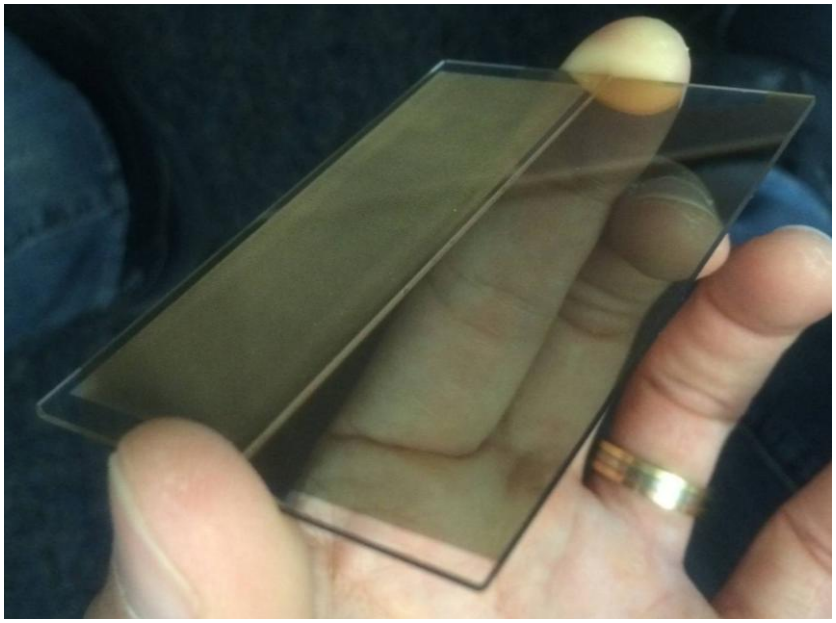

Figure 2.3.1: Glass slides plated with translucent gold
Thin gold films were utilized as a laser absorptive layers for micropallet ejection. The slide on the right is a 1 inch by 3 inch standard microscope slide with a 200 Å gold layer plated to its surface using E-beam vapor deposition. The slide on the left is also coated with the same gold layer and also has an array of 50 µm thick, 250 µm by 250 µm micropallets patterned on the surface of the gold.

The gold films exhibited strong adherence to the glass slide surfaces and passed standard tape-lift tests utilized for checking adhesion strength. The light transmission properties of the gold thin films were quantitated using an Ocean Optics USB2000 Spectrometer (Ocean Optics, Dunedin, FL) opposite to a tungsten halogen light source separated by the glass slides being analyzed. Along with being able to allow adequate light passage, the gold thin films were also required to maintain high conductivity to allow for electroplating to occur on their surface during later fabrication steps. To confirm adequate conductivity, the resistance of the gold films were recorded as a function of distance from a single corner of the films. The corner location was representative of where an alligator clip passing current would be placed during electroplating procedures.

2.3.2 Fabrication of Micropallet Arrays

The design of the colony sized micropallet arrays was similar to standard single cell style pallets, but were much larger. Arrays of square pallets were fabricated onto the gold coated glass slides with an addition design element which formed square through holes (also referred to as via holes) within them.

The gold coated glass slides were prepared for micropallet fabrication by washing their surfaces with isopropyl alcohol followed by a rinse in diH_2O. They were then dried in N_2 gas and dehydrated in a 135 ˚C oven for at least one hour or until ready for coating. 1002F photoresist was the standard resist used from single cell micropallet arrays due to its biocompatibility and low autofluorescence which were required traits for this array iteration as well. The resist was first prepared as previously reported [79] by dissolving EPON resin 1002F (Miller-Stephenson, Sylmar, CA) in γ-butyrolactone (GBL) (Sigma-Aldrich) with the addition of triarylsulfonium hexafluoroantimonate salts (Dow Chemical, Torrance, CA) to generate photosensitivity necessary for photolithography. The ideal concentration for each component for the formation of 50 µm tall micropallets had been previously established. Each component was added to a glass jar and mixed with an automated stirrer for 24 hours in order to break down all resin aggregates as well as completely degas the solution. The finished 1002F mixture had a honey-like viscosity and was sticky to the touch. 1002F was spin coated over the surface of the gold coated slides to a thickness of 50 µm and soft baked on a hotplate at 70°C for 20 minutes and then additionally heated to 105°C for 40 more minutes to evaporate all solvents from the photoresist and solidify the film. Over heating the slides would result in non-uniform films which was not ideal. After cooling the slides for 20 minutes, the 1002F films were photolithographically patterned with exposure to a collimated UV light source (AB&M INC, Scotts Valley, CA) at 1200 mJ/cm^2. The film mask used for patterning was a negative representation of the desired micropallet features. As the colony sized micropallets did not require patterning of features below 50 µm, low resolution printed masks worked with no negative effects on the final designs.

Four different photomasks were printed and utilized for this study. The first mask was designed for the purpose of fabricating large micropallets with dimension of 270 µm by 270µm and 50 µm gaps in between adjacent structures. This mask design was intended to be used for testing optical properties and biocompatibility of 1002F patterned on the gold thin films and did not include any via holes in the pallets. The three remaining mask designs were created using the same square dimensions of the first mask with the inclusion of a square via hole added to the corner of every pallet. Each of the three masks consisted of an array of via hole micropallets with the holes designed at either 50 µm by 50 µm, 75 µm by 75 µm and

100 µm by 100 µm. The different via hole sizes were referred to as small, medium, and large respectively. When included in the pallet designs, the via holes allowed for the exposure of the gold thin film within a micropallet which was required in order to form the ferromagnetic core which would later be added by electroplating. Appendix A figure 6.1.2 includes an image of the three core size designs after metal plating. In order to allow for uninterrupted cell growth on the micropallet surfaces, the via holes were placed as far to the sides of a pallet as possible while maintaining the structural integrity of the pallets. Each mask design also included 2.5 mm wide borders on each side of the glass slides so that there was enough room for an alligator clip to be connected to the arrays during electroplating without interference from the pallets. Figure 2.3.2 is a schematic of the photolithography process for microarray fabrication and an example of a completed array. Following UV exposure, 1002F coated slides were baked at 65°C for 7 minutes and then 95°C in a second oven for 18 additional minutes to finalize the photoinitiation of the resist. Once cooled, the slides were immersed in SU8 photoresist developer (MicroChem, Newton, MA) for four minutes to remove all uninitiated regions and quenched with isopropyl alcohol. Surface agitation of the slides during developing was required to fully develop the gap and via hole regions of the micropallets. Partial development of the holes could result in ferromagnetic core formation within the pallets thus ruining the function of the devices. Finally, the slides were dried with N_2 gas and hard baked in a programmed oven with a pre-set heating and cooling routine specifically designed for 1002F.

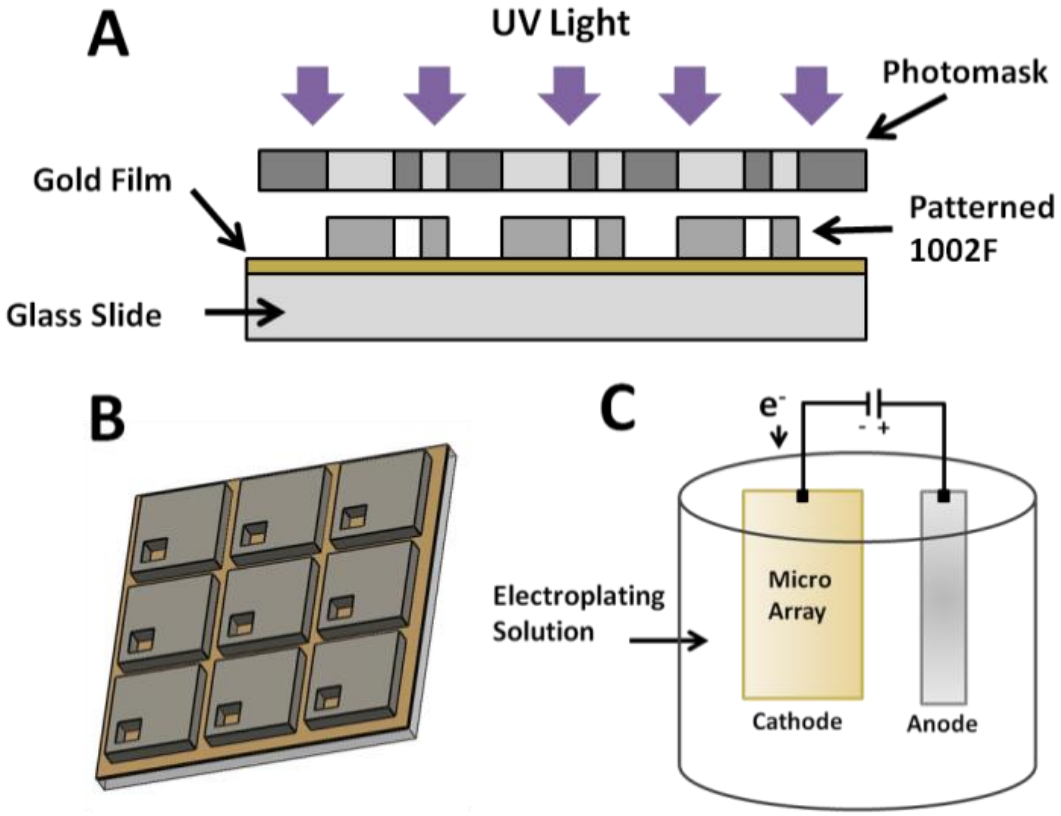

Figure 2.3.2: Fabrication of microstructure arrays containing via holes on gold thin films
A) Schematic of the photolithographic patterning process of the micropallet array. B) Representation of patterned structures. Regions of the gold thin film are exposed within each micropallet through a via hole for the electroplating of ferromagnetic nickel cores. C) Schematic of electroplating setup. Microarrays are linked to a power source and immersed in an electroplating solution along with an anode. Electroplating occurs on all exposed conductive surfaces of the micropallet array which in this case were the exposed gold thin film surfaces.

2.3.3 Gold and Ferromagnet Electroplating

The exposed gold thin film surfaces on the micropallet arrays with via holes were plated with gold coated nickel structures utilizing a multistep electroplating procedure. First, the photopatterned 1002F micropallet arrays were sonicated at 47 kHz for 5 minutes in a diH_2O bath at room temperature (27°C) in order to displace the air pockets trapped within the via holes that would form upon immersion in high surface tension liquid. While sonicating the arrays, a pipette was used to create additional agitation over the slides by repeatedly pumping water over their surfaces. Sonication was a necessary step

to include as not doing so would lead to several pallets having no electroformation within their via holes due to air bubbles stayed trapped for the duration of fabrication.

Gold coatings were created on the top and bottom sides of the ferromagnetic nickel cores. To create the bottom gold coating, the micropallet arrays were linked to a power source by alligator clip on one end while the other was immersed in Technigold 25E electroplating gold solution (Technic Inc, Cranston, RI). A pure gold high surface area mesh anode was placed in gold plating solution along with the sample to be coated and grounded. Figure 2.3.2 also includes a representation of the electroplating setup which was utilized for all three metal plating steps. Gold electrodeposition was conducted for 2 minutes at an applied current of 0.5 A / dm^2 at 60°C to create a 500 nm thin layer directly on the gold thin film surfaces. After the initial plating, the arrays were washed three times in diH_2O at room temperature to remove excess plating to prevent contamination of the nickel plating solution. The newly formed gold layer acted as a seed layer for the following ferromagnetic nickel plating. Sonication procedures did not have to be performed in between plating steps as a single removal of air in the via holes was enough to maintain liquid contact in the via holes throughout the rest of the fabrication procedures. A Watts nickel bath solution ($NiSO_4 \cdot 6H_2O$, $NiCl_2 \cdot 6H_2O$, H_3BO_3), was filled into a beaker and placed in a 50°C hot bath with constant low level agitation. The glass slides were linked to the power source again and placed in the Watts bath solution along with a nickel anode probe and a second dummy cathode. Although not necessary for all nickel electroplating procedures, the dummy nickel cathode was utilized in this instance to increase the overall surface area to be electroplated in the bath which increased plating quality. Nickel core formation was achieved with three discreet current application steps. First, 0.5 A / dm^2 was applied to the arrays for a span of just 3 minutes to form a very thin layer of nickel. The second current step was applied at 1 A / dm^2 and held for only 3 minutes once more. The first two current application steps were used as a safety measure in order to increase the conductivity of the arrays by placing a uniform layer of nickel over the entirety of the previously plated gold seed layer. Neglecting the first two steps and performing nickel electroplating at overly harsh conditions could result in non-uniform nickel formation and is not suggested. The final step involved raising the applied current to 2 A / dm^2 and holding this

setting for 112 minutes. The completed nickel core structures were on average 30 μm thick. After proper nickel formation was confirmed by inspection with a microscope, the arrays were triple washed in diH_2O and one more 500 nm gold layer was added over the surface of the nickel plating by repeating the first step of the process. The visual differences in nickel coated micropallet arrays and gold coated micropallet arrays can be seen in Appendix A figure 6.1.3. Once completed, the arrays were triple washed in diH_2O for a final time. Images of the completed arrays are shown in figure 2.3.3.

Although the ferromagnetic cores could theoretically be plated to any height within reason, it was necessary to aim for heights at least 20 μm lower than the height of the micropallets. It was empirically found that overplating the core structures would generate additional holding forces which would make laser ejecting the pallets near impossible. Forming the core structures at heights lower than the micropallets had no noticeable effect on device function and generated enough magnetic response for the ejected pallets to be collected by a magnetic probe. The 1002F pallets of the arrays were not affected by the electroplating procedure due to the pallets being unable to hold charge. The structures maintained their transparent features and all remained adhered to the surface of the gold films. Appendix A figure 6.1.4 shows an example of electroplated micropallet arrays with via holes as well as overplated samples.

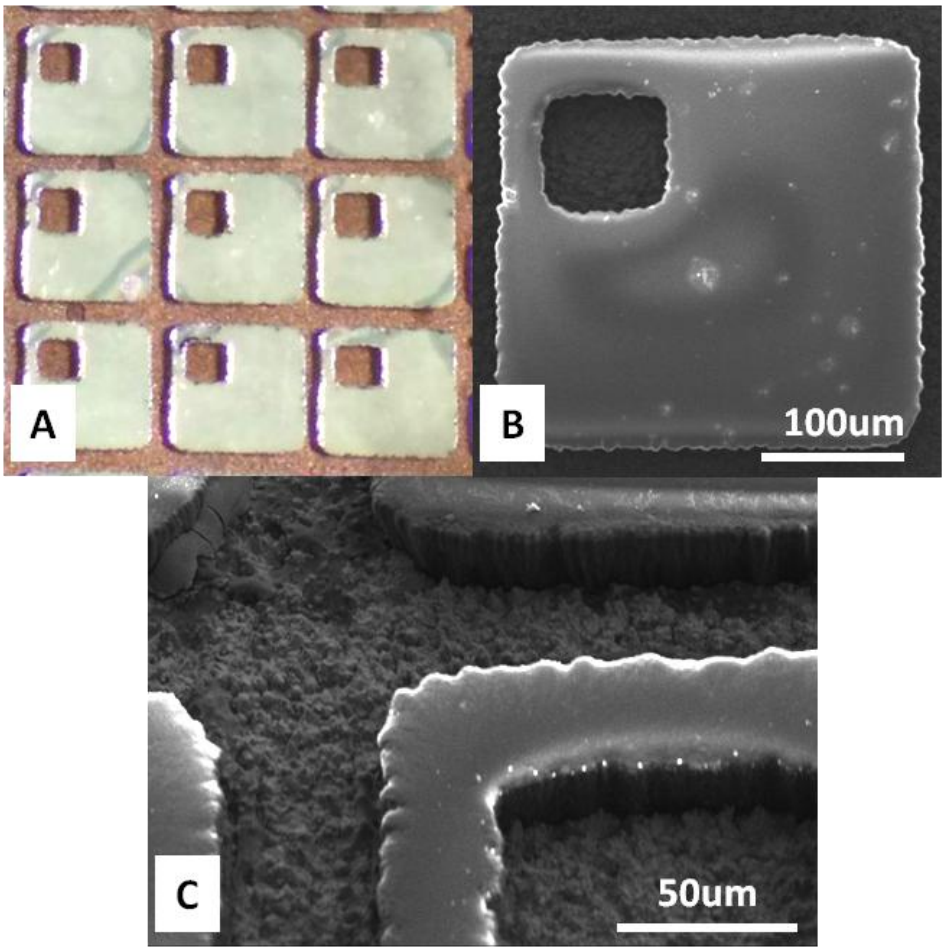

Figure 2.3.3: Large area magnetic micropallet arrays for cell colony sorting
A) Section of a completed array revealing the top layer of gold coated on both the borders surrounding the pallets and within their via holes. B) Scanning electron microscope (SEM) image of an individual magnetic micropallet. C) SEM image of a corner section of an individual pallet. The metal plating can be seen rising to 30 µm along the sides of the 50 µm tall structure.

2.3.4 Magnetic Response Analysis

For the magnetic cores embedded into the pallets to be useful, they had to be shown to generate enough magnetic response force to enable pallet collection. Furthermore, the attraction of the ferromagnetic nickel elements would need to be sufficiently strong when attracted towards a magnetic probe with a magnet small enough to be utilized for individual pallet collection. To test the magnetic attraction strength of the three different nickel core structures, pallets from each completed array shape were physically ejected from the arrays by pressing on the pallets with an 18 gauge need tip. Each individual ejected pallet was then placed onto its own sheet of double sided tape which was then adhered

to the surface of a scale. The pallets were tested one by one. A 1 mm diameter, cylindrical gold coated neodymium rare earth metal magnet with a peak magnetic field strength of 225 Gauss was aligned perpendicularly to the scale surface at 0.1 mm above the pallet being tested, which had to be identified with an ink blot as they were too small and transparent to spot by eye. The magnetic was secured onto a sliding ruler which was slowly raised from the pallets enabling the measurement of distance from the pallet surface and correlate it to the amount of attractive force by noting the positive change in weight as the magnetic was drawn away from the pallet. Background forces generated by the scale surface reacting to the magnetic force was recorded ahead of time and subtracted from all readings. The small, medium, and large ferromagnetic cores were tested with this set up.

2.3.5 Virtual Airwall Preparation

The formation of "virtual air walls" during cell seeding on micropallet arrays has been utilized since the onset of the technology.[80] In order to capture air within the gaps, and in this case the via holes, of the micropallet arrays it was necessary to chemically alter the surfaces of the devices to a more hydrophobic form. To do so, the magnetic micropallet arrays were silanized as previously described.[80] 200 µL of (heptadecafluoro-1,1,2,2-tetrahydrodecyl)trichlorosilane (Gelest, Morrisville, PA) was placed into a small weigh boat which was then put into a dry-seal desiccator with the micropallet arrays. An oil-free vacuum pump was linked to the desiccator and the internal pressure of the system was brought down to 7 Torr. The air sealed desiccator was then kept under pressure for at least 24 hours or until the arrays were ready to be used.

2.3.6 Protein Surface Coating for Cell Culture

Although 1002F is biocompatible, it is not cell growth ready on its own. Past work has shown that it is greatly beneficial to the cell seeding and expansion process if 1002F structures are first coated with extracellular matrix proteins or certain types of antibodies.[82,83] The magnetic micropallet arrays were coated in human fibronectin protein by utilizing the methods described in the cited work. First, to allow liquid retention on over the micropallet arrays, 8-well polystyrene cell culture chamber slides

(LabTek, Nunc, Naperville, IL) were adhered to the surface of the arrays. Poly(dimethylsiloxane) (PDMS) in a viscous liquid form was used as an adhesive to bond the chambers to the arrays by first applying the PDMS to the understand of the chambers and then pressing them to the array surfaces. The arrays were then placed in a 65 ˚C oven for 15 minutes to solidify the PDMS which effectively formed a liquid seal around each chamber. The arrays bearing the chambers were sterilized in 70 % ethanol and left to dry in a sterile environment. Figure 2.3.4 displays the appearance of a completed magnetic micropallet array device ready for use.

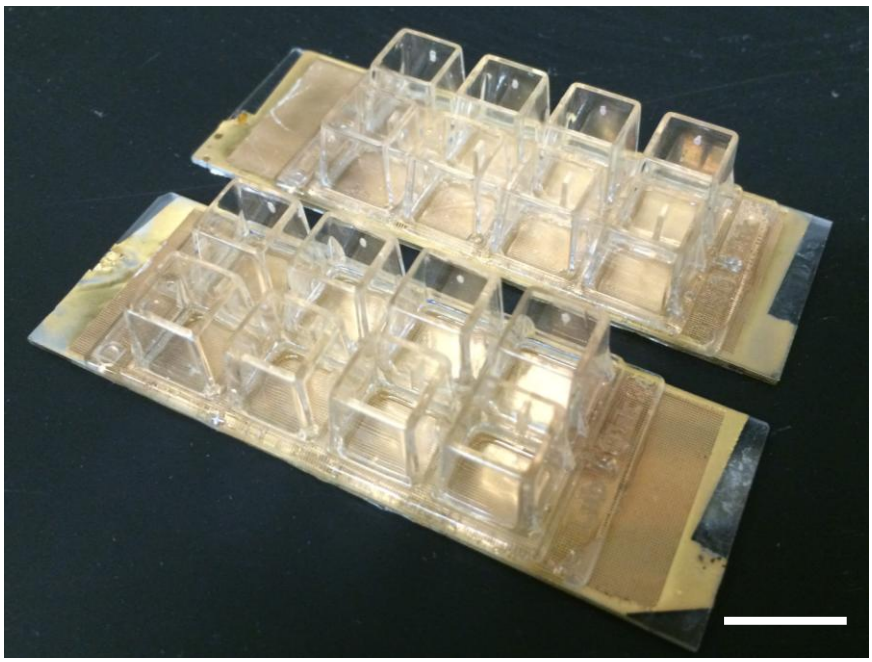

Figure 2.3.4: Completed magnetic micropallet arrays ready for use
Two completed magnetic micropallet arrays with 8-well cell culture chambers are shown. This was the final form of the arrays and were ready for all sample seeding at this point. These devices were sterilized in 70% ethanol and kept in a sterile biosafety cabinet until use. The scale bar is 12.5 mm.

Each cell culture chamber on the slides were filled with a 300 µL solution of human fibronectin at a concentration of 20 mg/mL suspended in filtered double-distilled water (ddH_2O) and incubated for one hour. Any excess fibronectin that did not adhere to the arrays after one hour was displaced and removed with a series of half volume exchanges with fresh ddH_2O. The ddH_2O washes were followed up with further half volume exchanges with 70 % ethanol to break down any fibronectin bridges which may have formed between adjacent micropallets.[82] Ethanol's low surface tension allowed the fluid to easily flow

through gaps between micropallets and displace air trapped in these spaces as well as the core holes, removing any fibronectin which may have settled on top of the air. Ethanol washes following fibronectin seeding were always performed as failure to do so could result in cell motility from pallet to pallet if protein bridges remained on the arrays. Following the ethanol washes, the arrays were completely emptied of their contents and sterilized a final time with an ethanol spray. The magnetic micropallet arrays coated in fibronectin were kept in a sterile environment until cell seeding.

2.3.7 Adherent Cell Culture and Seeding Procedure

Three different adherent cell lines were used to monitor cell growth and interaction with the magnetic micropallet arrays. HeLa, NIH/3T3 and rat208F cells were prepared and cultured following vendor (ATCC) suggestion. Each of the cell types were grown in polystyrene culture flasks incubated at 37°C in 10% CO_2. When the micropallet arrays were completed and ready for use, cells were removed from their growth flasks by trypsin-EDTA digestion (0.25% trypsin; 1mM EDTA) and vigorously pipetted following their removal to ready them as single cell suspensions in conical centrifuge tubes (Falcon, BD Biosciences, San Jose, CA). Collected cell numbers were manually assessed using a standard hemocytometer (Reichert, Buffalo, NY) and viability of the cells was confirmed by Trypan blue stain exclusion.[96] Recovered viable cells were diluted to 1000 cells/mL and one mL was pipetted into the 8-well LabTek slides. To first assess whether cells seeded onto the 1002F pallets fabricated on the gold thin films could be adequately imaged, HeLa and 3T3 cells were plated together within a shared chamber at a 1:1 ratio to test whether morphological differentiation was possible on the microarrays. The micropallet arrays used in this study were fabricated form the mask described in section 2.3.2 without any via holes. The arrays used in this study were also not electroplated. To test the ability for cells to grow on magnetic micropallets, rat208F cells were seeded to the arrays in the same manner as described above and expanded for ten days to form cell colonies. After first seeding the cells, initial cell adhesion was confirmed at three hours after which point the cells were observed in 24 increments and checked for

viability and growth. The cell culture media was completely replaced every 72 hours. Figure 2.3.5 displays the progression of cell seeding to their eventual confluence on the micropallets.

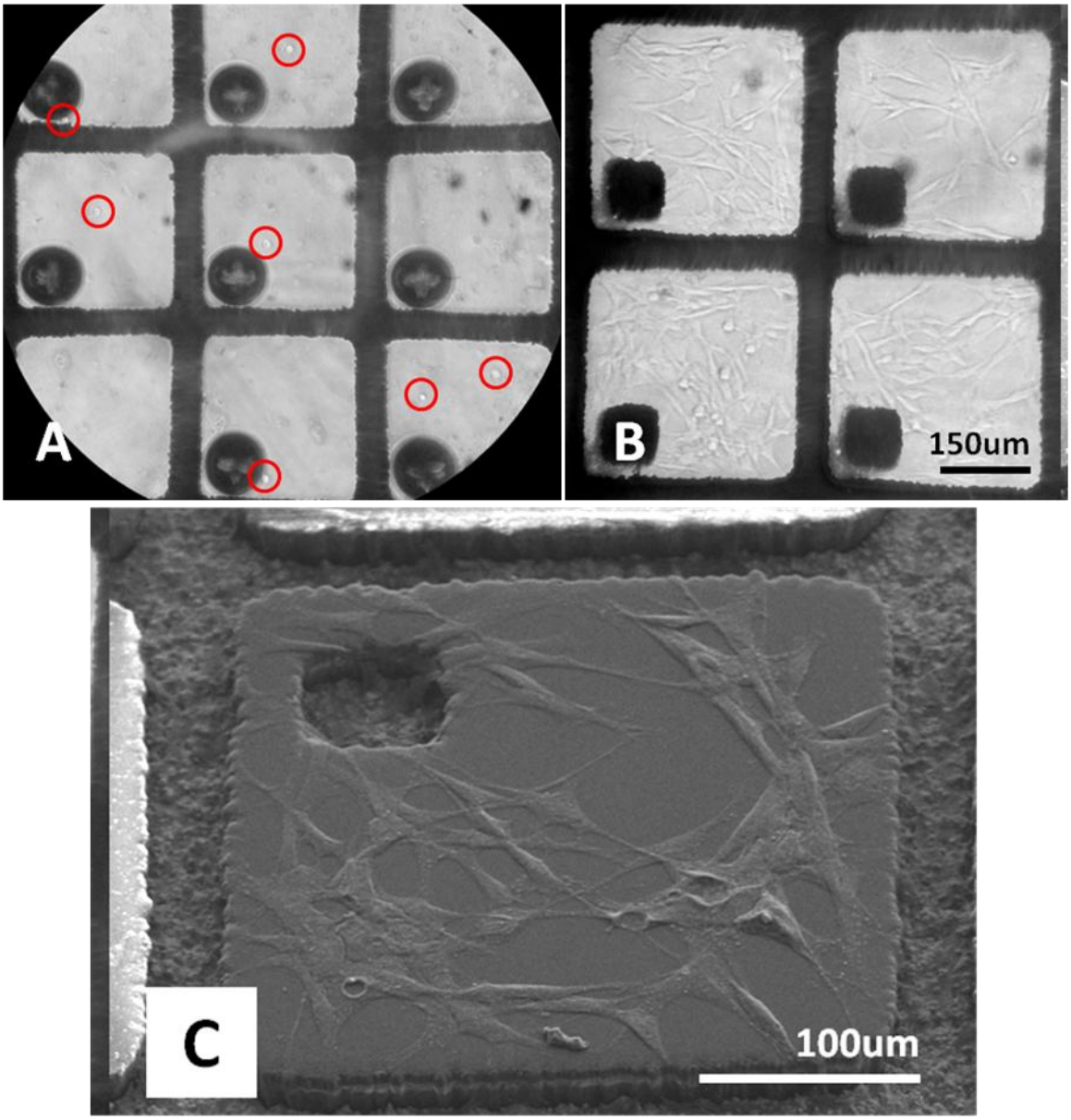

Figure 2.3.5: The capture and growth of cells on magnetic micropallet arrays
A) Cells seeded on micropallets. Individual cells are circled in red. Air bubbles captured within via holes and the borders surrounding the structures constrained cells to the transparent surfaces of the arrays. B) Rat208F cells grown to confluence on micropallets. C) Scanning electron microscope image of an individual micropallet with fixed rat208F cells.

2.3.8 Cell Viability Test

The biocompatibility of magnetic micropallet arrays with and without the final biocompatible gold coating were directly compared to one another. The results formed on the two types of pallets were directly compared to those achieved on a standard micropallet array consisting of 1002F pallets fabricated on glass slides. Each well of the 8-well culture chambers adhered to the arrays were readied for the addition of cells by first adding 300 µL of rat208F culture media. Seven of the eight culture wells were filled with a rat208F cell suspension to a concentration of 1000 cells/mL. After seeding to the arrays, the cells were grown for seven days in an incubator maintained at 37 ˚C with 10% CO_2. A 60 percent media exchange was performed on day three and day six of culture. On the seventh day, a the cells of a single well from each slide were fixed with 2% paraformaldehyde to create a control positive for cell death. To fix the cells, the media of the selected wells was replaced slowly by four half volume exchanges of RPMI 1640 media (Life Technologies, Carlsbad, CA) and finally emptied to a volume of 150 µL. A 150 µL volume of 4% paraformaldehyde was then added to the control wells and the cells were incubated in the fixing solution for 20 minutes. Once the cells were fixed, the paraformaldehyde solution was completely removed and replaced with 300µL of RPMI 1640. The 7 wells of each of the slides had their media replaced with RPMI 1640 solution by four half volume exchanges to a final volume of 300 µL.

The viability of the cells cultured in each of the wells was assessed with a combination of 7-Aminoactinmycin (7AAD) and Annexin V conjugated to CF647 fluorescent dye (Annexin V) (EMD Millipore, Hayward, CA). Annexin V targeted phosphatidylserine, a component of the phospholipid membrane found on cells, which can become exposed on early apoptotic cells. 7AAD will readily fluoresce upon intercalating with DNA, but cannot access the genomic DNA of cells unless their cell membranes are compromised, which is an event that occurs late in the cell death process. By using a combination of two different viability stains, it was possible to assess varying levels of cell health with Annexin V staining cells early in the apoptotic process and 7AAD staining late apoptotic and necrotic cells. Cells from six of the non-fixed wells were exposed to both of the stains at a 2.5% concentration. The fixed wells were also stained in the same manner and the arrays were incubated for 20 minutes

before being inspected. The 8th remaining well on each array slide was left as a negative control for fluorescent emissions and did not have the addition of the stains. The magnetic micropallet arrays with seeded rat208F cells were imaged with an LSM 780 confocal microscope (Carl Zeiss, Oberkochen, Germany) with a two channel setup emitting lasers at 633 nm and 561 nm for Annexin V and 7AAD excitation respectively. The positive cell death controls were imaged first in order to set up the imaging conditions based on fluorescent peak emissions of 670 nm and 650 nm emitting from the stains.

2.3.9 Micropallet Release and Magnetic Collection

An LSM 780 confocal microscope with a paired Ti:sapphire multiphoton laser system (MaiTai, Spectra-Physics, Santa Clara, CA) was used for all cellular evaluations. The multiphoton laser served the purpose of ejected targeted magnetic micropallets by focusing its laser energy at the surface of the gold thin film below a target pallet. The laser's emission wavelength was set to 790 nm which translated to an effective 395 nm wavelength at the focus point of the laser which was then absorbed the gold. During array observation, if a cell colony of interest was located the LSM microscope software, Zen, was used to draw a square region surrounding just the perimeter of the target pallet. This drawn region defined the multiphoton laser irradiation region. While focus height during cell observation was located at the top surface plane of the pallets, laser ejected was an event which took place at the bottom side of the pallets and so that focus height had to be shifted to just below the pallets at the surface of the gold thin film. The ideal focus height for ejection could be repeatedly found for every pallet by imaging for autofluorescent emissions emitted from the glass slide by excitation with a 488 nm observation laser. The focus height had to be accurate or micropallet ejection by the excitation of the gold thin film could not occur. The top side of the gold film below a target pallet was irradiated with the MaiTai laser with an average energy of 88 mJ created by around 8 passes of the laser through the region defined by the Zen software. Previous work has shown that exposing the bottom surfaces of micropallets with highly focused lasers resulted in the formation of localized plasma which in turn would generate an upward force capable of ejecting standard sized micropallets.[76] Although this plasma generation was not capable of ejecting the larger

magnetic micropallets outright, it did lead to partial delamination of random regions of the pallets. This delamination which typically occurred on the outskirts of the pallets allowed for the influx of the surrounding culture media below the pallet. At the same time, the gold thin film heated as it absorbed the laser energy which resulted in the vaporization of the media over the heated gold. Media vaporization created gas microbubbles which formed between the glass film surface and the bottom of the target pallet. As the bubble were formed, they expanded and preferentially rose upward, displacing the remaining sections of the pallets adhered to the glass slide surface and causing them to float upward away. The upward force generated by the bubbles dislodged the pallets, but was not strong enough to cause the adhered cells to disconnect from the pallet. Adjacent pallets were also unaffected by the ejection process. The LIFT process described at the beginning of this chapter has previously proven that laser interaction with metals for the purpose of sample ejection did not show significant detrimental effects on the viability of biological samples. Figure 2.3.6 displays the micropallet ejection process.

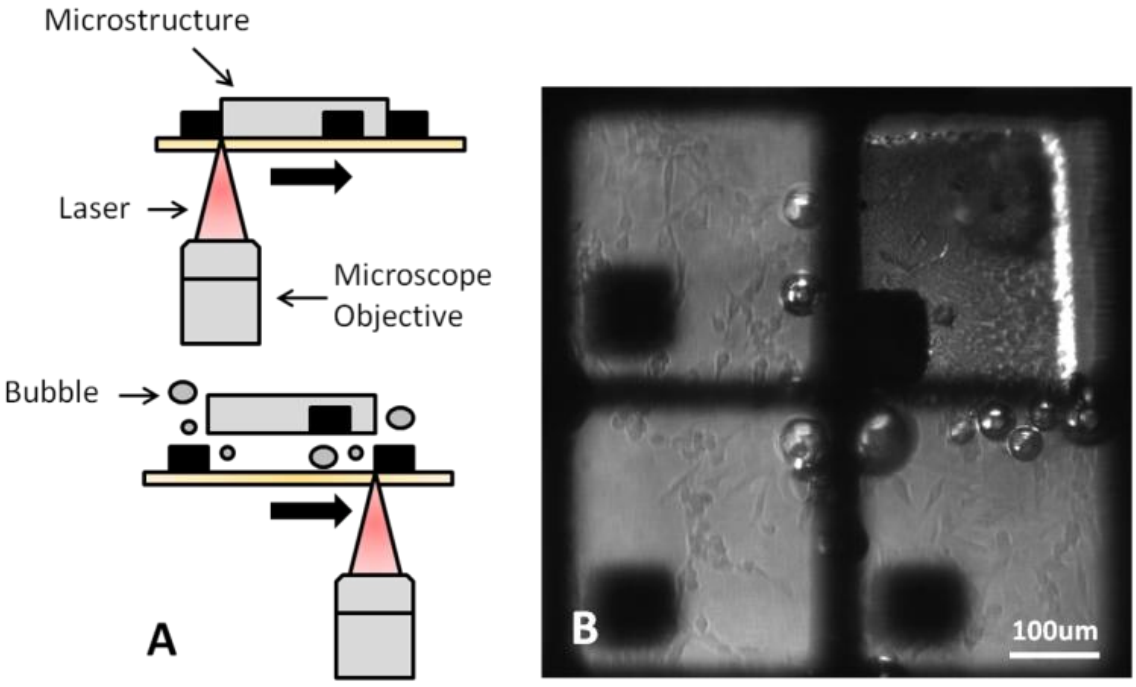

Figure 2.3.6: Ejection of micropallets from gold thin film substrates
A) Schematic of the bubble assisted release of micropallets with a multiphoton laser. B) Image taken with a confocal microscope mid-ejection. Partial release of the structure on the top right of the image can be observed along with the formation of bubbles. Rat208F cells adhered to the surface of surrounding structures were unaffected by the ejection process.

The target pallets that were laser ejected typically settled on top of the surrounding pallets at a distance ranging from 30 µm to 500 µm from the drawn target site. There were, however, instances where the bubble formation caused by the heated gold thin films would generate large, singular bubbles due to the combination of the microbubbles. These large bubbles would continually expand during laser excitation and succeed at pallet ejection, but the pallets would stay adhered to the surface of the bubbles. This even was seemingly random and did not have a negative effect on the collected cell colonies. Appendix A figure 6.1.5 shows an image of a pallet stuck to a large vapor bubble following ejection. In order to collect the released pallets, a 1.5 mm diameter polystyrene probe with a removable neodymium magnet which was previously developed for other magnetic pallet collection protocols was used.[84] First, the probe was sterilized with 70% ethanol and completely dried by air. The probe was then lowered into the culture well with the ejected pallet and the magnetic attraction of the ferromagnetic core caused the ejected pallet to connect to the probe. The pallet was then transferred over to a separate culture plate and the magnet within the collection probe was removed causing the pallet to fall into the well by gravitational forces. Any culture plate could be utilized, but for experiments using these pallets it is suggested that a 96-well culture plate (Falcon, Corning, Tewksbury, MA) be used so that location of the collected pallet is not too time consuming. Large culture wells may make it difficult to find the deposited pallets. The wells were filled with fresh cell culture media in order to promote further growth of the collected cell colonies. Between pallet collections, the probe was washed in sterile ddH_2O to prevent cross contamination from well to well.

2.4 Results and Discussion

2.4.1 Gold Thin Film Characteristics

24 different glass slides coated in gold thin films were assessed to record the average electrical resistance of the slides as a function of distance from an alligator clip. The resistance followed a linear progression with a resistance of 12.4 Ω at a distance of 1 mm from a corner of the slides to 23.8 Ω at a distance of 80 mm. All recorded resistance values were deemed acceptable for electroplating and so no

changes were required of the gold thin film fabrication process. An additional note regarding resistance of the films is that these recorded values only had an impact on the very first electrodeposition step due to additional metal plating drastically lowered the resistance of the slides. As an example, the average recorded resistance over the entirety of the slides was as low as 0.5 Ω following 30 µm thick nickel structure plating.

The optical features of the gold thin film were just as important as the conductivity due to a primary function of the magnetic micropallet arrays being the ability to analyze the physical appearance of cells captured to the pallet surfaces. 20 slides were divided into four groups each prepared with a different level of surface alteration. These groups included five uncoated slides, five glass slides coated with just 50 µm thick 1002F, five slides coated with just gold thin films, and finally five slides coated with gold thin films and then subsequently layered with 50 µm thick 1002F. The average measured light transmission properties of each group is shown in figure 2.4.1.

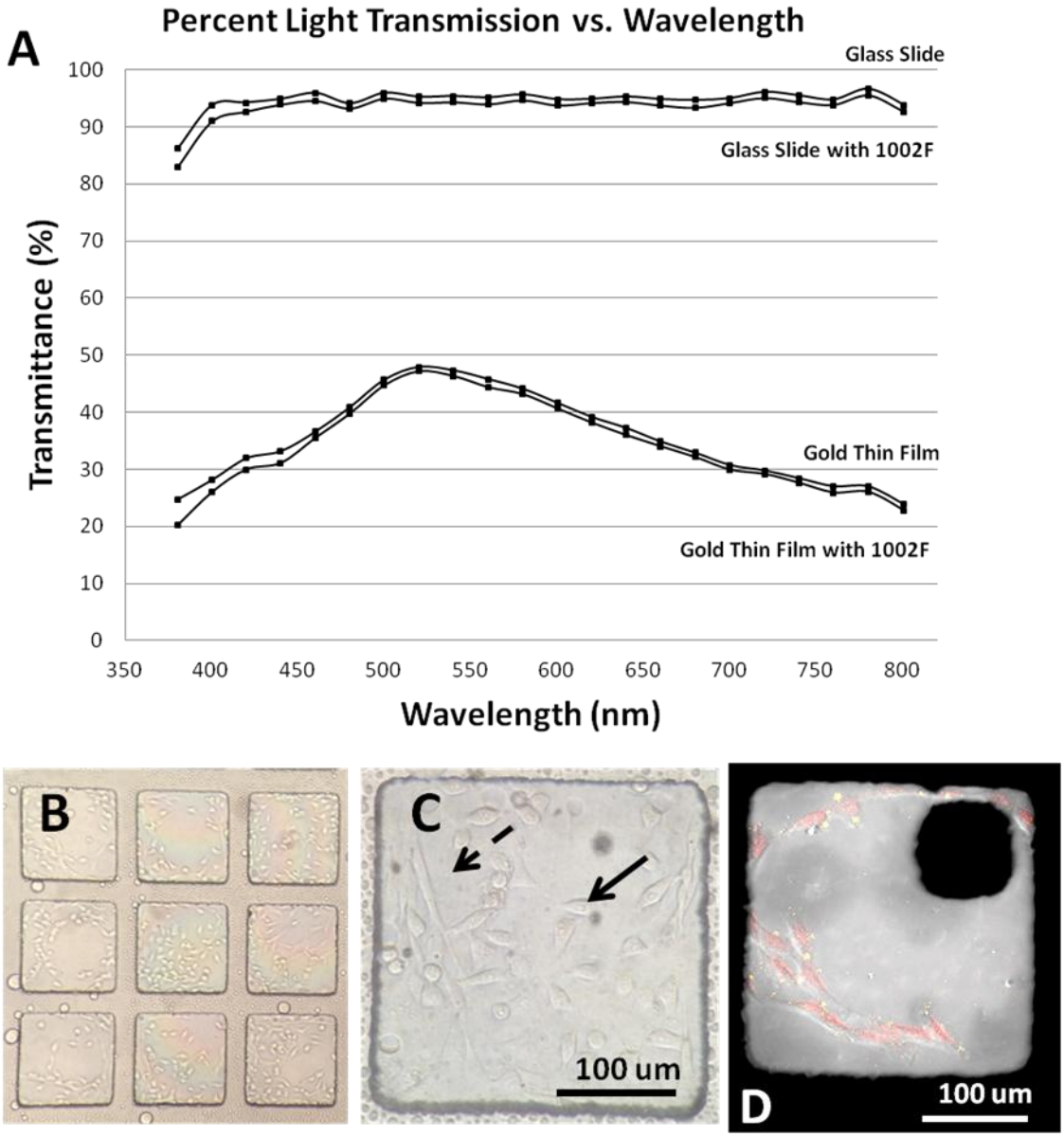

Figure 2.4.1: Light transmission of gold thin films deposited to glass microscope slides
A) Chart comparing transmittance of glass slides, glass slides coated with a 50 µm layer of 1002F photoresist, glass slides coated in a gold thin film, and glass slides coated in a gold thin film with a 50 µm layer of 1002F photoresist to represent the final transmittance properties of the cell colony arrays. B) Image of an array of 1002F micropallets on a gold thin film with cells grown on their surfaces. Each structure is a 270 x 270 µm square with a 50 µm height. C) Individual 270 x 270 x 50 µm micropallets on gold with a mixture of seeded HeLa and NIH 3T3 WT cells. The dotted arrow is pointing to a 3T3 cell and the solid array is pointing to a HeLa cell. D) Magnetic micropallet with 7AAD (red) and Annexin V (yellow) stained rat208F cells.

It was found that micropallet arrays formed on gold thin film coated glass slides definitely exhibited a loss in light transmission when compared to micropallets formed on plain, uncoated glass

slides. This fact was very apparent from the onset of this project as shown in figure 2.3.1. The arrays formed on the gold thin films, however, were still plenty functional as cell colony imaging devices. When cells adhered to the pallets on gold thin films were viewed by standard phase contrast microscopy there were still very clear and differences in cell morphology were still very apparent and distinguishable. While any level of excess absorbance can be detrimental to immunofluorescent imaging of cells, the peak transmittance through the gold films was located within a range of wavelengths which are most commonly used for stain visualization. As an example, the biocompatibility study conducted on the arrays involved 7AAD and Annexin V staining, which had peak fluorescent emissions at 650 nm and 670 nm respectively, were clearly visible. This result suggests that other commonly utilized fluorophores such as FITC should be detectable on the arrays as well. Chapter 3 discussed in detail the use of H2b-mCherry stain which was clearly visible on the arrays as well.

2.4.2 Magnetic Property of Micropallets

Every ferromagnetic core size discussed earlier in the chapter resulted in successful capture of ejected micropallets. The magnetic probe used for pallet collection could capture ejected pallets settled to the surface of the arrays without generating enough force to dislodge pallets untouched by the multiphoton laser thus preventing any unwanted pallet collection. Figure 2.4.2 displays the average measured force response of the three different nickel core structures to the magnetic probe as a function of probe distance to the sample.

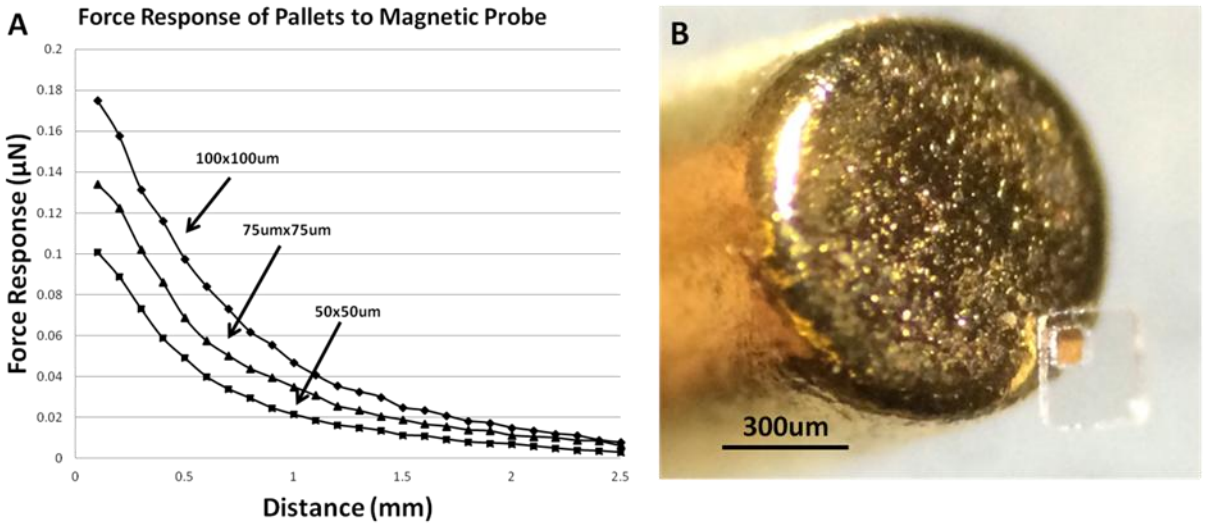

Figure 2.4.2: Magnetic properties of micropallets with ferromagnetic cores
A) Force response of three different ferromagnetic core sizes. B) Individual captured micropallet on a 1 mm diameter neodymium magnet. The magnet was unsheathed (as shown) during micropallet force response experimentation in order to record the maximum force response to the 225 Gauss magnetic field.

The recorded magnetic attraction force of the micropallets was directly related to the distance at which the magnetic probe was able to collect the pallets. The average capture distance for the small, medium, and large cored micropallets was equal to 0.2 mm, 0.5 mm, and 0.6 mm respectively during this study, but could vary depending on subtle differences in the state at which a pallet was captured. For example, if any bubbles that were generated during laser release were left stuck to the pallet after ejection, the pallets would preferentially stay adhered to the bubbles and the probe had to be brought closer for collection. The average collection distance values were most repeatable when the ejected pallets were settled over the surface of other pallets, away from their original position on the arrays. The collected pallets would typically stay connected to the collection probe in an orientation which favored cell colony health by keeping the growth surface of the pallet away from the probe due which the side edges of the pallets making contact instead. When the probe with a retrieved pallet was removed from the cell culture well on the arrays, a droplet of culture media would encompass the pallet and keep the cells wetted during the short transfer procedure as previously shown in a separate work.[84]

2.4.3 Magnetic Micropallet Release and Recovery

The ferromagnetic cores within every micropallet enabled cell colonies that were ejected from the arrays via vapor bubble pallet ejection to be collected by magnetic probe. During ejection, the cores would stay held within their respective released pallet while the larger metal mesh surrounding the pallet remained in contact with the gold thin film below. The vapor bubble ejection event required the magnetic micropallet arrays to be used in liquid environments and was not reproducible during dry testing of the devices. While this limitation was not necessarily important due to the intended use of the devices, it is a limitation nonetheless that is worth noting. Figure 2.4.3 shows the progression of a pallet being ejected with an LSM 780 confocal microscope controlled with Zen software.

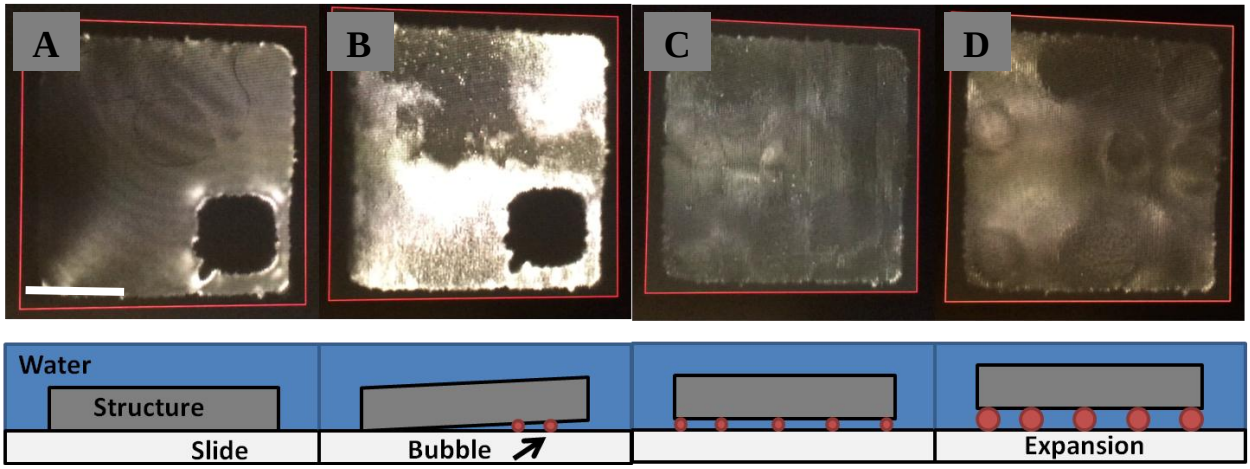

Figure 2.4.3: Absorptive gold layer aided laser release of large pallets using vapor bubbles Time-lapse of the progression of a magnetic micropallet being ejected from the surface of the slide. A) Pallet imaged with a Zeiss LSM 780 confocal microscope before laser irradiation. The scale bar on the bottom left of the image is 100 µm. B) Same pallet after 1 second of irradiation with 2-photon laser. C) After 3 seconds. Bubbles can clearly be seen where the pallet used to reside. The pallet has been pushed up above the focal plane of the microscope and thus can no longer be seen. The disappearance of the black ferromagnetic core indicated successful pallet ejections. D) After 4 seconds. The bubbles become larger and more mobile as the gold surface is continually heated.

Most cell colonies remained adhered to the ejected micropallets immediately following laser release and for the duration of the magnetic probe collection and transfer process. Cell colonies with especially low adhesion strength characteristics could still be retained on the pallets, but extra care had to be taken in order to not shake the cells too much during collection. If cells with weak adhesion strength are the primary target for a work, it is suggested that smaller core sizes are used so that the pallets express

a lower attraction force to collection probes. As an aside, a quick experiment was run along with the cell colony sized micropallets which tested the capabilities of the vapor bubble release system with even bigger pallets than those primarily utilized for this study. Four separate sized pallet arrays composed of square pallets with dimensions of 200 µm by 200 µm, 300 µm by 300 µm, 400 µm by 400 µm and 500 µm by 500 µm were fabricated over the surface of gold thin film coated glass slides. Each pallet size was successfully ejected via laser generated vapor bubble formation with greater than 90% success rate (n = 30 for each pallet size). The successful release of larger pallets using this method has the potential to enable different types of biological research requiring larger scale pallets such as those opting to sort for microscopic animals typically larger than cell colonies. The laser energy required for larger pallet release has yet to be optimized, however, and if larger pallet release is sought then more experiments will be required. As for the standard pallets of 270 µm by 270 µm primarily used for cell colony collection, vapor bubble ejection resulted in a 95.1% success rate with n = 60 pallet ejections. Figure 2.4.4 shows a pallet following ejection hovering over surrounding pallets as well as an SEM image of an ejection site after release. Although these early results showed great promise, there were some confounding issues that would occur on occasion from poor fabrication. It was mentioned earlier that overplating of the metal structures in and surrounding the pallets would cause impossible to release pallets. Another issue that could occur was the over use of PDMS during cell culture chamber adhesion to the pallet surfaces. With too much, or too low a viscosity, the PDMS would flow into the gaps between pallets and add an extra securing force. The pallets surrounded by excess PDMS could still be ejected, but magnetic recovery of the pallets would be hindered by lingering PDMS meshes holding the pallet down. Overall, the high success rate of pallet ejections was a great sign for use of the magnetic micropallet arrays for cell colony sorting as the previous standard release system was primarily optimized for releasing pallts with dimensions smaller than 200 µm by 200 µm.[76]

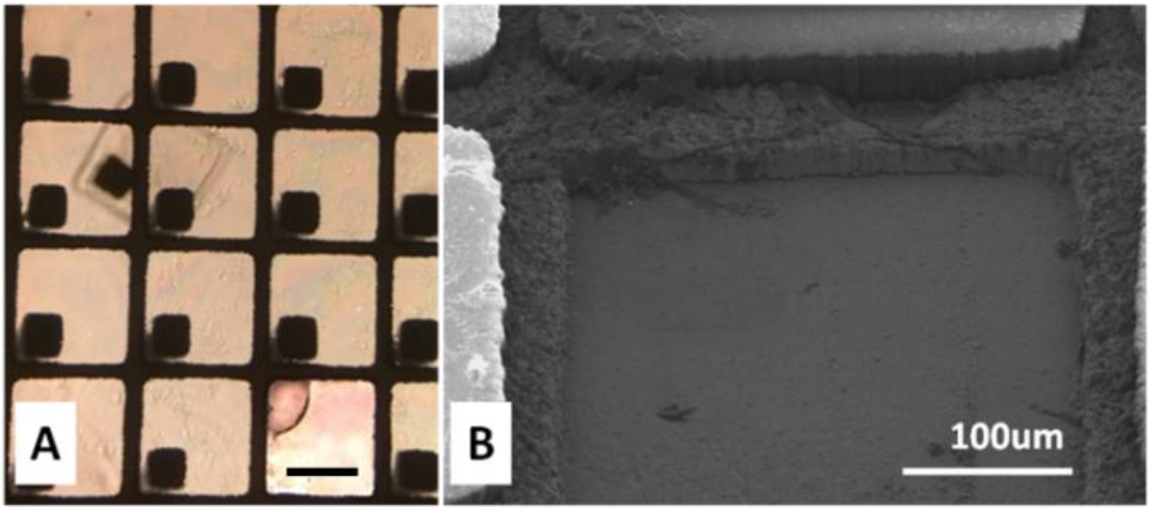

Figure 2.4.4: Released micropallet with adhered cell colony
A) Phase contrast image of a released magnetic micropallet resting on top of surrounding structures. The structure's original location can be observed on the bottom right of the image. The scale bar is 200 µm and located on the image at the site of the released pallet. B) Scanning electron microscope image of the pallet ejection site. The metal walls which previously surrounded the structure are maintained during the ejection process.

2.4.4 Cell Viability and Growth

The viability of cells grown on the magnetic micropallet arrays was significantly affected by the presence of the gold layers surrounding the ferromagnetic nickel structures. The pallets with only the nickel plating showed losses in the viability of the cells adhered to the pallets as expressed by both 7AAD and Annexin V signals present on the arrays. For the purpose of this study, any cells that were expressing one or both of the stains were considered to have lost their viability on the arrays. With an n = 1410 observed cells on the arrays, 9.9% of the cells were found to be unviable which equated to a 90.1% viability rate after seven days of growth. There was no trend related to the cell growth proximity to the nickel structures. An even distribution of compromised cells was found over the entirety of the pallets including the innermost areas of the 1002F away from the edges and cores. Cells that were grown concurrently on magnetic micropallet arrays with gold coated nickel structures maintained a 99.9% viability with an n = 1563 which reflected the viability results obtained on standard micropallet arrays fabricated on plain glass microscope slides with n = 1521.

The cellular viability immediately following multiphoton laser enabled vapor bubble ejection was also tested by using a Trypan blue exclusion test immediately following laser release of colonies.[96] HeLa cells that were cultured on the arrays for one week to an average colony size of 35 individual cells were 93% viable immediately following release and collection in a 1:1 solution of Trypan blue stain in 1x phosphate buffered saline (PBS). NIH/3T3 cells were tested in the same manner as the HeLa cells and exhibited 84% viability. Both cell types were tested with n = 5 pallets ejected and immersed in the Trypan test solution.

Equally important to the viability of individual cells grown on the arrays and collected after ejection was the capacity for the collected cell to expand into full grown cell lines post transfer. Using the methods described in section 2.3.9, individual targeted cell colonies of rat208F cells were collected from the gold coated magnetic micropallet arrays and transferred to a 96 well culture plate with wells filled with 300 µL of fresh culture media. A sample size of n = 20 rat208F colonies were collected from the arrays and grown for a span of two weeks with total media changes every three days. Every single collected cell colony grew to confluence within the wells which boded well for the success of future colony selection experiments to come. Figure 2.4.5 shows a progression of rat208F cell colony growth seeded to a micropallet over a span of 7 days.

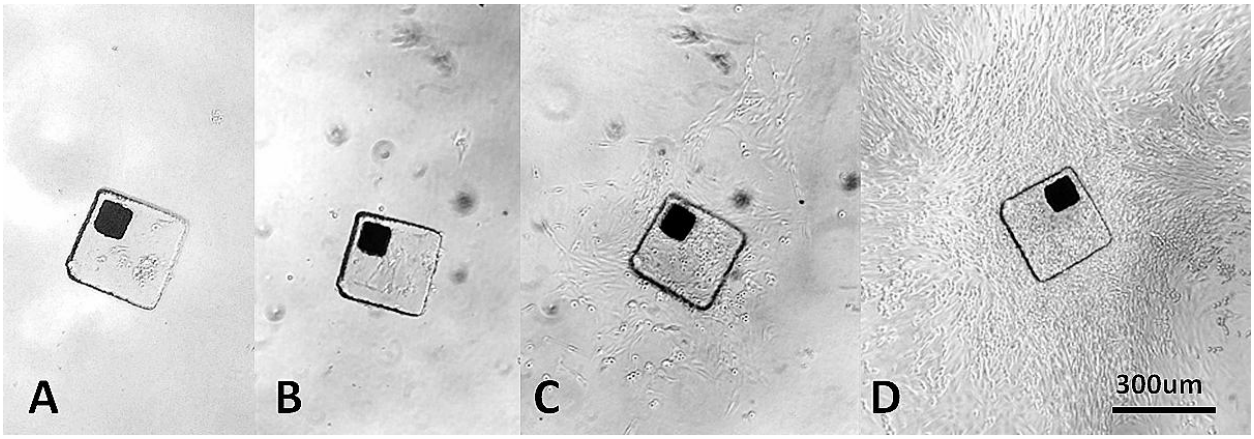

Figure 2.4.5: Growth of a rat208F cell colony captured to a magnetic micropallet
A) 3 Hours, B) 24 hours, C) 72 hours, D) 152 hours. The cells were facing down towards the bottom of the polystyrene culture well when initially seeded. The ferromagnetic core within the structure is 75 by 75 µm.

2.5 Chapter 2 Conclusion

This chapter discussed the invention, fabrication, and testing of a brand new type of micropallet array specifically designed for cell colony sorting. A new type of pallet ejection modality was achieved through the use of gold thin films patterned onto glass slides below large area micropallet arrays. The gold layers could be heated by using a highly focused multiphoton laser which in turn generated vapor bubbles between the gold and the above pallets which forced the pallets to release from the array. Vapor bubble ejection enabled the consistent and reliable release of micropallet structures ranging from 200 µm by 200 µm to 500 µm by 500 µm which was previously shown to be difficult using standard ejection methods. The conductive qualities of the gold layer also enabled the first use of electroplating techniques applied to the fabrication of micropallet arrays. Electroplating was used to create magnetically responsive micropallets with ferromagnetic cores created within via holes that were patterned into each individual pallet. This inclusion of the core allowed for unhindered cell imaging through the transparent 1002F pallets while still allowing magnetic manipulation of released structures for downstream assays.

The large area magnetic micropallet arrays were shown to be biocompatible and capable of supporting cell growth over extended periods of time for the purpose of cell colony formation. Three different adherent cell types including HeLa, NIH/3T3, and rat208F cells were tested on the arrays and each line was able to successfully grow while sequestered on the arrays and expanded after transfer to separate culture wells. Use of the arrays resulted in minimal loss in cell viability showing that the addition of the gold coated nickel structures was not detrimental to cell retention. Each of the cell types also stayed sequestered throughout their colony expansion on the arrays which meant that the final colonies had spawned only from the cells that were originally seeded to their corresponding pallet at the start of a study. This result showed that the magnetic micropallet arrays had the potential to be used as cell sorting tools designed for clonal expansion of single cells differentiated based on both their single cell morphologies as well as their final morphologies once cell colonies were grown which could reveal additional details of specific cell behavior. The work accomplished in this chapter laid a foundation for future work with the arrays more focused on specific, impactful biological work.

Chapter 3: Highly Efficient Purification of Transfected Cells on Magnetic Micropallet Arrays

3.1 Introduction

The previous chapter described the creation of a novel micropallet sorting platform capable of cell colony sorting with the added benefit of simplified magnetic collection of released cell colonies. While it was proven that the technology could benefit cell sorting research, it was necessary to further examine the utility of the technology. It was important to prove that actual, useful biological sorting procedures could be performed using the large area magnetic micropallet array. Furthermore, for the arrays to be found particularly useful, it had to be shown that there was an added benefit to using the micropallet arrays as opposed to simply following standard guidelines for cell colony sorting. This chapter focuses on two specific types of cell sorting procedures which are regularly performed in biology and examines the improvements made to the procedure with the increased ability for cell selection specification during collection as well as the enhanced speed enabled by use of the magnetic micropallet arrays. The first primary sorting procedure involved the purification of cells transfected with a fluorescent nuclear stain and the second was the purification of virally transformed cells based on morphological differentiation from the remaining untransformed cells. The work described in this chapter was made possible by the help of Trisha Westerhoff of the Nelson lab.

3.1.1 Purification of transfected cells on magnetic micropallet arrays

The transfection of cells with foreign DNA is a common practice in modern biology and has become an important tool for understanding the specific cellular functions that the expression of certain genes control.[97, 98] By inserting predefined segments of DNA into cells, researchers have been able to make direct connections between protein expression and the resulting cellular functionality in transfected cells. In a similar manner, researchers have also been able to shut off certain protein expression and observe changes resulting from the gene shut-off. Both types of analysis are key to gaining a better

understanding of how cellular function is controlled by their DNA. One standard use of cellular transfection is the generation of stably transfected cell lines composed entirely of cells expressing the specific genomic alteration desired by a researcher. Stably transfected cells exhibit intentionally introduced, predictive behaviors which are important controls used in cellular analysis experiments. With DNA transfection, researchers have been able to establish several new cell lines with extremely desirable features that would otherwise not exist in naturally occurring wild type cells. Some examples of the usage of transfected cell lines include specific protein over-production and cultivation, immunofluorescent imaging and analysis of cells and cellular functions, and the study of cancer behavior by the transformation of cells.[99] Although there are many different types of methods for transfecting cells with equally varying levels of success,[100-102] there is always the need for a series of purification steps in order to completely remove the population of cells that failed to take in and integrate the foreign DNA sequences. Cell line purification typically requires cells to endure survival pressure oftentimes generated by inserting some form of cell-lethal antibiotic resistance along with the target DNA sequence and culturing the cells in media containing that antibiotic. By doing so, over time only cells that have successfully been transfected with the DNA, and thus the antibiotic resistance, will continue to grow while the cells that were not successfully transfected are killed by the cytotoxic media. Another type of cell sorting procedure that is commonly used is the focus forming assay for cancerous cell transformation studies.[65] Focus forming assays rely on the ability for cancerous cells to continue to expand even under conditions that would otherwise result in contact inhibition and cell quiescence. As a sample of partially transformed cells grow on a culture surface, they eventually reach confluence and limit the growth of the wild type cells. The transformed cells, however, continue to grow in the vertical direction on top of the surrounding cells and form colony foci. Researchers then locate these foci and locally extract the transformed cells to be expanded in a separate culture. Although the aim of this protocol is to only collect transformed cells, due to the tightly packed growth of the cells, many untransformed cells end up being collected along with those that are cancerous, limiting the purity of those that were collected. The focus forming assay must then be performed again with the new population of cells to continually lower the

total number of untransformed cells. In these instances, survival pressure brought on by artificially introduced antibiotic resistance may not be possible as may cancerous transformation studies aim to study preexisting retro viral DNA found naturally in the world. Radioactive cell transformation research also negates the possibility of including such resistances as DNA is not introduced at all in these instances.

While the process of establishing stably transfected cell lines is well understood and commonly practiced, there is a need to develop methods to expedite the procedure. As it currently stands, cell line purification requires the repeated growth and passage of cells as the non-transfected and transiently transfected cells get weeded out of the population. This can be quite time consuming and outcomes may be constrained due to several factors relating to potential changes in cell growth characteristics caused as secondary changes resulting from the foreign DNA integration. Due to the transfected and non-transfected cells sharing the same growth space, competition over the available nutrients and surface area of the culture flask may limit the rate of expansion of the desired cell populations especially if successfully transfected cells have any kind of hindered robustness when compared to the untransformed counterparts. Slow growth of the target cell populations further lowers the rate at which purification can be achieved. Cell purification procedures performed using the magnetic micropallet arrays described in chapter 2 (henceforth referred to as Ferrocore micropallet arrays) solved many of the issues associated with the standard process. The most obvious improvement that was generated by the use of the Ferrocore micropallet arrays was that they provided individualized growth regions for every single cell seeded to the arrays. Due to each pallet being separated by a relatively large gap, when single cells were sequestered to pallet surfaces, the cells were able to grow and expand over the surface of their pallets without competition from other cell lines. The wide gaps between pallets also successful prevented most cells from branching to adjacent pallets with the exception of some cancerous cells with extremely low adherence strength. Without competition, even cells with low growth rates had ample chance of expanding to full colonies for extraction from the arrays without losing out to the faster growing cells in the same seeded cell population. Another benefit of using the Ferrocore arrays was the ability to assess individual cell colonies without visual interference from other uninteresting cells. When growing cells on

shared substrates, a common issue that occurs is crowding of different cell types with one another. With single cell colony sequestering, however, visualizing each colony was quick and simple. Finally, the greatest benefit to using the arrays over standard purification procedures was the ability to extract target cell colonies with no fear of retrieving unwanted cells in the process. In this way, it was possible to directly go from heterogeneous sample populations seeded to the arrays to completely pure and separated cell colonies with different genetic and phenotypic features in one collection step. Figure 3.1.1 is a visual representation of the differences in cell procedures performed on micropallet arrays from standard ones.

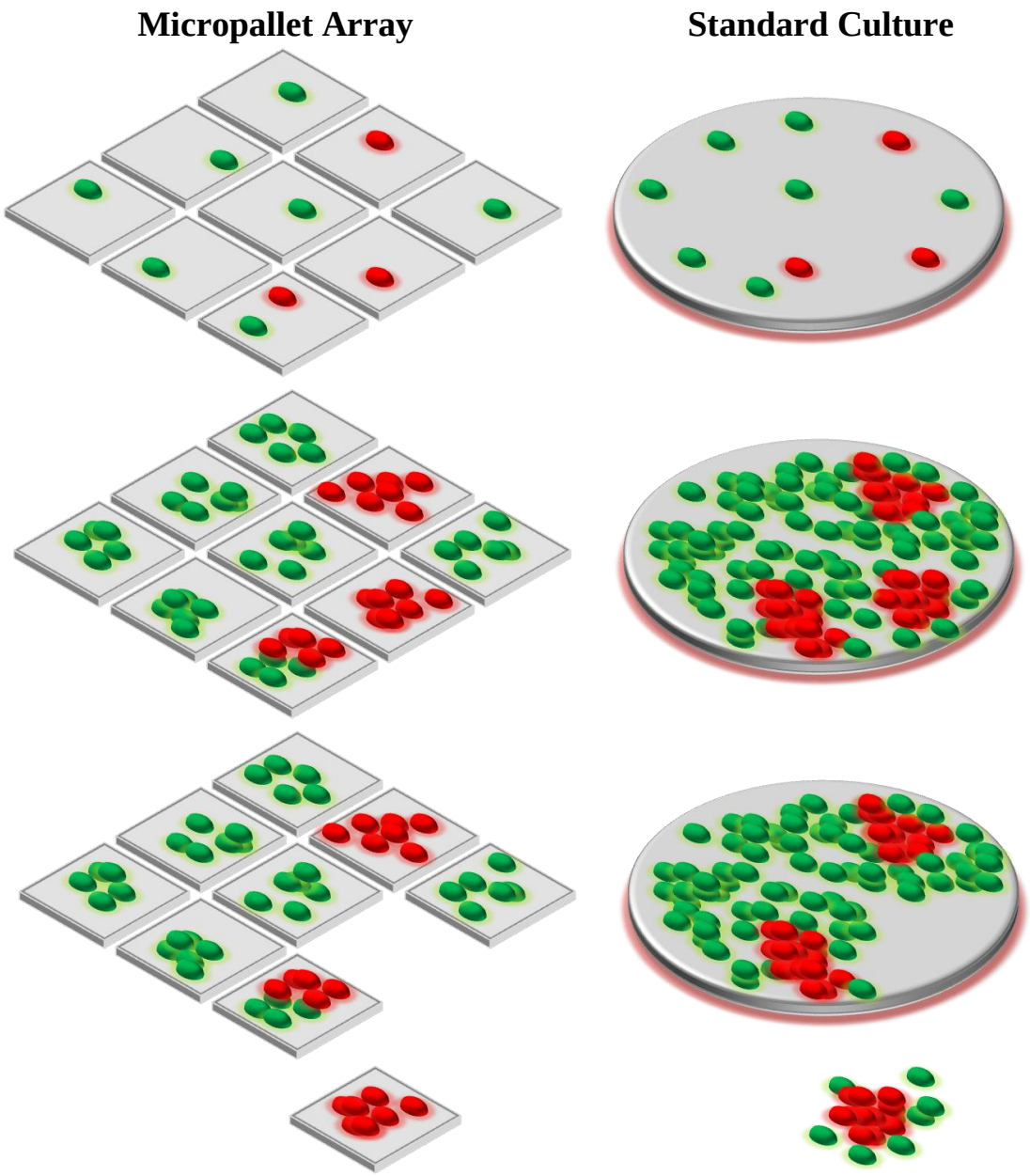

Figure 3.1.1: Cell purification workflow on micropallet arrays vs. standard culture dishes
This schematic represents the differences in work flow when comparing cell purification procedures performed with micropallet arrays (left column) versus standard methods utilizing shared culture dishes (right column) for cell growth. The small oval shapes represent biological cells with the two different colors (green, red) signifying different cell lines with red representing those of interest. Micropallet arrays enabled individual cell sequestering upon sample seeding to the arrays. These single cells would then expand to form clonal colonies formed from the single cells. Individual micropallets with cells of interest could easily be identified and collected for further expansion without unwanted cells. Cells seeded to standard culture dishes are forced to compete for space and crowd one another. This crowding may make target cell identification impossible depending on the type of cell that is sought for a particular study. When cells are collected from shared dishes, unwanted cell collection is unavoidable and further purification work is required to establish clonal cell lines.

3.2 Fabrication of Ferrocore Micropallet Arrays

Large area magnetic micropallet arrays fabrication for cell purification procedures was very similar to the process described in section 2.4.2 and the reader is suggested to look at that section for specific component vendor information and granular process details. This section details improvements made to the technology through design and fabrication to improve on their utility. First, higher quality photomasks were utilized in order to generate sharper microstructures, enhancing the overall visual appeal of the micropallets. Second, in order to better track single cell colonies from the beginning of experimentation to the end, different regions of the micropallet arrays were uniquely demarcated to distinguish them from one another. Third, a technique for roughening the surfaces of the micropallets was included in fabrication to improve cellular adherence strength to the arrays. Fourth and finally, a new method of creating liquid barriers in the gap spaces between pallets was established to replace the need for silanizing the arrays.

3.2.1 Demarcated micropallet arrays for improved cell tracking

In the same manner as described in section 2.4.2, 200 Å thick translucent gold absorptive films were plated to standard 1 in. by 3 in. glass microscope slides with e-beam vapor deposition. Micropallet arrays consisting of square microstructures with dimensions of 250 μm (w) by 250 μm (l) by 50 μm (h) were photolithographically fabricated from biocompatible, transparent 1002F photoresist onto the surface of the gold thin films.[79] The pallets were separated from one another by 50 μm gaps. A high resolution photomask was purchased from CAD / Art Services, Inc. (Bandon, OR) and used to pattern the arrays. Using the higher quality mask than the ones used for the original creation of the magnetic micropallet arrays resulted in the formation of very clean cut structures which were much more reflective of the features designed on the mask. The new masks also enabled the creation of smaller structural features than the previous set of masks. Every micropallet structure was fabricated in such a way as to form a single 60 μm by 60 μm square through hole located in a single corner region of the pallets. These through holes exposed the gold thin film layer through the pallets and enabled the electroformation of

ferromagnetic cores in each structure. Micropallet arrays composed of pallets with ferromagnetic cores will henceforth be referred to as Ferrocore micropallet arrays.

As a newly included fabrication step, different regions of the Ferrocore micropallet arrays were demarcated to visually differentiate 5 by 5 sections of pallets from one another. A marking system created by including notches on the sides of pallets was established on the arrays by designing the pallets to have individual 15 μm by 15 μm squares missing from the sides opposite to the ferromagnetic core region. The location of the notches along the pallet edges as well as the combination of which notches were included on a pallet varied from region to region and enabled simpler tracking of specific sections of the arrays during studies. A secondary marking scheme involving the inclusion of numbers on micropallets was also explored. Instead of taking up more cell growth surface area on the Ferrocore micropallets to draw the numbers, the through holes themselves were drawn as numbers with 50 μm wide "lines". The lines expanded through the entirety of the pallets in the same manner as the regular square through holes in order to expose the conductive gold layer below. The magnetic strength tests conducted in chapter 2 already verified that any ferromagnetic core size larger than 50 μm by 50 μm would generate sufficient magnetic attraction strength to carry pallets to the magnetic probe used for collection. Figure 3.2.1 displays both types of completed Ferrocore micropallets.

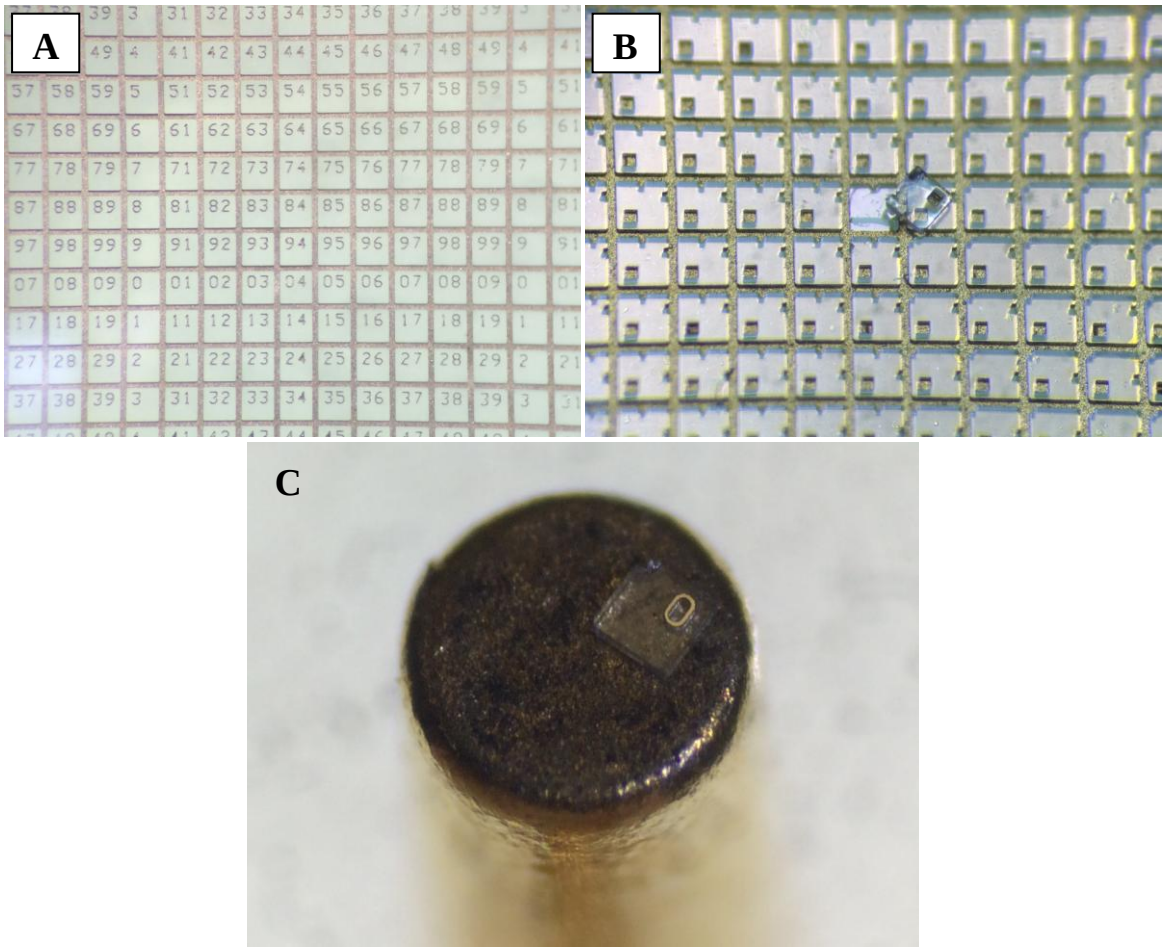

Figure 3.2.1: Ferrocore micropallet arrays with demarcation for easy identification
A) Ferrocore array demarcated with numbers to distinguish between regions of pallets. The numbers were plated with 50 µm wide lines making up the font. All micropallets shown in this figure are 250 µm by 250 µm. B) A second type of demarcated array using notches located at the sides of the pallets. The notched marking system was used for all experimentation in this section. A dislodged pallet is shown in the middle to show how the ferromagnetic cores are retained within ejected pallets. C) Ejected pallet marked with the number zero electroformed into the number shaped hole. An interesting note is that without the metal, the center of the zero would not have stayed joined to the pallet. This displays the adhesion strength of the metal within the pallets.

As seen in the above image, the demarcated Ferrocore micropallet structures were electroplated to form gold coated structures on all exposed gold thin film surfaces. The plating process is thoroughly described in section 2.4.4. One improvement that was made to the plating process was a change in the way that liquid was initially introduced into the hard-to-plate core regions of the pallets. Previously, sonication was utilized to displace air bubbles from within the cores in order to ensure that plating solution could enter those regions during plating. Without the sonication, many of the core regions of the

pallets were left unplated due to the air bubbles preventing plating solution penetration. It was discovered empirically that an equally effective and much simpler method for core filling was to simply flush liquid over the surface of the pallets with a rushing faucet of deionized water (diH_2O). Before plating, every Ferrocore array was roughly washed with the faucet before plating solution immersion. All other methods were maintained from the previous chapter. The ideal metal plating thickness ranged from 25 μm to 35 μm. Thinner electroplating resulted in Ferrocore arrays with lower energy requirements for laser assisted pallet release, but also were more likely to have the cores pop out from the micropallets during collection. The thicker plated arrays, on the other hand, had near zero chance of having the cores come out of the pallets due to the higher surface area of contact within the pallets, but also required greater laser energy to release. In general, it was better to aim for thinner ferromagnet plating as high laser irradiation during pallet ejection risked loss in cell viability.

3.2.2 Pallet roughening for better protein and cell adhesion

In order to improve on cell interactions with the Ferrocore micropallet arrays, a pallet surface roughening technique was integrated into the fabrication process. The first iteration of the arrays described in chapter 2 kept pallet surfaces unaltered as there has been much success with single cell sorting without the need for physical changes to normal 1002F surface topography. While the very robust cell lines used in the previous chapter, including HeLa and NIH/3T3 cells, had no problem growing on the Ferrocore arrays, other groups have shown that some specialized cell colony types greatly benefit from roughened pallets.[103] For the Ferrocore micropallets to be better ready for diverse cellular study, it was necessary to establish a repeatable process for surface roughening for cell lines less robust than the typical model cells. A different group has already established a well researched roughening technique specifically designed for 1002F photoresist.[104]The work described in this paper were adapted for use with the Ferrocore arrays.

Alumina particles (Al_2O_3) sized at 1-2 μm were purchased from Atlantic Equipment Engineers (Upper Saddle River, NJ) and mixed at a 1:1 ratio with diH_2O to form a slurry solution. 5 mL of the slurry

was then placed onto a flat surface, such as a smoothed aluminum foil sheet, to form a 4 in. by 4 in. circular region. To roughen the Ferrocore pallet surfaces, arrays were flipped face down onto the slurry and rotated in a figure eight pattern fifty times while force was applied uniformly on the back side of the slide. The slides were then washed in an alternating sequence of diH_2O and 70% ethanol three times. Once washed the slides were left in a sterile environment to completely dry. The roughened Ferrocore micropallet arrays had a slight loss in image clarity when observed by phase contrast microscopy, but adhered cells were still adequately visible and morphological differentiation of cells could be made. The decision of whether or not to roughen the pallet surfaces was decided by the needs of the specific types of cells that were to be sorted on the arrays and will be discussed later on in this chapter. Figure 3.2.2 shows a comparison between unroughened pallets and roughened pallets when viewed with an inverted microscope.

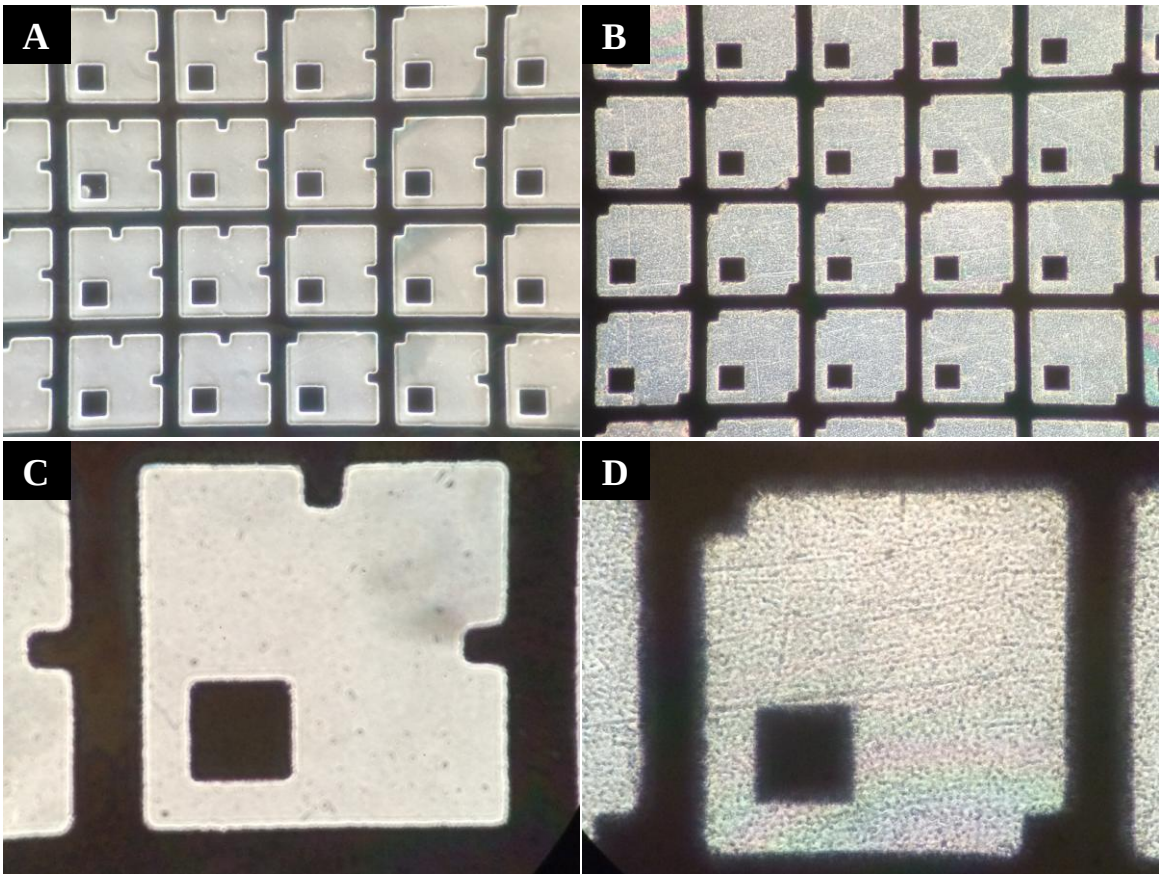

Figure 3.2.2: Ferrocore micropallet arrays before and after surface roughening
A) Ferrocore micropallet array before surface roughening with a slurry of 1 µm alumina particles. Individual micropallets are 250 µm by 250 µm. B) Same array as in image A after roughening procedure. C) Zoomed in image of single pallet before roughening. D) Single pallet after roughening. A combination of elongated scratches and dimples created by the roughening led to a higher surface area on the pallets for cell adhesion.

3.2.3. Formation of liquid barriers with high density Fluorinert

Up to this point, most if not all variations of the micropallet array technology has relied on the formation of virtual air walls to keep seeded cells from falling into the gap regions surrounding pallet structures.[80] In order to create virtual air walls, the arrays must be silanized to alter the surface chemistry of the pallet gaps to be hydrophobic. While effective for most array types, the ability for virtual walls to sequester cells on the Ferrocore arrays was inconsistent due to the differences that would arise from batch to batch when electroplating the arrays. Depending on the final thickness of the gold coated ferromagnet layer as well as the topography of the top surfaces of the structures, virtual air wall stability

ranged from being perfectly normal to absolutely ineffective. Because electroplating has an enormous number of factors that lead to the final result, it was decided that a more consistent form of micropallet wall formation was necessary. Attempting to use different materials to form walls aiding pallet sequestering is not new and a study involving the use of poly(ethylene glycol) (PEG) to form barriers between micropallets has been published.[81] While effective for wall formation, PEG patterning on the arrays requires an extra fabrication step and would be cumbersome to include to an already elongated process for Ferrocore array creation. Previous promising work in the Bachman lab explored the use of high density liquids to form temporary walls during cell seeding. Early work showed that a fluorinated liquid with a density near two times that of water could be used to form walls over the gaps of the micropallet arrays when placed in wells before cell culture media is added. This idea was taken and successfully expanded upon to be used with the Ferrocore micropallets.

The concept of using liquid barriers for Ferrocore arrays is quite straight forward. Any biocompatible fluid with a density great enough to stay separated below added culture media would theoretically be able to form walls during cell seeding for sequestering purposes. For this study, a previously tested fluid, Fluorinert FC43 (3M, Saint Paul, MN) was selected for wall formation. The fluid, typically used for coolant purposes, had a liquid density of 1860 kg / m^3. Water's density, for reference, is 1000 kg / m^3, nearly half that of the FC43. Althoughs it was previously found that the FC43 could be used to form barriers on micropallets, the biocompatibility of the fluid was not explored. To quickly test for cytotoxicity, a mixing experiment involving small concentrations of FC43 introduced into cell cultures was performed. Due to only an extremely minute amount of FC43 being required to form walls between the pallets, the FC43 concentration levels tested only consisted of 0%, 0.5%, 1%, and 1.5% by volume. Three different adherent cell lines of HeLa, rat208F, and NIH/3T3 were cultured at low densities in their respective medias with the various concentrations of FC43 mixed in for 7 days. On the 7th day, the cell media was replaced with a solution of Trypan blue mixed with PBS at a 1:1 ratio in order to perform an exclusion test to observe their viability.[96] It was found that all cell types at every concentration retained above 99.9% viability with negligible differences between the different concentrations. It was thus

concluded that FC43 could safely be used for liquid wall formation. This study did not include concentrations higher than those listed above and so it cannot be concluded that FC43 Fluorinert as a whole is biocompatible, but that at such low concentrations it does not have a noticeable effect on cell health. For this study, however, the tested concentration levels of the liquid were more than adequate and the viability results were promising.

Liquid walls made up of the Fluorinert FC43 were formed just before all cell seeding procedures conducted on the Ferrocore micropallet arrays. For arrays fitted with 8-well Labtek chambers, a 0.5 µL droplet of FC43 was placed in the middle of each chamber and allowed to spread through the gaps between the pallets. Due to its low viscosity, the liquid quickly flowed through all of the gaps between the pallets. The array slide was tilted back and forth to make sure than any excess FC43 left on the top surfaces of the pallets fell into the gaps. 500 µL of cell culture media was then immediately added over the FC43 in each well to prevent the barriers from evaporating. Finally, cells were added to the wells and to seed to the micropallets. All volumes were doubled if 4-well chambers were being used. Figure 3.2.3 is a schematic representing the procedure for liquid wall formation.

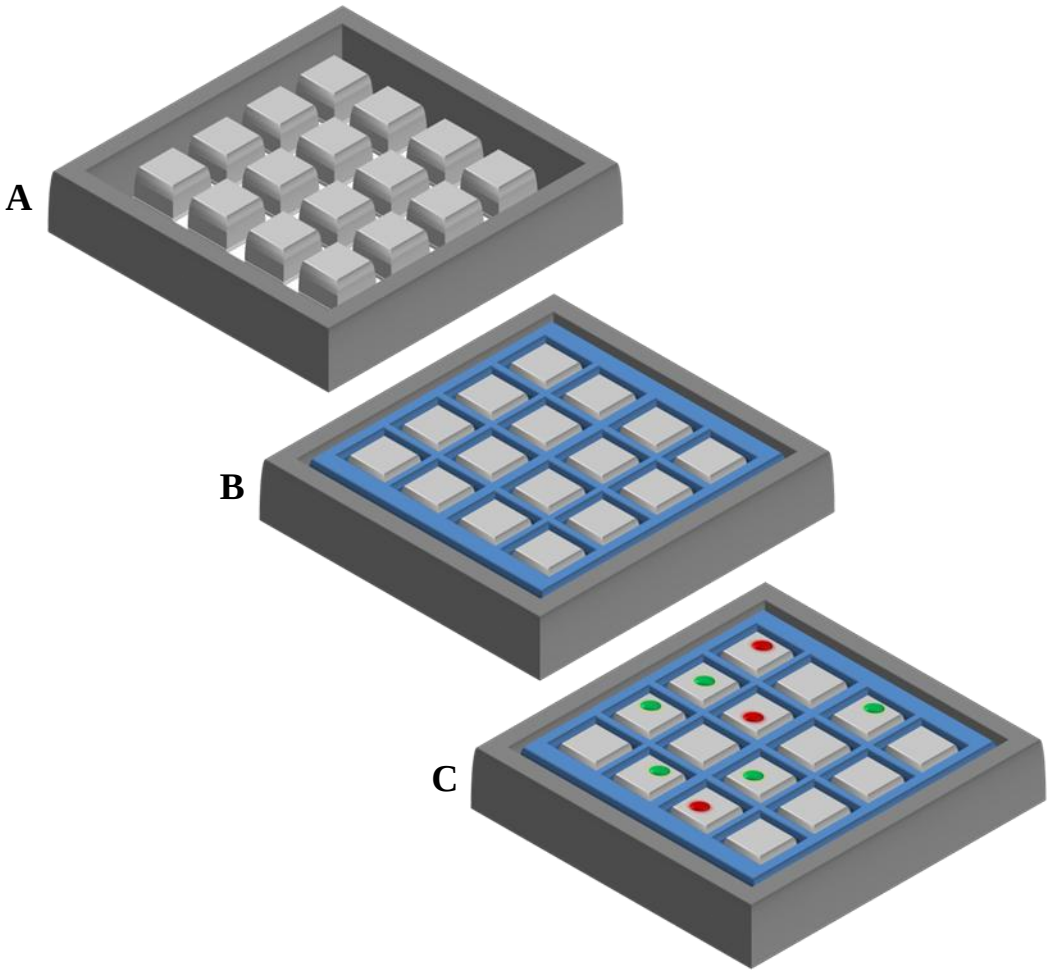

Figure 3.2.3: Formation of liquid barriers for cell sequestering on micropallet arrays
A) Schematic representation of a micropallet array surrounded by a culture chamber. B) Liquid walls were created with high density Fluorinert FC43 which rushed in between pallets when dropped into the culture well. The liquid formed physical barriers to stop cells from falling between the pallets. C) Representation of cells being sequestered to pallet surfaces after seeding. Fluorinert barriers would typically remain in the solution until cell culture media exchanges were conducted or until evaporated.

The formation of liquid walls using FC43 Fluorinert was an effective means of sequestering cells to the top surfaces of the Ferrocore micropallet arrays. Although a quantitative analysis was not conducted, every cellular sorting procedure described in this chapter utilized the formation of these walls and so confidence is high for this process due to tangible results being obtained. Liquid wall formation negated the need for the time consuming silanization procedure. Furthermore, the quality of silanization can diminish over time and micropallet arrays are sometimes made months in advance as experiments are being conceived. By using the liquid wall formation, there was no worry of any aspect of the completed

arrays deteriorating during storage. Although FC43 is quite volatile, when kept in air tight containers the shelf life is long and so a single purchase of a large volume can last a very long time.

3.3 Cell Preparation for Experimentation

The main goal of this work was to show that two primary cell purification procedures relying on the identification of unique, outstanding traits exhibited by cells of interest could be performed on the Ferrocore micropallet arrays. Rat 208F cells acquired from the labs of Dr. Hung Fan (University of California, Irvine, Irvine, CA) were selected as a model adherent cell line to be transfected for the experiments performed in this section. A second set of adherent cells including wild type NIH/3T3 cells and two different lines of transfected 3T3 cells gifted from Dr. Fan were also tested with the Ferrocore arrays in order to analyze the technology's consistency and efficiency with varied cell types.

All materials used for the cellular research such as chemicals, cell culture reagents, and disposables were purchased from Fisher Scientific (Pittsburg, PA) unless otherwise noted. The wild type cells were cultured according to ATCC suggestion until transfection. The Ferrocore design consisting of notched markings were used for all cellular work described in this section for consistency.

3.3.1 Rat208F transfection plasmid preparation

Both wild type rat208F cells and NIH/3T3 cells were transfected with two different plasmids to form a total of six cell types, including wild type cells, grown on the Ferrocore arrays. Rat208F cells were transfected using a Fugene6 transfection reagent (Roche Diagnostics, Indianapolis, IN) in order to generate H2b-mCherry (Addgene, Cambridge, MA) expression to represent cell purification based on fluorescent signal detection. A second cell line was established from rat208F cells using a Jaagsiekte retro virus sequence with an additional fluorescent marker,[105, 106] JSRV-ENV-FLAG obtained as a gift from Dr. Fan. These cells were transformed with the intent of performing purification studies by identifying morphological differences between transformed and wild type rat208F cells.

To transfect the cells with the desired DNA sequences, transfection plasmids were prepared ahead of time. Plasmids with the JSRV-ENV-FLAG sequence were transfected into E. coli DH5α for propagation of the plasmid using previously established protocols. Briefly, 10 ng of JSRV ENV-FLAG was added to a purchased solution of E. Coli DH5α in 50 µL transformation tubes (Falcon #2054, BD Biosciences, San Jose, CA) and incubated on ice for 30 minutes. The E. Coli cells were then heat-shocked using a 42 ˚C water bath for 1 minute and once again returned to ice for 2 minutes. SOC media warmed to 37 ˚C was added to the transformed cells to a 1 mL total volume and incubated at 37 ˚C while mixing constantly at 200 RPM for a total of 1 hour. This time span was necessary to allow the E. Coli cells to express the antibiotic resistance written into the JSRV-ENV-FLAG plasmid. After the hour incubation, 100 µL of the cell solution was added to an LB agar plate supplemented with 100 µg / mL of ampicillin to purify the samples. Single surviving colonies of E. coli transformed with JSRV-ENV-FLAG were inoculated in a 5 mL volume of fresh Luria Broth (LBroth) supplemented with 100 µg / mL ampicillin and grown as pure starter cultures for 8 hours at 37 ˚C with constant mixing at 200 RPM. Cell cultures that survived this second purification step were then used to inoculate individual 250 mL cultures overnight using a 1:1000 dilution of the original culture in the Lbroth with ampicillin. Plasmid DNA from the cultures maintained overnight were isolated using a Qiafilter midiprep plasmid purification kit (Qiagen, Valencia, CA) according to the manufacturer's suggestions.

Purified samples of the plasmids were quantified with a nanodrop ND-1000 Aspectrophotometer (ThermoScientific, Waltham, MA), with the JSRV-ENV-FLAG sequence verified with restriction enzyme digestion visualization with agarose gel electrophoresis. In this instance, the restriction enzyme *Ncol* was utilized. This enzyme double digested the JSRV-ENV-FLAG plasmids to DNA bands of 2.1 and 4.1 Kb in length. The plasmid digestion was accomplished by following the manufacturer's instructions and applying them to 1 µg of plasmid DNA. A 1.2% agarose gel purchased from SeaKem LE (Lonza, Allendale, NJ) in 1X TAE buffer was prepared and cooled to 60 ˚C and supplemented with 0.5 µg / mL ethidium bromide before being cast. The 1X TAE running buffer was also supplemented with ethidium bromide. 0.25 ng of *Ncol* digested JSRV-ENV-FLAG DNA was mixed with loading buffer

(bromophenol blue, xylene cyanol FF in glycerol) to a 1X concentration and then loaded into a gel lane. Undigested JSRV-ENV-FLAG plasmid was prepared as well and loaded onto the gel as a control. The gel was then run at 70 V excitation for 3 hours on ice and then visualized with UV light with a gel imaging station (Biorad, Hercules, CA).

A second type of plasmid was purified in order to generate samples ready for H2b-mCherry transfection. E. Coli DH550α transformed with H2b-mCherry plasmid gifted from Robert Beneza (Addgene plasmid #20972) was grown in LBroth with 100 µg / mL ampicillin and processed in the same way as described above. Once purified, the finalized plasmids were quantified using a nanodrop ND-1000 spectrophotometer. The H2b-mCherry sequence was digested with 2 separate restriction enzymes. *Aatll* was first used to digest the sequence at 5 discreet locations to form 5.78, 0.37, 0.19, 0.08, and 0.05 Kb length sequences. The longest DNA band could be visualized with gel electrophoresis. *Xbal* was also used to digest the mCherry sequence at a single size which linearized the complete plasmid and allowed it to be used as a control. Both the purified H2b-mCherry plasmids and JSRV-ENV-FLAG plasmids were stored at -20 ˚C until use.

3.3.2 Rat208F and NIH/3T3 cell transfection

Wild type rat208F and NIH/3T3 cells were both transfected to form two more separate cell lines from each. To transfect the rat208F cells with either the previously prepared H2b-mCherry plasmids or the JSRV-ENV-FLAG plasmids, 100,000 cells were first seeded into each well of a 6-well culture dish. After being given 24 hours to settle, the rat208F cell culture media (DMEM supplemented with 10% fetal bovine serum, 4.5 g/L glucose, 2 mM L-glutamine, 1 mM sodium pyruvate, and 100 U / mL penicillin 100 µg / mL streptomycin (Mediatech, Manassas, VA)) was replaced with the same media without the added antibiotics to 2 mL per well. Fugene6 (Promega, Madison, WI) was used to transfect the cells as according to the manufacturer's instructions. In short, 200 µL of OptiMEM media (Lifetechnologies, Carlsbad, CA) was mixed into 16 µL of the Fugene6 solution in an eppendorf tube and incubated at room temperature for 5 minutes. For H2b-mCherry transfection, 2.5 µg of the plasmid was mixed into the

Fugene6 solution in an OptiMEM tube and incubated for 15 minutes at room temperature and finally placed into a single well of a 6-well culture dish with the cells to be transfected. The same step was used for JSRV-ENV-FLAG plasmid but with only 4 µg of the plasmid being deposited. 24 hours after the cells were introduced to the plasmids, the culture media was removed and replaced with fresh media once again mixed with penicillin / streptomycin. After an additional 48 hours, the cell cultures transfected with H2b-mCherry plasmid were mixed with 600 µg / mL of G418 antibiotic in order to establish a positive selection survival pressure. JSRV-ENV-FLAG transfected cells did not require a survival pressure step due to it not being likely for cancerous cells, such as those properly transformed by Jaagsiekte retro virus, are unlikely to be outcompeted by untransformed cells.

Successful rat208F transfection was confirmed by fluorescent confocal microscopy as well as flow cytometry targeting nuclear mCherry expression. Positive JSRV-ENV-FLAG expression was also quantified by confocal microscopy and flow cytometry by immunofluorescent staining directed at the FLAG tag included in the plasmid. In the case of the JSRV transfection, the successfully transfected cells could also be distinguished from wild type cells based on their morphological features representing an oncogenic transformation. Figure 3.3.1 shows examples of successfully transfected rat208F cells from both populations.

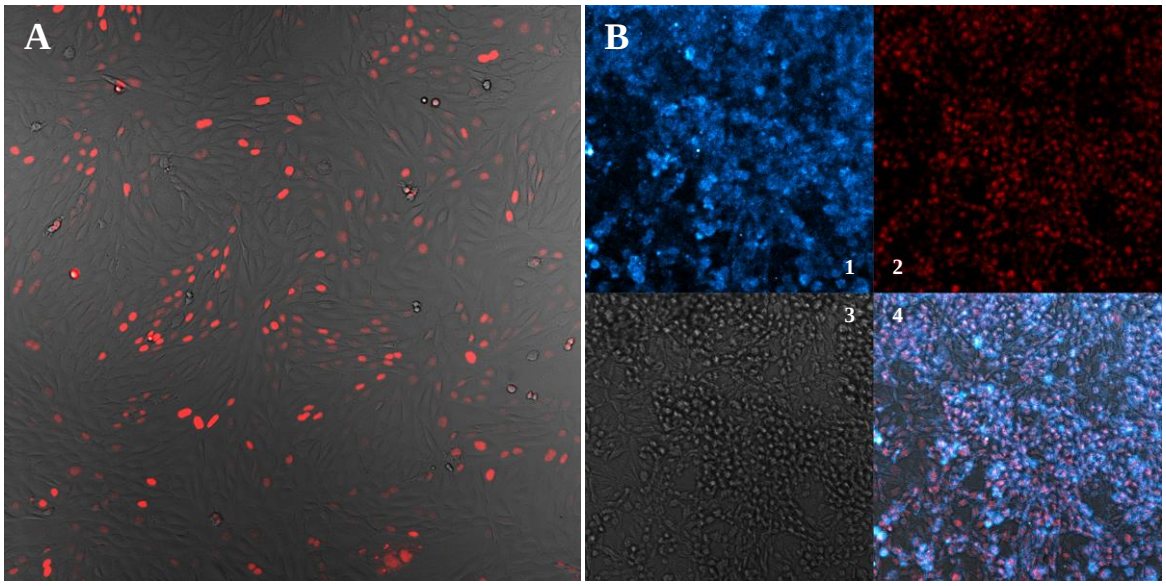

Figure 3.3.1: Rat208F cells transfected with H2b-mCherry and JSRV-ENV-FLAG
A) Mixture of wild type rat208F cells with those transfected with H2b-mCherry. Cells that were transfected properly can be seen expressing the red stain after being excited by a 561 nm laser. The morphology of the transfected cells closely resembled that of the wild type cells although it was empirically found that they exhibited slower growth rates. B) Stably transfected JSRV-ENV-FLAG rat 208F cells. Image 1 displays the FLAG tag expression. Image 2 displays a sytox red non-specific stain. Image 3 imaged the cells with all fluorescent signal shut off displaying just the morphology of the cells. Image 4 shows the combination of all images. JSRV-ENV-FLAG transformed cells had a much faster growth rate than wild type rat208F cells and also did not exhibit contact inhibition when confluence was reached. The cells also preferentially balled together at high numbers. Wild type rat208F cells preferentially stretched over the surface of their growth substrates and would not ball together.

In addition to rat208F cells, NIH/3T3 cell transfection procedures were also performed to enhance the total number of cell types tested on Ferrocore micropallet arrays. The first cell line was generated by infected NIH/3T3 cells with the FrKP strain of murine leukemia virus (MuLV) which transfected the cells with plasmid 8065-2/*. The second cell line was created by infected wild type cells with the Akv strain of MuLV with 8065-2/* plasmid which would in addition express a modified Glyco-Gag protein found in Moloney MuLV. These cells were received as stably transfected cell lines from Dr. Hung Fan. Both cell lines were cultured in standard NIH/3T3 media (DMEM supplemented with 10% bovine calf serum, 2 mM L-glutamine, 1 mM sodium pyruvate, 1X non-essential amino acid mixture, and 100 U / mL penicillin with 100 µg / mL streptomycin) with an added 25 µg / mL of zeocin for positive selective pressure. Although the two cell lines were visually identical when observed through confocal

microscopy, the line transfected with the FrKP strain grew at a much slower rate than those created with the Akv strain and were found to be less robust overall. Figure 3.3.2 shows FrkP and Akv transformed NIH/3T3 cells grown in culture flasks.

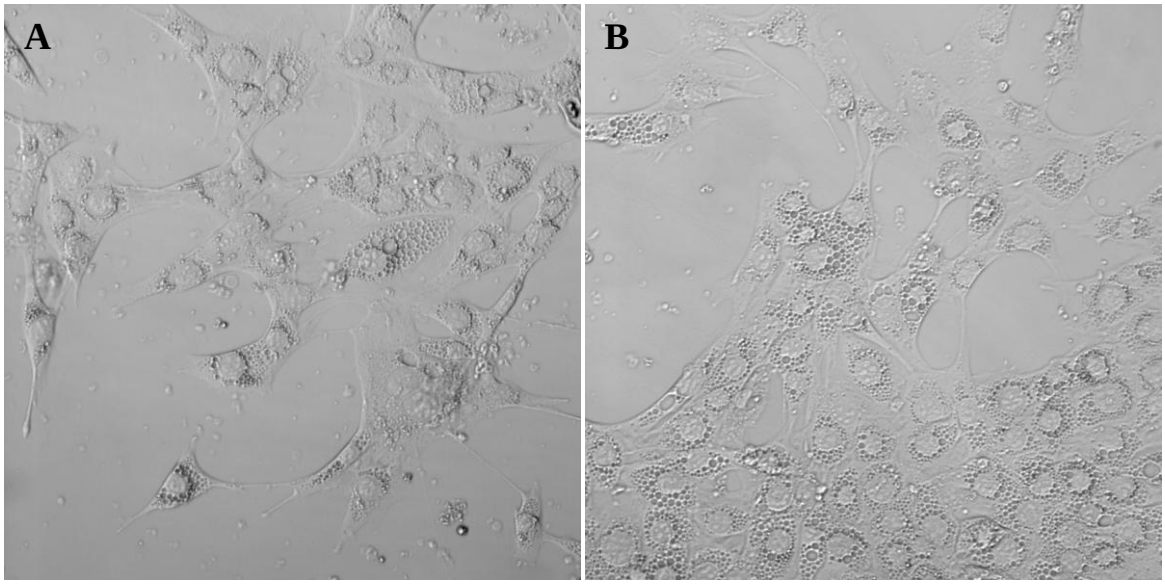

Figure 3.3.2: NIH/3T3 cell variations by transfection with murine leukemia virus
A) 3T3 cells stably transfected with FrKP strain. B) 3T3 cells stably transfected with Akv strain. FrKP transformed cell morphology was similar to the Akv transformed cells, but had a much slower growth rate. Both cell types exhibited high amounts of vesicle production as can be seen in the images as bubbles within the cell cytoplam. Both cell types were cultured in 3T3 media spiked with Zeocin antibiotic to maintain purity.

3.4 Purification of Transformed Cells on Ferrocore Micropallet Arrays

Two separate transfected rat 208F cell cultures were prepared alongside two cultures generated from NIH/3T3 cells and maintained as described in section 3.3. All six cultures (including the wild type lines of each parental cell) were used to test the utility of the Ferrocore micropallet arrays. As mentioned in section 3.1, cell purification after transfection procedures is a necessary, yet very time consuming and labor intensive process in its current form. The goal of this section was to show that purification procedures could be expedited using the Ferrocore arrays.

3.4.1 Cell seeding to Ferrocore micropallet arrays

Ferrocore micropallet arrays mounted with 8-well Labtek chambers were prepared as described in section 3.2. Rat208F cells transfected with mCherry (RmCherry cells for short) were cultured in rat208F media spiked with G418 antibiotic at 37 ˚C with 10% CO_2 until ready for use. The cells were not allowed to grow to confluence before use in order to limit the number of cells in a state of quiescence which could occur if the cells were too tightly packed within their culture flask. The RmCherry cells were removed from their culture by replacing the media with a solution of trypsin-EDTA solution (0.25% trypsin; 1mM EDTA) for five minutes. The cells were then vigorously pipetted to form a single cell suspension and resuspended in fresh media. The cells were then counted manually using a hemocytometer (Reichert, Buffalo, NY). In order to best achieve single cell seeding to the Ferrocore pallets, the total number of cells placed in each Labtek well equaled 1/3 of the number of pallets within each of the wells. For the 8-well Labtek chambers this translated to 250 cells / well. By seeding the cells in this way, the sample was completely random and thus each of the wells would theoretically be filled with a percentage RmCherry cells reflecting that recorded by flow cytometry before the start of the Ferrocore pallet experiment. In this case, the first experiment had 30% RmCherry cells and the second had 8%. For purification of rat208F cells transfected with JSRV-ENV-FLAG, the stably transfected cell were mixed with wild type cells at a 5% total cell concentration. For NIH/3T3 variants, the cells that were used were already stably transfected and were cultured primarily to test for the viability of the cells through the entire purification process. Once the cells were seeded to the arrays, they were left to grow for seven days with a 60% media change at 72 hours and at 144 hours. After one week of culture, the cells were imaged with a confocal microscope system in order to identify cells of interest grown on the arrays.

3.4.2 Purification of rat208F cells transfected with H2b-mCherry plasmid

Rat208F cells transfected to express the H2b-mCherry nuclear stain were prepared following the process highlighted in the previous section. Two purification procedures were performed on the Ferrocore arrays. The first utilized the transformed cells one month after the initial transfection was conducted.

These rat208F cells were found to express around 30% mCherry with flow cytometry before being seeded to the arrays. When the second purification was performed two weeks later, it was thought that the cells would be expressing the same, if not more mCherry, but in fact when quantified by flow the number of cells with stable mCherry had dropped to near 8%. Although this result was puzzling at the time, the lower transfected value actually benefited the study in terms of allowing for a potentially larger impact if purification successes came from extremely low concentrations of desired cells. With both mCherry transfected populations the same procedure was used to purify the cells.

On day seven, the Ferrocore arrays were viewed using the same LSM 780 microscope with attached 2-photon laser described in section 2.5.3. To excite immunofluorescent emissions from the RmCherry cells, the confocal microscope was set to emit a laser at 561 nm at 6% the total power. The 6% power level was selected by initially scanning the arrays at higher than ideal power until fluorescent signal from cells was observed. The power levels were then reduced to a balanced setting where fluorescent emissions were still bright, but there was little to no background noise caused by overexposure. RmCherry emissions signals were used to check the purity of each cell colony grown on the arrays. Pure colonies were defined as those that were adhered to the surface of a pallet with no cells without signal mixed within them. Figure 3.4.1 displays one example of a pure RmCherry cell colony grown on a Ferrocore micropallet as well as an example of an non-pure colony.

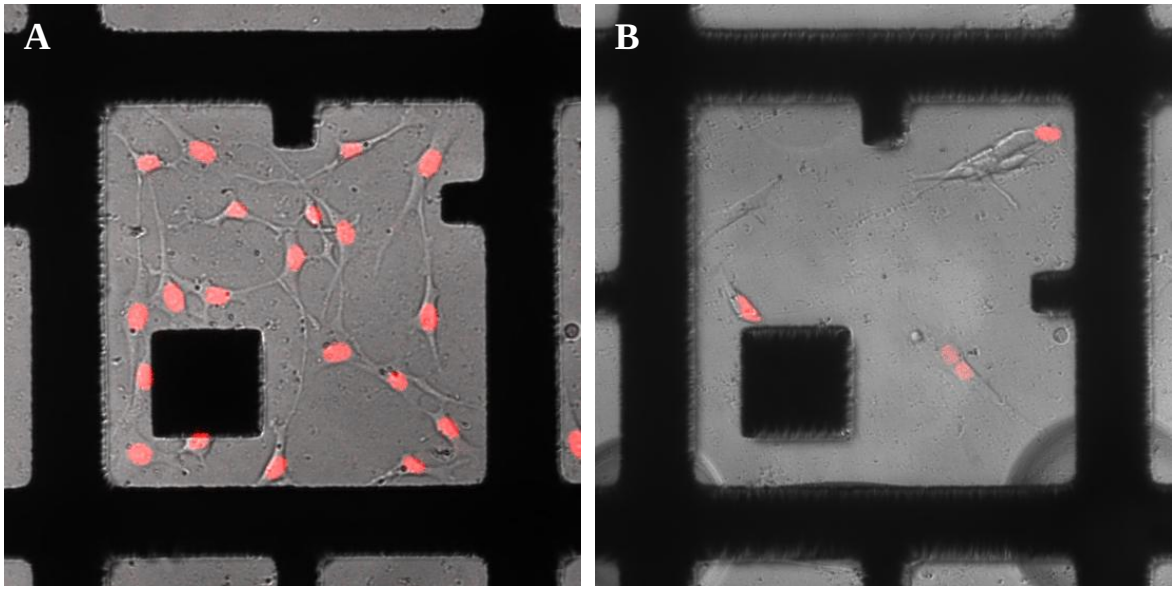

Figure 3.4.1: Pure colony of rat208F cells transfected with H2b-mCherry on micropallet
A) A pure colony of rat208F cells transfected with H2b-mCherry stain were grown on the surface of a ferrocore micropallet. This image was taken seven days after a heterogeneous population of cells were seeded to the array as single cells. This particular sample consisted of 30% successfully transfected rat208F cells, but pure colonies were also located in samples with a positive concentration as low as 8%. The pallet is 250 µm in length and width. B) An example of a non-pure cell colony growing on a ferrocore pallet. Although these pallets bore some transfected cells, they were avoided during collection as the final colony grown from such a pallet would not be a pure cell line.

Once a pure colony was located, the pallet bearing the colony was ejected from the array with the 2-photon laser as described earlier in section 2.4.9. The collected colonies were transferred via magnetic probe to individual wells of a 48 well plate filled with a 1:1 ratio of conditioned RmCherry media and fresh RmCherry media. The collected pallets were observed with the LSM 780 microscope at two distinct time points, 24 hours and one week after the collection, in order to verify that colonies considered pure when retrieved from the arrays were still pure after prolonged growth in their new cultures. Several colonies that were observed to be a mix of RmCherry cells and cells with no fluorescent emissions were also collected along with colonies with no emissions at all in order to provide negative control examples displaying how cells would look if not properly purified. Figure 3.4.2 shows the progression of RmCherry cells seeded to the Ferrocore arrays as single cells to after the cells had been collected and grown for two weeks in a 48 well culture dish.

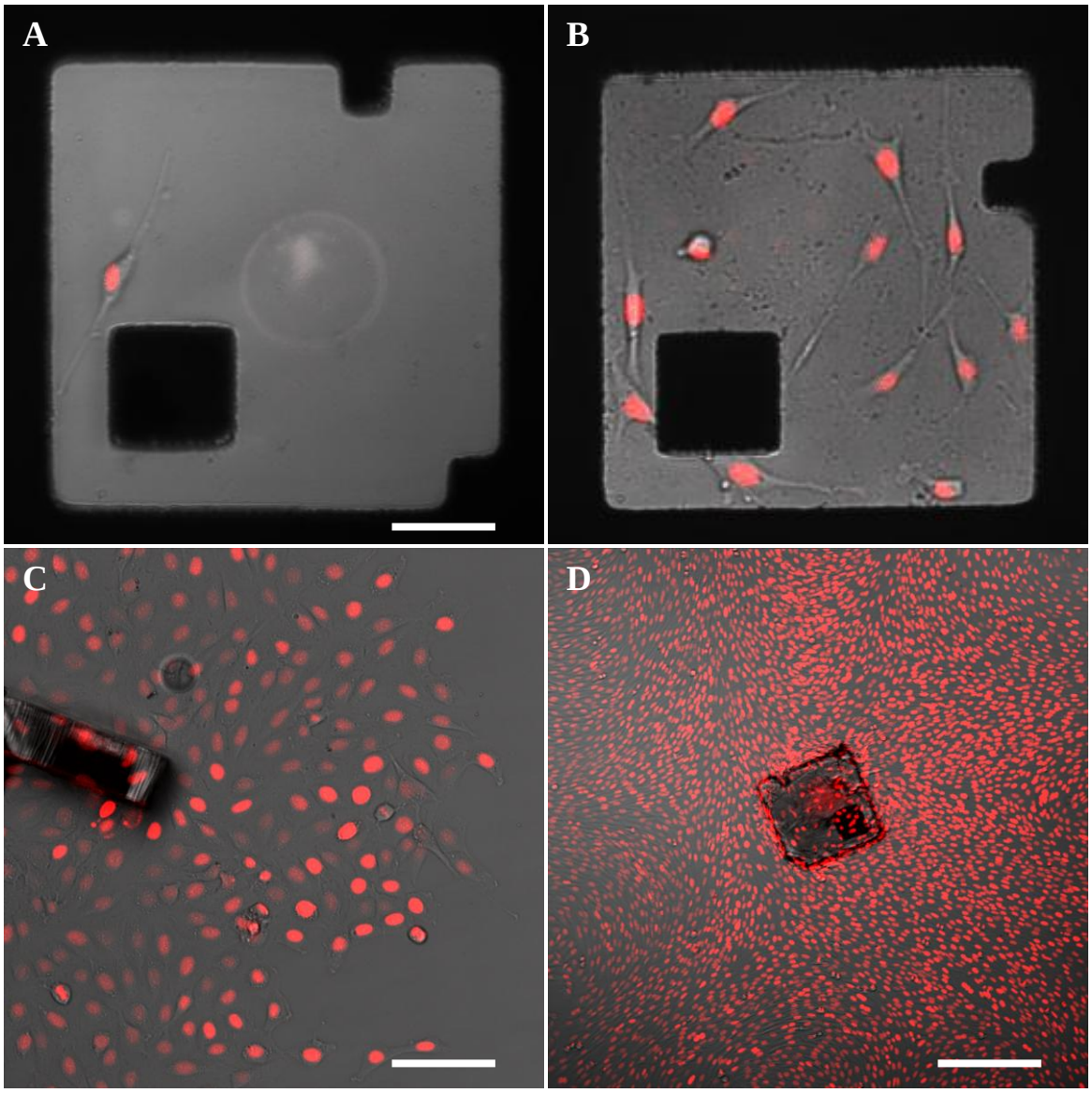

Figure 3.4.2: Purification of H2b-mCherry transfected rat208F cells on Ferrocore micropallets
A) Single transfected rat208F cell expressing H2b-mCherry fluorescent signal. Transfected cells were seeded to the ferrocore micropallet arrays at an 8% positive transfection concentration within a sample mixed with untransformed cells. Scale bar is 50 µm. B) Pure cell colony formation on a ferrocore micropallet after one week of growth on the array. The pallet shown in image A is not the same as B due to the colony in image B growing to more representative numbers, however the seeded cells were from the same studied population. C) Collected pallet after one week of growth in a 48 well culture plate. Every single cell expressed H2b-mCherry stain. D) Same culture well shown in image C after two weeks of growth. The pallet was brought down parallel to the culture well by the force of the cells. Every cell in the culture still maintained H2b-mCherry stain expression.

3.4.3 RmCherry purification results

For both experiments it was found that there were several pallets that bore cell colonies that had thrived during the seven days of growth, but were expressing no fluorescent emissions. Keeping in mind that these cells had been cultured in media spiked with a lethal dose of antibiotics, it was concluded that the H2b-mCherry transfection of rat208F cells resulted in two primary types of transformed cells. One type was those that were considered the cells of interest for this experiment, expressing both antibiotic resistance as well as H2b-mCherry. The second were cells only exhibiting the antibiotic resistance, but not expressing the mCherry stain. Another key difference that was found among the cells was that those with the antibiotic resistance without mCherry expression were much more robust than the properly transfected RmCherry cells and grew at a much faster rate after collection from the arrays. This fact explained why when grown in a shared culture over time the total percentage of RmCherry cells had diminished as they had been outcompeted by the cells not expressing mCherry. Of the colonies that were collected as pure samples from the population originally seeded at 8% transfection, 10 out of the 11 colonies, 91%, successfully maintained purity at one week after collection. The one cell colony that did not have any cell growth after collection most became disconnected from its pallet during the collection process as no cells were observed on the pallet even as early as 24 hours after transfer. Five mixed cell colonies were also collected and each continued to expand in culture exhibiting 100% viability post collection. Three colonies expressing the brightest mCherry signal and exhibiting the healthiest looking morphology were selected to be further expanded and analyzed by flow cytometry to quantify the purity level of the grown samples. Figure 3.4.3 is a plot showing the levels of H2b-mCherry expression identified in each cell colony. The cells were also frozen down cryogenically in order to preserve the cells to be used as stably transfected cell line.

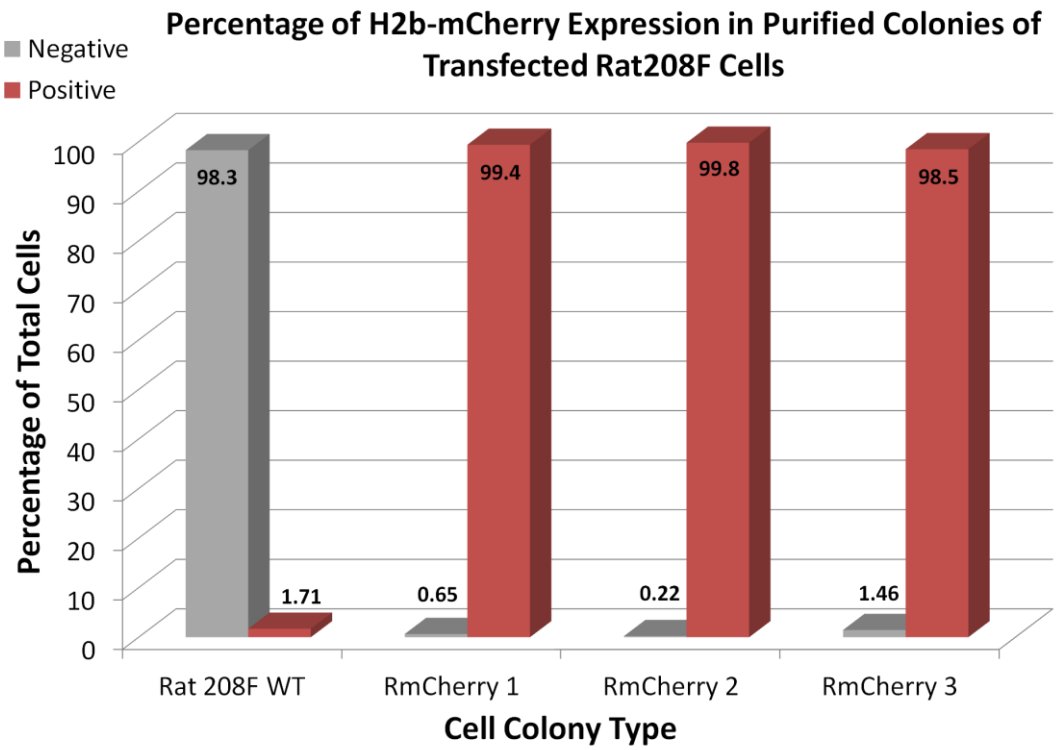

Figure 3.4.3: H2b-mCherry expression of transfected rat208F cells purified on ferrocore arrays The fluorescent expression of H2b-mCherry of three transfected rat208F cell colonies (RmCherry) purified with the ferrocore micropallet arrays was analyzed by flow cytometry. Each colony was identified as a pure colony while growing on the arrays and then clonally expanded in a separate culture after collection for two weeks. The left most set of data was acquired from a rat208F wild type control which was expected to express no mCherry signal. Each purified RmCherry cell colony expressed near pure mCherry signal with the negative expression values falling within expected noise levels.

3.4.4 JSRV-ENV-FLAG transformed rat208F cell purification

The previous section covered the purification of transfected rat208F cells based on the identification of immunofluorescent emissions artificially introduced to the cells via transfection. These signals were bright and obvious when observed with a confocal microscope making distinction of target cells very straight forward. While fluorescent signal transfection is very common and an important process to address, other commonly utilized cell transformation studies include cell transformations with no fluorescent signal generated by the transfection. One such example is cellular transformation through retroviral infection. Retroviruses are a family of viruses that reproduce by infecting hosts and using DNA machinery to integrate their genetic information into the host DNA. The hosts will then replicate the

inserted genetic sequences as if it were their own and produce the molecular components leading to virus replication. In some rare cases, the addition of the viral DNA within a host can lead to oncogenic transformation of the cells making them cancerous. These transformations are of great interest to scientists because they create a one to one translation of cause and effect which can be tracked to a well defined source.

Intentional cellular transfection using retroviruses oftentimes only uses the raw viral samples to infect cells without any alteration, such as the addition of fluorescent tags, so purification can no longer rely on immunofluorescent detection the way it could be in the earlier H2b-mCherry case. For these transformation studies, the most straight forward and commonly utilized method of locating successfully infected cells is to use what is known as a focus-forming assay.[65, 66] These assays rely on differences in cell morphology generated by the oncogenic transformation of target cells to differentiate them from the surrounding wild type cells in the shared population. First, cells are seeded at low density to a culture flask and then a transfection procedure is performed using the cancer causing retroviruses.[107] The cells are then left to grow until they reach confluence. Once confluent, untransformed cells enter a state of quiescence and no longer expand in number. The transfected cells, however, will continue to grow above the surrounding cells and form foci at which point they can be spotted and collected. Another common trait among cancer transformed cells is a weakened adherence to one another and to their surrounding substrates which can lead to rounded cell phenotypes when compared to the parental cells.[108] This trait specific to cancer transformed cells was true in the case of rat208F cells transformed with JSRV-ENV-FLAG and was used as a marker for locating cells of interest from a mixed population of wild type and JSRV-ENV-FLAG transected rat208F cells. Figure 3.4.4 is an image comparing wild type rat208F cells to transformed ones.

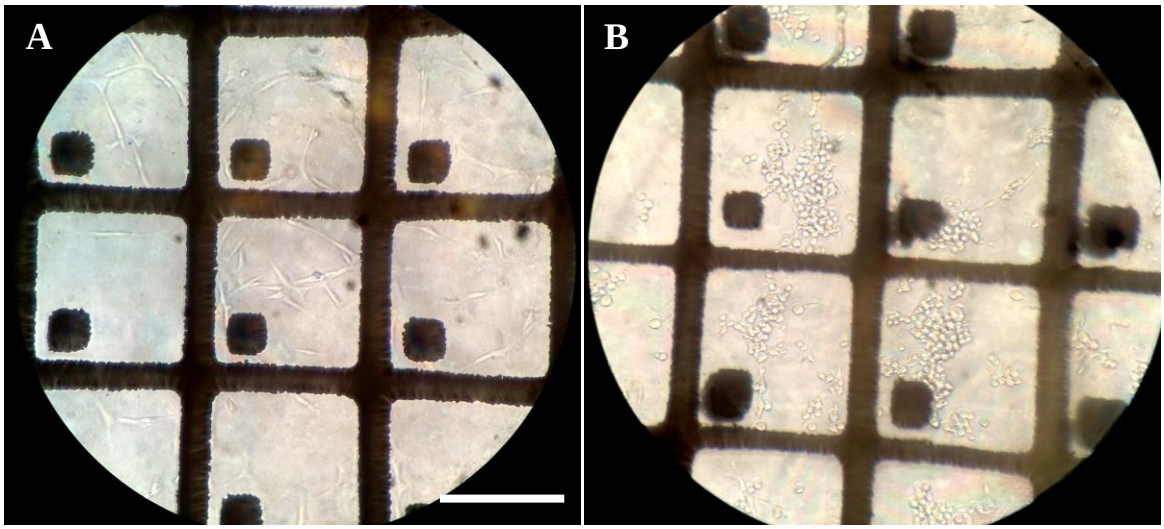

Figure 3.4.4: Comparison of wild type rat208F cells to JSRV-ENV-FLAG transformed cells
A) Wild type rat208F cells grown on micropallet arrays. The cells are visualized as elongated and spaced out from one another. The scale bar is 250 µm. B) JSRV-ENV-FLAG transformed rat 208F cells. The phenotype for these cells was a much more balled up due to lower adhesion strength of the cells. The cells also preferentially stuck to one another and formed masses of cells when cultured long enough to grow to high numbers. As seen in the image, the transformed cells were very easy to distinguish from the untransformed cells purely based on their morphology.

Cell purification experimentation was performed by mixing a known concentration of JSRV-ENV-FLAG transformed rat208F cells (RJSRV cells) with wild type cells and seeding the cells to the Ferrocore micropallet arrays as described above in section 3.4.1. A mixed cellular solution was prepared with a 5% concentration of RJSRV cells mixed into 95% wild type cells and suspended in rat208F cell media. The cells were seeded into wells of an 8-well Labtek chamber mounted to the Ferrocore micropallet arrays as described in section 3.4.1. When imaged with the LSM 780 confocal microscope, there was no need to set up fluorescent imaging channels. A 488 nm laser was used to illuminate the samples at 3% total output energy. Proper image setting eliminated any background noise from the laser while stay creating a bright enough image to see all cells on the arrays. When identifying cells of interest, pure RJSRV colonies were determined as those growing with balled up morphologies with no cells exhibiting the stretched out phenotype typical of the wild type cells. Once located, pallets bearing the pure RJSRV colonies were release and collected as mentioned in section 2.4.9 and transferred to a 48 well culture plate filled with a 1:1 ratio of conditioned rat208F cells collected from RJSRV cultures and fresh

rat208F cells. The cells were then grown for one week in order to expand the number of cells. Figure 3.4.5 shows a pure RJSRV colony growing on a Ferrocore micropallet.

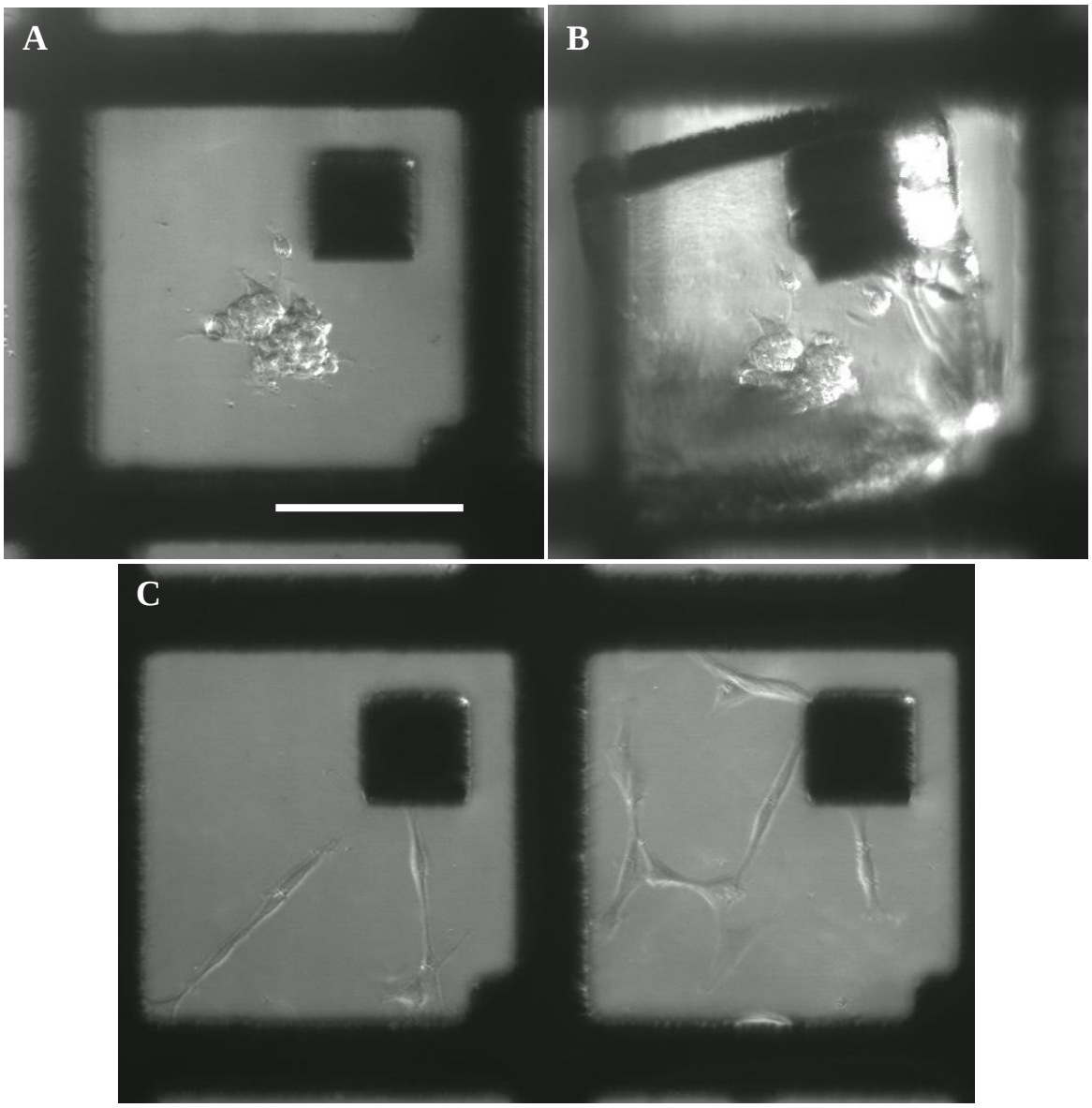

Figure 3.4.5: Pure RJSRV cell identification by LSM 780 confocal microscope
A) Pure JSRV-ENV-FLAG infected rat208F (RJSRV) cell colony on ferrocore micropallet as imaged by LSM 780 confocal microscope. When transformed, rat208F cells tended to be circular and preferentially adhered to one another to form spheroid colonies. The scale bar is 125 µm. B) The pallet showed in image A was ejected with a 2-photon laser . The bubbles generated to eject this pallet were brushed away with a needle to better show the colony adhered to the surface of the pallet. C) Untransformed rat208F cells growing on pallets in the same chamber as the colony in image A. Wild type rat208F cells looked stretched out over the surfaces of the pallets. The differences in phenotype between the two types of cells were quite distinct.

In order to confirm whether the collected RJSRV cells were pure after one week of growth in the culture wells, an intercellular immunofluorescent staining procedure was performed on the cells targeting the FLAG tag section of the transfected JSRV strain. The stain targeting the FLAG tag could only be utilized on dead cells and thus could only be used for purity verification on fixed cells and not cells that were grown on the Ferrocore arrays that were intended for further expansion following laser release and collection. To visualize the FLAG tag, expanded RJSRV colonies that were grown in the 48 well cuture dish were fixed with 4% paraformaldehyde using standard methods. The fixed cells were then tagged with anti-Flag mouse mAb followed by a FITC goat-anti-mouse igG (H+L) secondary antibody. Each antibody was introduced to the cells and incubated for thirty minutes followed by several gentle washes with RPMI buffer. After the FLAG tags were bound to FITC, the cells were immersed in a solution of Sytox Red DNA stain at a 5 nM concentration in RPMI buffer and incubated for 10 minutes. To visualize FLAG expression with the LSM 780 confocal microscope, a 488 nm laser set at 9% total energy output activated the FITC fluorescent emission spectra ranging from 500 to 550 nm. A second laser emitting at 633 nm with 5% energy was used to visualize the Sytox Red stain emitting a signal ranging from 630 to 690 nm which marked all cells in the culture. The phase contrast image was also analyzed. Figure 3.4.6 shows a pure RJSRV cell colony expanded in the 48 well culture dish. An image of a mixed population of RJSRV cells with untransformed parental rat208F cells is also shown.

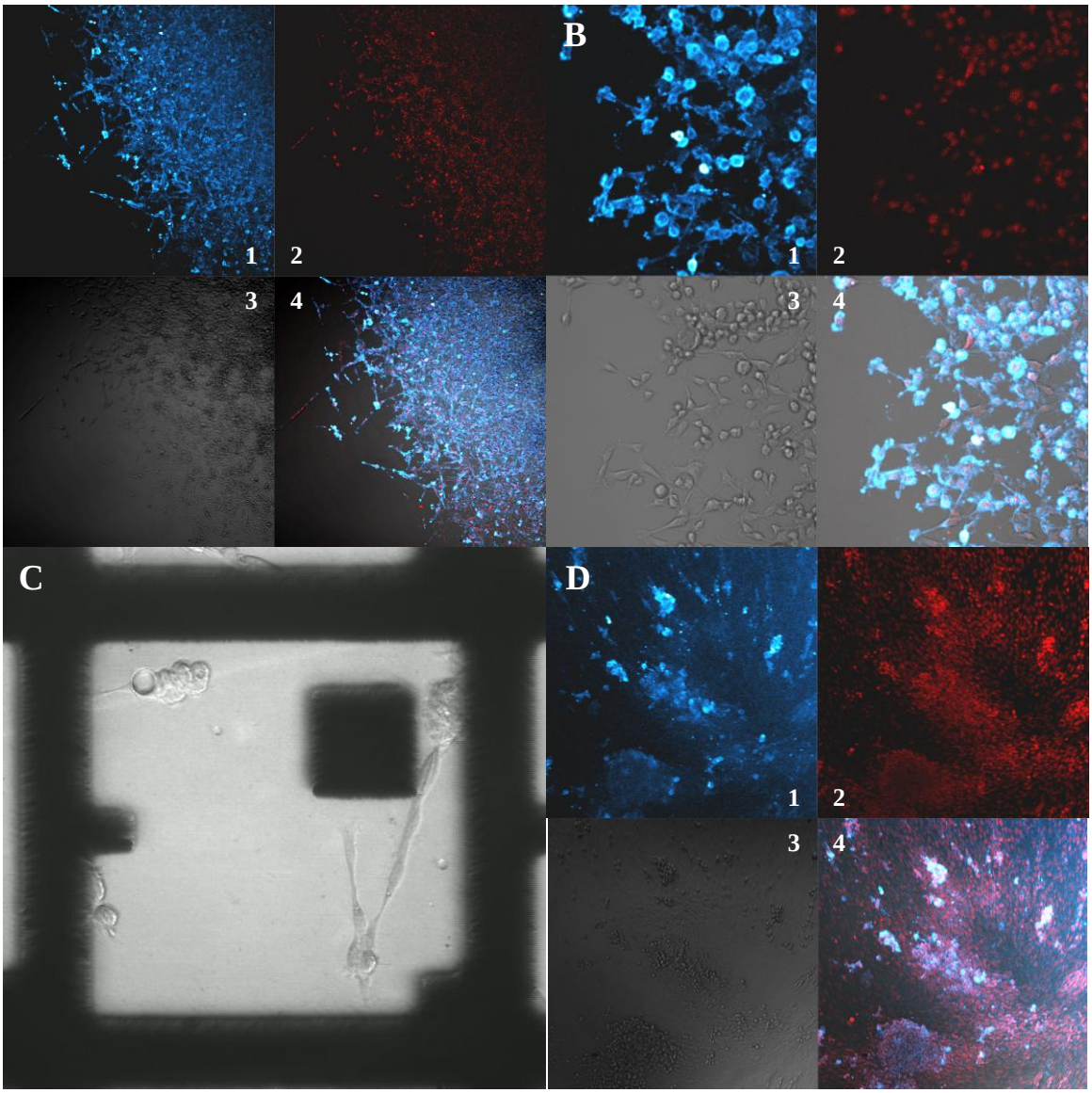

Figure 3.4.6: Visualization of Flag tag expression on purified RJSRV colonies
A) FLAG tag visualized by antibody linked FITC stain (Blue) on JSRV-ENV-FLAG transformed rat208F cells (RJSRV cells) expanded from a pure colony collected from ferrocore micropallet arrays. A Sytox Red nuclear stain is also included in order to highlight all cells in the image. Images 1-4 all represent the same viewing channels for pictures A, B and D. Image 1 shows just the fluorescent channel showing FITC expression on Flag tag. Image 2 shows Sytox Red. Image 3 is the phase contrast channel. Image 4 is the combined image of each channel. B) Zoomed image of a second pure RJSRV colony also collected from the arrays. Purity of the collected cells were further analyzed by zooming on sections of the expanding colonies and confirming FITC expression on every imaged cell. C) Example of pallet with a mixture of both RJSRV and parental rat208F cells. Spherical cells presumed to be RJSRV cells can be seen near the top of the pallet and wild type rat208F occupy the bottom right section. This pallet was collected and expanded to create a negative control for failed cell purity. Image D) Visualization of the colony grown from the pallet shown in image C. Unlike in image A and B, only clustered cells forming foci displayed FITC expression. Parental cells formed a flat layer beneath the RJSRV cells and only expressed the Sytox Red stain. The dark regions of the Sytox Red stain are due to the confocal microscope focal plane having to be set above the bottom surface of the culture due to transformed cells primarily clustering vertically away from the lower parental cells.

3.4.5 JSRV-ENV-FLAG purification results

Several purification procedures with RJSRV cells were performed on both Ferrocore micropallet arrays as well as the first rendition of the arrays earlier referred to as large area magnetic micropallet arrays. Every purification was performed with a 5% RJSRV concentration mixed into wild type rat208Fc cells. The total accumulated number of pure RSRV colonies collected from Ferrocore micropallet arrays was 40. Of the 40 collected pure colonies, 34 resulted in successful establishment of pure colonies grown within the 48 well culture plates (85% success). The six colonies that were unsuccessful did not work due to there being no cell growth at all within the wells that they were transferred to from the arrays. It was likely that the cells had become dislodged from their corresponding pallets during the laser ejection and collection process. This was not a surprise as a common trait shared amongst RJSRV cells was their weak adhesion to their growth substrates. 40 pallets bearing pure wild type rat208F cells were also collected with 37 of colonies successfully growing after transfer, or 92%. Two of the failed colonies faced apoptosis at 24 hours after collection and one exhibited no growth at all. Complete loss in cellular viability after transfer was a very rare event so these two instances were considered an anomaly.

The purification of cells based on their morphologic differences was highly successful and results were consistent. Two main factors could be used to differentiate RJSRV cells from wild type rat208F cells. First, there were distinct visual differences between the two populations as shown in figures 3.4.5 and 3.4.6. Another factor that contributed to observable differences among the cells was the increase in growth rate that was caused by the JSRV-ENV-FLAG transformation. When grown on the Ferrocore micropallet arrays for one week, the RJSRV cells exhibited an average growth rate near double that of the parental cells. It is important to note that not all transfected cell types exhibit faster growth rates than their wild type forms. The differentiation of these particular cells based on their growth kinetics was found to be useful only after much observation and understanding of their growth tendencies. Figure 3.4.7 compares the two growth rates. The ability to establish pure cell lines based just on morphological differentiation was an important result to accomplish using the Ferrocore arrays. Being able to purify cell

lines not exhibiting obvious signals such as immunofluorescent emissions greatly enhances the versatility of the technology, allowing researchers to work with a variety of cell types.

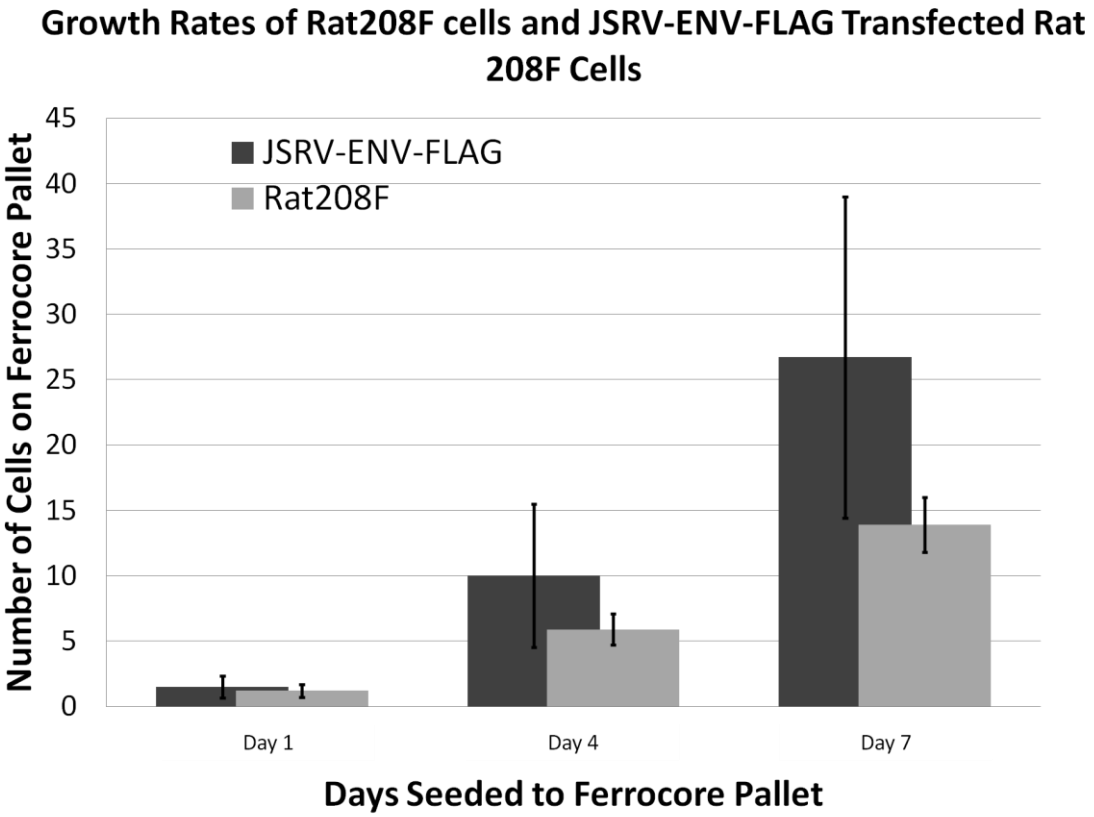

Figure 3.4.7: Growth rates of rat208F cells and RJSRV cells when grown on ferrocore arrays A) The growth rate of JSRV-ENV-FLAG transformed rat208F cells and wild type rat208F over a span of seven days are compared. The error bars represent the standard deviation of the population. Day 1 n values for RJSRV and wild type cells were 67 and 38 respectively. Day 4 n values were 74 and 41 and day 7 n values were 100 and 28. Large sample sizes were analyzed for the RJSRV cells due to the high variability in cell numbers on the ferrocore pallets. The faster growth rate of JSRV transformed rat208F cells was a specific identifier only used for this sorting study. The growth rate of other transfected cell types may not reflect the rates observed with these particular cells.

An additional result that was observed during this work was differences in results that occurred due to pallet surface roughening. As explained in section 3.2.2, the surfaces of the Ferrocore pallets were roughened in order to better promote cellular adhesion and viability. As it turned out, the increase in cellular adhesion to the arrays actually made differentiating JSRV cells from wild type cells more difficult due to the RJSRV cells exhibiting a more stretched phenotype than when cultured on unroughened pallets. The total number of pure colonies collected was from a combination of both unroughened pallets

and roughened pallets so results were not confounded by using the surface roughening technique. These results, however, did reveal that the surface roughening of pallets is a step that may be worth skipping if cell morphological differentiation dependent on surface adhesion to the pallets was the target for cell purification.

3.4.6 NIH/3T3 variant culture on Ferrocore micropallet arrays

The use of the transformed NIH/3T3 cell lines described in section 3.3.2 was primarily to test whether a wide variety of cells could be consistently grown on the Ferrocore micropallet arrays and clonally expanded following collection from the arrays. It was also important to note whether the collected cell were representative of the cells originally seeded to the arrays. FrKP and Akv transformed NIH/3T3 cells (FrKP and Akv cells respectively) were seeded to the arrays as single cells as described in section 3.4.1 and grown for seven days. In the case of FrKP and Akv cells, there was no specific phenotypic or immunofluorescent trait that was sought during collection as the seeded samples were homogeneous. Rather, any pallet with a confluent colony of cells surrounded by empty adjacent pallets were selected as targets and collected via laser ejection from the arrays. Following the procedure performed for all previous cell types, the FrKP and Akv cells were transferred to a 48 well culture plate filled with half conditioned NIH/3T3 media and half fresh media spiked with Zeocin antibiotic. Figure 3.4.8 includes images of populations of Akv and FrKP cells growing from pallets after one week in culture.

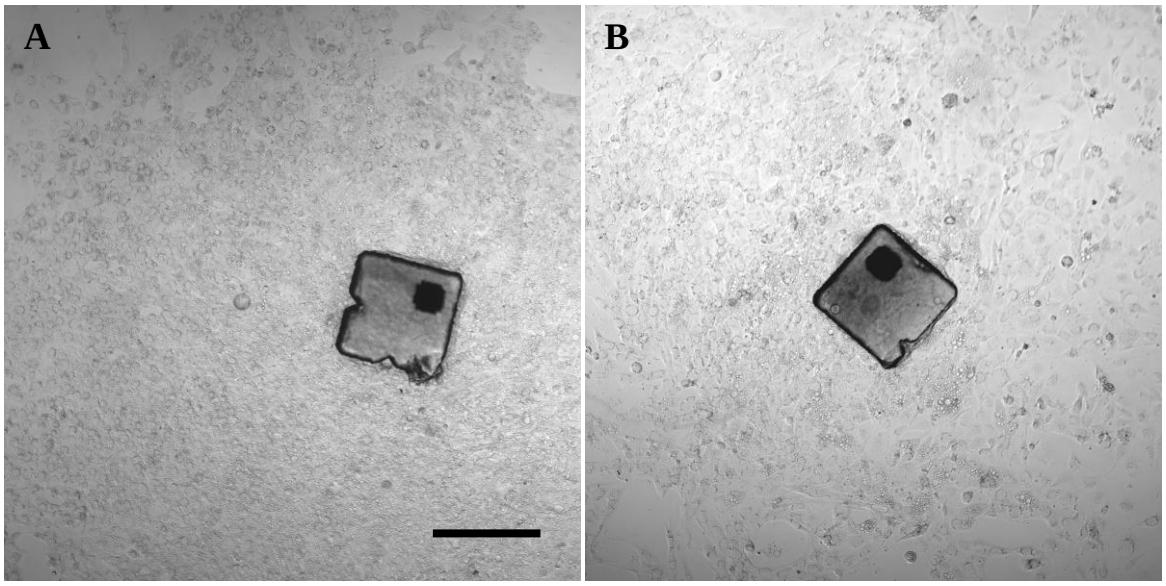

Figure 3.4.8: Akv and FrKP transformed NIH/3T3 cells collected on ferrocore pallets
A) Clonally expanded NIH/3T3 cells transformed with Akv strain murine leukemia. B) NIH/3T3 cells transformed with FrKp strain murine leukemia. The FrKp cells were less robust than the Akv cells but were still capable of growth after collection from the ferrocore micropallet arrays.

The NIH/3T3 cell variants were not quite as robust as the rat208F variants when grown and collected from the Ferrocore micropallet arrays indicating that different cell types have difference survival capabilities with use of the technology. Of the 20 wild type NIH/3T3 pallets collected, 17 were viable and grew into colonies after transfer. 21 total Akv cell colonies were collected and 17 of those remained viable as well. For the FrKP cells, 22 pallets were collected and only 13 of those continued to expand clonally after collection. Although the positive growth results for FrKP were much lower than all other tested cell types, this result was consistent with the growth dynamics that were observed for this particular cell line before seeding to the arrays showing that outcomes can be predicted and accounted for before purification studies are conducted.

3.5 Chapter 3 Conclusion

Cell purification studies conducted on the Ferrocore micropallet arrays were highly efficient and effective while maintaining ideal culture settings for adherent cell lines by allowing them to stay connected to a growth surface from start to finish. No harsh chemical treatments required for more typical types of sorting methods such as FACS or MACS were necessary to sort the cells. When compared to

standard purification practices, Ferrocore arrays enabled faster overall cell purity acquisition, better selection capabilities for individual cell colonies grown from a single cell, and greater versatility for cell colony manipulation directly following collection which was enabled by the magnetic micropallets. Stably transfected cell lines could be established from heterogeneous populations with initial target cell concentrations as low as 5%. Pure cell lines were established with just one retrieval event of target cells from heterogeneous samples. This result was an overwhelming success as normal cell purification using standard means such as focus forming assays typically take at least two collections of target cells (followed by multiple days of cell growth) but usually even more to completely ensure purity of grown cell samples. This process has been described as taking anywhere from 3 months to 6 months. Using the Ferrocore micropallet arrays completely circumvented the need for repeated cellular collections for purification with a one shot approach.

The work accomplished in this chapter also proved that multiple characteristics of the adherent cells being sorted could be identified directly during growth on the arrays for collection and purification targets. Growth rate, phenotype, immunofluorescent signal, and general cell behavior could all be tracked on individual pallets by utilizing the newly designed demarcation system allowing consistent observation from start to finish. This level of observation of individual cells grown to corresponding colonies would not be possible with standard sorting and purification methods.

3.5.1 Future work for the improvement of Ferrocore micropallet arrays

This chapter discussed two major types of cell purification procedures that could be greatly enhanced with the use of ferrocore micropallet arrays. While the biology was sound and use of the technology improved on the conventional methods for cell purification, there are still a number of improvements that could be made which would further ready ferrocore arrays for mass appeal. Array fabrication on the surface of semi-transparent gold thin films enabled the simple and consistent ejection of large area pallets by utilizing the formation of vapor bubbles upon laser irradiation. Although the imaging quality loss was not greatly significant, there was still a noticeable loss in light transmission through the

gold layer. For these experiments described in this section the transmission loss was not an issue, but if researchers were to target cells with incredibly dim immunofluorescent signals, the signals may be lost due to the absorptive layer. Gold was selected for this purpose because of its biocompatibility as well as its absorption properties, but other conductive materials and metals besides gold would theoretically work as well. As a next step to this work, however, it is suggested that gold layer formation be continued, but that strategic patterning of the gold layers should be attempted. Although vapor bubble formation enabling pallet ejection appears to occur at random locations, it would be worth attempting to pattern the gold layer underneath pallets to some distinct regions and not just a continuous sheet all across the surface of the glass slide. It could be possible that just having a gold layer underneath the gap regions surrounding individual pallets and extending to the core formation location may be enough to still cause pallet ejection.

The next major endeavor that should be attempted is the integration of Ferrocore micropallet arrays into larger chip systems with further downstream biological assays. The inclusion of the magnetic cores enabling the magnetic manipulation of cells following ejection does not just have to be utilized for pallet transfer to other culture plates. It is also possible, in theory, to control the pallets within microfluidic systems by an external magnet, especially because pallets with larger ferromagnetic cores could be controlled from relatively far distances as shown in chapter 2. It would be interesting if a microfluidic system were to be linked to a Ferrocore magnetic micropallet array and released pallets could be instantly transferred through microfluidic channels to perform specified assays on target cell colonies. Appendix B figure 6.2.1 includes a set of images representing the magnetic control of a released Ferrocore micropallet within a microfluidic channel. The use of magnetic control of samples through microfluidic channels would allow for closed fluidic systems without any external pressure sources for sample movement which further lends the technology's readiness for on chip integration. A second worthy pursuit would be to begin writing automated imaging algorithms for Ferrocore micropallet arrays. Unlike standard micropallets, the Ferrocore arrays had great contrast differentiating the cellular growth surfaces and the surrounding gaps which were visualized as white and black respectively with phase

contrast microscopy. The ferromagnetic cores could also be used as imaging fiducials to quickly locate pallet locations corresponding to cell colony growth, enabling speedy analysis of whole arrays.

Chapter 4: Metal Side-Coated Micropallet Arrays

4.1 Overview

This chapter diverts from the common theme of colony sized micropallets described in chapter 2 and 3 and revisits the historically standard sized micropallet arrays fabricated for single cell sorting. At the time of this work, collaboration with Kanto Gakuin University in Japan had just started and our group decided to test the potential impact of their unique electroless plating technique on micropallet technology.[109] The primary goal of this chapter was to explore the types of improvements that could be made to the micropallet technology without changing the base standard micropallet fabrication process or features such as size and shape. A major discovery that we made through this work was that direct electroless plating of nickel could be conducted on patterned 1002F photoresist using short wavelength UV surface pretreatment. Furthermore, these thin nickel walls (around 500 nm thick) possessed strong enough magnetic response qualities that they could be collected using the same collection probe described in chapter 2.[84] Optical properties when compared to other existing magnetic micropallet array systems for single cells were much better due to the 1002F photoresist making up the pallet structures did not have to be altered in anyway. In fact, the work described in this section showed that the formation of reflective nickel walls coating the transparent walls of the micropallets improved some optical properties and also created greater contrast between dead zones and areas of interest. This contrast was very similar to the contrast generated by electroformation of nickel structures on the ferrocore micropallet arrays (chapter 2, 3) and has the potential to ease automated visualization and analysis of micropallet arrays long term.

4.2.1 Abstract

We describe a method of enhancing the imaging properties of micropallet arrays by electrolessly plating opaque, reflective sidewalls to every individual array element. Short wavelength UV light was used to chemically and physically modify the surfaces of the pallets in order to enable optimal nickel

plating conditions. After nickel plating, the sidewalls were electrolessly plated with a thin layer of gold to insure biocompatibility of the completed devices. In addition to improved optical properties, the ferromagnetic nickel sidewalls provided further micropallet enhancement by enabling magnetic recovery of individually released pallets. We characterized the optical properties of metal side coated micropallet arrays and compared them to those that were unaltered. The viability of cells seeded to the arrays was assessed by propidium iodide stain.

4.3 Introduction

The micropallet array is a powerful tool for adherent single cell and cell colony sorting.[72-74] Much work has been devoted to optimizing adherent cell sorting to better understand cell behavior that cannot be analyzed with more commonly utilized fluidic forms of sorting such as flow cytometry.[18-21] The general embodiment of the micropallet array is of transparent photoresist patterned to form thousands of individually addressable micro pedestals on glass microscope slides. Each structure of the micropallet array forms an independent growth surface for seeded cells, which can then be characterized and recovered via laser catapult. The most commonly utilized method for cell selection described in this work was ejection by local plasma formation by the highly focused irradiation of a 2-photon laser at the micropallet / glass slide interface.

Since its initial invention many variations to the micropallet array have been developed to generate better functionality for different cell sorting applications, but work has yet to be done to improve on the imaging properties of the technology. Due to the transparent nature of each pedestal within an array, immunofluorescent emission from tagged cells captured on pallet surfaces are free to spread from one pallet location to the next during imaging, leading to potential decreased sensitivity and "bleed through" that may manifest as false positive signals. Optical distinctions between one pallet and the next can prove challenging as there is very little contrast distinguishing pallets from the empty space between them. These constraints become even more apparent when trying to design automated micropallet

imaging systems for speedier cell sorting to work towards matching the output of more commonly utilized cell sorting systems.

We report on a method for improving both the intensity of fluorescent signals generated on the surface of individual pallets and the signals' containment to their corresponding micropallet areas by electrolessly plating nickel walls to the sides of each pallet and glass slide surface. The nickel plating also enabled the magnetic collection of individually released pallets for targeted cell collection, improving upon the current standard of micropallet adhered cell retrieval. Both of these improvements could better enable automated systems built for micropallet analysis and control.

4.3 Experimental Details

4.3.1 Fabrication of standard micropallet arrays

Micropallet arrays were created by the photolithographic patterning of a transparent photoresist onto the surface of glass microscope slides as previously described.[84] 1002F photoresist, selected for its low autofluorescence and biocompatibility,[79] was prepared by dissolving EPON resin 1002F (Miller-Stephenson, Sylmar, CA) in γ-butyrolactone (GBL) (Sigma-Aldrich) with triarylsulfonium hexafluoroantimonate salts (Dow Chemical, Torrance, CA), a photosensitizing agent. Each component was prepared at the previously described ratio. Glass microscope slides were washed in piranha etchant solution (H_2SO_4 and NH_4OH) before spin coating 1002F photoresist onto their surfaces to 50 μm in thickness. Slides were then baked until all solvent was evaporated from the photoresist at which point arrays were exposed to a UV light source (AB&M INC, Scotts Valley, CA) through a photomask bearing the micropallet pattern at 1200 mJ/cm^2. Following another bake step, the slides were immersed in SU8 developer and baked once more using a predefined heating protocol.

4.3.2 UV surface modification of micropallet arrays

Micropallet arrays were exposed to a low pressure mercury lamp UV light source (Koto Electronics Co., JPN) emitting 254 nm and 184.9 nm wavelength light for three minutes at a distance of 50 mm from the fluorescent light source. These settings were previously proven successful by the

company and were adhered to for the entirety of this work. UV exposure resulted in the microroughening of the pallets and exposed glass surfaces to aid electroless deposited metal adhesion strength and uniformity due to increased wettability of the exposed surfaces.[109] Electroless metal plating is a wet process and thus requires that samples be hydrophilic in order to produce consistent results. While testing the surface treated 1002F pallets, it was discovered that there was a considerable increase in autofluorescent emissions from the UV exposed pallets when compared to standard pallets. Laser emission and collection settings were adjusted accordingly for this work. Research involving extremely low fluorescent detection may prove to be difficult when using these sorts of pallets. Further work involving the side coating of pallet should focus on testing various UV exposure distances and times to best eliminate autofluorescence while still maintaining plateable surfaces on the pallets.

4.3.3 Electroless Coating of Micropallets

The electroless plating of metal side coatings onto micropallet arrays consisted of several reagent immersion steps as is standard for this process. Following an initial wash in deionized water (diH_2O), arrays were dipped into a solution of 50g/L NaOH in diH_20 (Sigma-Aldrich) for five minutes at room temperature to degrease the arrays. The arrays were then prepared for side-only coating by placing an adhesive sheet on the top surface of the micropallet arrays. Pressure was uniformly applied to the adhesive by gently pressing an acrylic block over the surface of the adhesive strip. A second strip was placed over the bottom-sides of the arrays to prevent unwanted bottom plating to maintain optical clarity through the devices. The arrays were then sonicated at 47 kHz for five minutes in diH_2O to allow for fluid flow between the pallets and displace any trapped air. Covered arrays were dipped in CC-231 (Dow Chemical Company) prepared at 50 mL/L in diH_2O to coat exposed surfaces with conductive metal salts. CC-231 immersion was conducted for one minute at 45°C. The surface adhered metal ions were then catalyzed in an agent consisting of 0.3 g/L $PdCl_2$ (Sigma-Aldrich) in diH_20 for two minutes at 45°C. Sodium hypophosphite (Sigma-Aldrich) was prepared at 30 g/L in diH_20 to create the accelerating reagent into which samples were immersed for one minute at 60°C. The arrays were then placed in an electroless

nickel plating solution at 80°C for five minutes. This process resulted in a thin, uniform plating of nickel-phosphorous at a thickness of 500 nm across all exposed regions of the micropallet array. Coated micropallets were characterized with a scanning electron microscope (SEM) as shown in figure 4.3.1. The final step of the plating consisted of the immersion of nickel coated arrays into a bright gold electroless solution (Transene Company, Danvers, MA) for ten minutes at 90°C resulting in a 2000 Angstrom gold layer coating over the nickel. The gold layer provided a safer material for biological study while leaving the magnetic properties of the nickel intact.

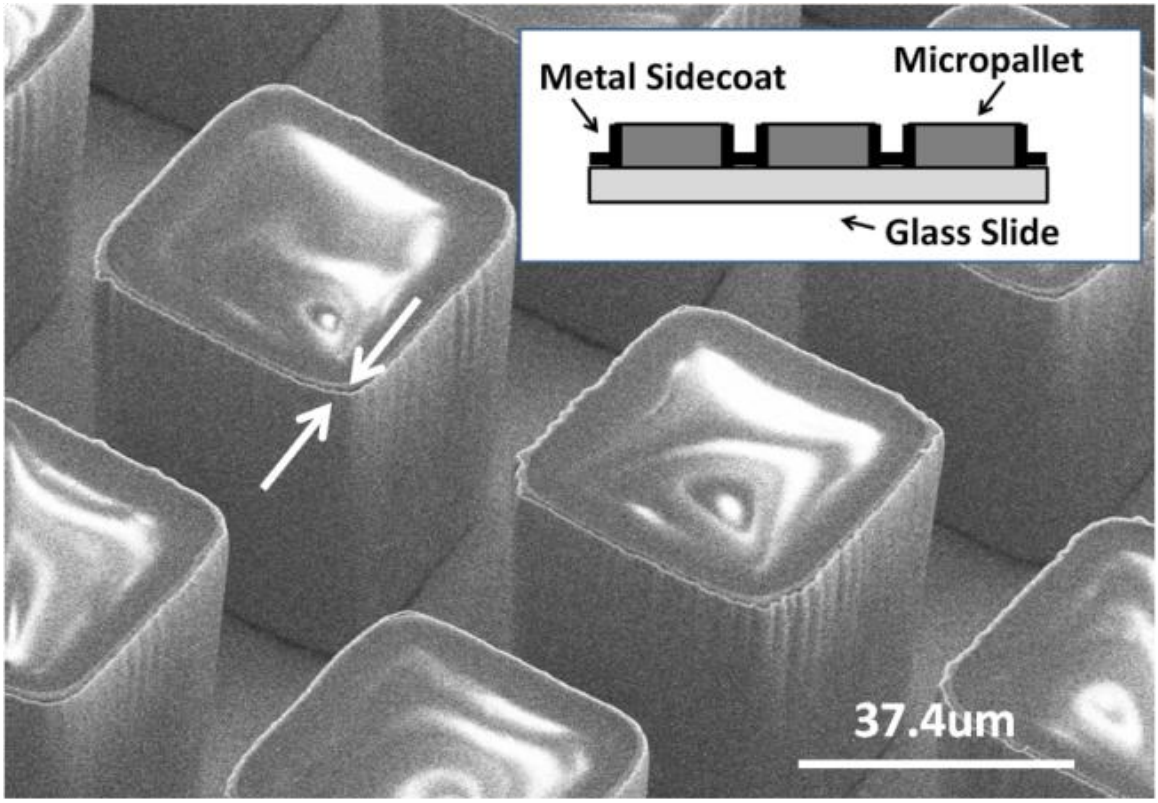

Figure 4.3.1: SEM image of nickel side coated micropallet arrays
Nickel sidewalls were plated to 500 nm and are highlighted by arrows on a single pallet. The white accumulation in the middle of the pallets was due to charge accumulation during imaging due to there being no nickel coating on the top surfaces of the pallets. The sidewalls could be subsequently plated with gold to increase biocompatibility using a second electroless plating procedure. The inlet image shows a 2D representation of a cross section of the array.

4.3.4 Sidecoated Array Surface Modifications

Surface modification to prepare for virtual walls and protein seeding were conducted in the exact same manner as was done for the magnetic micropallet arrays in chapter 2. Sections 2.4.5 and 2.4.6

provide a more in depth walkthrough. Gold side coated micropallet (GSM) arrays were silanized with (heptadecafluoro-1,1,2,2-tetrahydrodecyl)trichlorosilane (Gelest, Morrisville, PA) in a vacuum chamber as previously described to enable the formation of virtual air walls for cell sequestration on the tops of the micropallets.[80] The arrays were then coated in extra cellular matrix proteins prior to cell seeding to optimize cellular adherence strength in the same manner as described in section 2.4.6. While multiple types of proteins have been tested for cell compatibility on micropallets, fibronectin has been shown to result in the most consistent cell adhesion (nick protein paper) and was selected for use in this study.[82] GSM arrays were coated following the methods described in the previously published work as well as in chapter 2. Protein coated GSMs were stored in a sterile environment until use. The metal surfaces on the sides of the pallets and on the glass surfaces in the gaps did not appear to have any noticeable effect on silanization or air wall formation quality.

4.3.5 Light transmission and spread analysis

In order to study the light transmission properties of GSMs, fluorescent beads were used in place of fluorescently labeled cells to provide greater consistency. Yellow-green, 25 μm diameter polystyrene beads with 486 nm emission wavelengths (Polysciences, Inc) were used as cell surrogates. 8 well LabTek chambers (Nunc, Naperville, IL) were adhered over the surface of the arrays and filled with 500 uL of phosphate buffered saline. Chambers were then filled with 10,000 beads each, equaling the number of cells that would normally be seeded to best achieve single cells on single pallets based on a random Poisson distribution. The settled beads were imaged with an LSM 780 confocal microscope (Carl Zeiss, Oberkochen, Germany) and excited with a VIS laser emitting at 440 nm and analyzed with Zeiss' Zen microscope software as shown in figure 4.3.2.

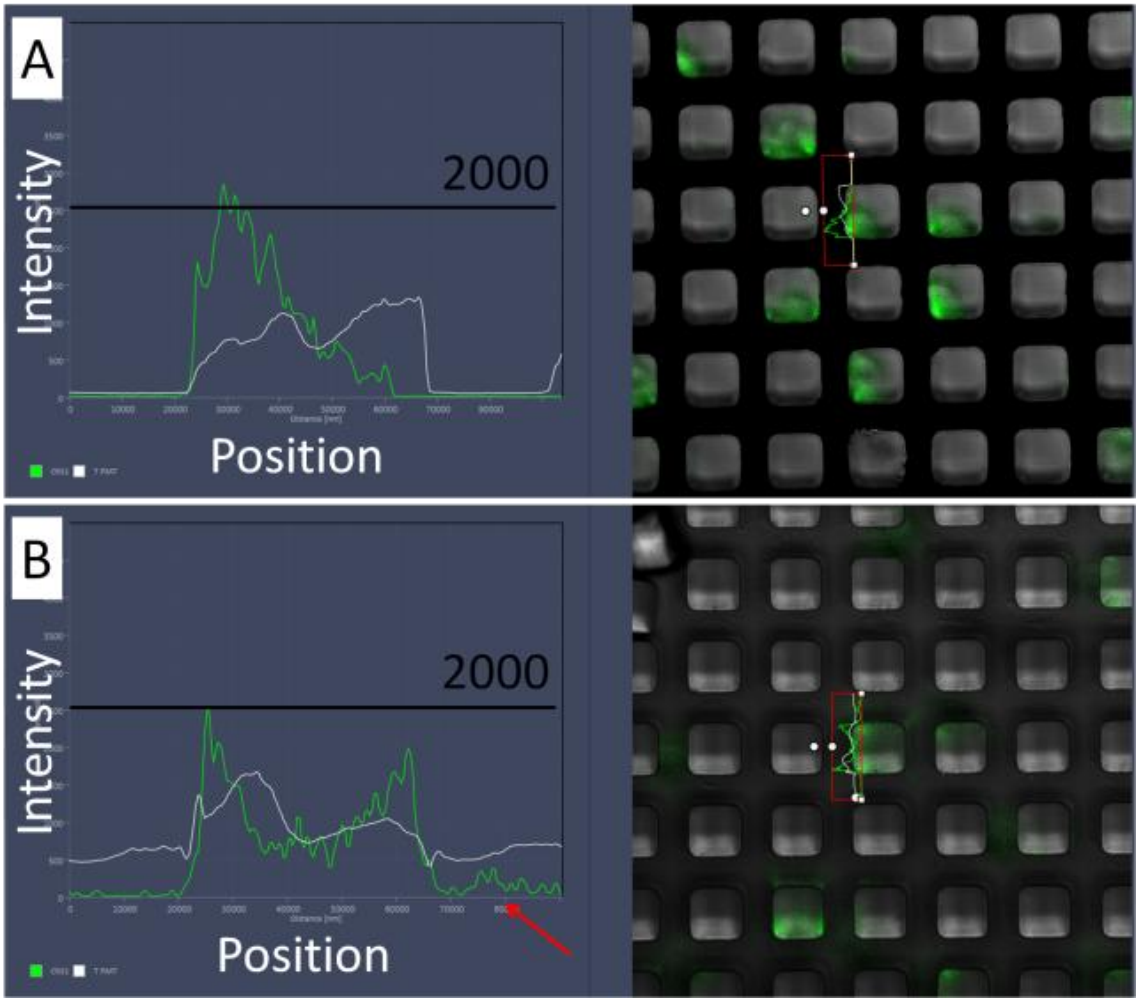

Figure 4.3.2: Light transmission properties of gold side coated arrays
A) Bead intensity and image of Side coated micropallet array. All fluorescent signal coming from the beads is contained within the pallet perimeter due to the opaque walls created on the glass slide as well as the reflective walls containing light within the pallet. B) Bead intensity and image of a standard array. The red arrow highlights signal spread from a standard pallet perimeter. While the spread may seem of minimal intensity when compared to the main signal, cell signals can range from very bright to extremely dim so any signal spread could indicate a seeded cell. The spread signal could be bright enough to confuse automated imaging systems into a false positive result on incorrect pallet locations.

The fluorescent beads seeded to the arrays were much brighter than what would typically be expected of wild type cells, but were nonetheless an important model to study before moving on to biological cell evaluation. Although bright, the level of fluorescent emissions that were collected from the beads were not out of the questions for cells with high density stain expression. Cell sorting studies performed with these types of especially bright cells would normally lead to high level of false positive detection when raw fluorescent signal is used as an indicator of cell existence like would be the case when

using automated cell detection on micropallet arrays. The nickel sidecoating on the pallets was highly effective at eliminating signal transmission emanating from the pallets bearing the bright beads and also created much more contrast between micropallet locations and the surrounding gaps which would most likely be used for automated analysis of pallet location.

4.3.6 Sidecoated array biocompatibility study

The viability of cells seeded to GSM arrays was monitored for a 24 hour span. This time frame was deemed appropriate as the regular use of micropallet arrays only requires cells to be sequestered to pallet surfaces for up to six hours before analysis and sorting. Each chamber of a GSM mounted 8-well LabTek chamber were filled with 400 µL of 3T3 fibroblast media along with 10,000 3T3 WT cells cultured following cell provider (ATCC) guidelines and selected as model adherent cells. The GSM captured cells were incubated for 24 hours at 37˚C in 10% CO_2 before viability confirmation.

In order to compare cell viability on GSM arrays and standard micropallet arrays a propidium iodide (PI) stain protocol was used to differentiate living cells from non-viable cells. Three GSM and standard arrays each were prepared with 48 total chambers for independently loaded sample cell populations. Four chambers on each array were dedicated as controls with half being positive controls defined as chambers containing cells fixed with 4% paraformaldehyde and stained with PI. The other half of chambers were left unaltered.

4.3.7 Magnetic collection of ejected pallets

Prior efforts to ease the collection of captured cells on micropallet arrays led to the invention of pallets with imbedded ferromagnetic iron nano particles[5] in order to enable collection with a magnetic probe.[84] Nickel sidewalls resulted in similar magnetic retrieval capabilities as the internal iron particles without the corresponding light transmission loss. Although the sidecoated pallets were collectable, they exhibited much weaker magnetic response forces and thus required the collection probe to be brought much closer to a desired pallet during collection. Thicker nickel plating may be beneficial to ease the

proximity requirements for probe attraction. Figure 4.3.3 displays an example of pallet ejection and transfer.

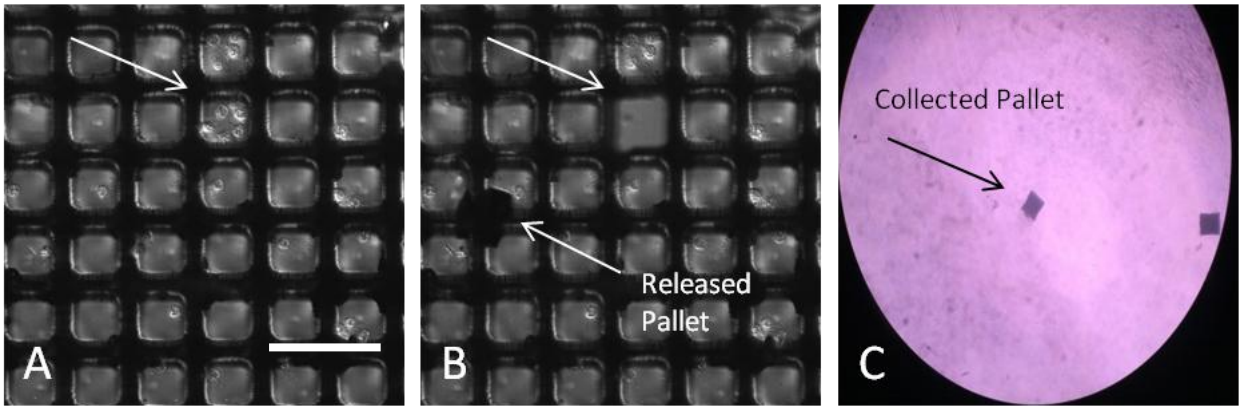

Figure 4.3.3: Ejection of sidecoated pallets and collection in cell media
A) An individual pallet with seeded cells is selected for laser release as indicated by the white arrow. The scale bar is 110 µm. B) The released pallet can be found a short distance from its original location after ejection. The settling point is typically within 300 µm of the ejection site. C) The pallet is then collected with a magnetic probe and released into a separate multi-well plate.

A method of ejecting pallets by laser has been previously described[9] and was successfully utilized for GSM release before retrieval.[76,77] The laser ejection process described in section 2.4.9 was very similar to the method used for GSM pallet ejection except less energy was required, around 1 mJ, to accomplish a full ejection. Theoretically there should have been a greater adhesive force generated by the formation of the nickel layer spanning from every pallet to the glass slide surface, but this force did not change any of the laser ejection settings required for consistent pallet release. Released pallets were located on the surface of surrounding pallets within a 300 µm radius of the ejection site and collected with a magnetic probe.

4.4 Results and Discussion

4.4.1 Modeling imaging properties of side coated micropallets

FRED ray tracing software (Photon Engineering, Tucson, AZ) was used to model the light transmission properties of standard micropallet and GSM arrays. Geometric shapes representing the size and scale of each GSM feature were generated within the software and a point light source emitting 526

nm wavelength light was simulated at the surface of an individual pallet to represent the fluorescent emission of a captured cell. 600,000 individual photon paths were modeled with a 180° spread from the source. GSMs and standard micropallet arrays were generated using different surface features corresponding to their real life material properties. For GSMs, the walls of micropallets were set as reflective boundaries with 65% total energy retention per ray interaction while the standard pallets were generated as completely transparent features. 1002F photoresist structures had an internal refractive index of 1.6 while the glass slide surface had a value of 1.5. Water was modeled to span the surfaces of the arrays and had a refractive index of 1.33. Gaps between the pallets would be expected to contain air walls due to hydrophobic surface properties and had a refractive index 1. The top facing surface of the glass slide on GSMs was covered with a 7000 Å reflective layer while standard arrays were created with unaltered glass surfaces. The reflectance for the nickel surfaces was set to 65% corresponding to the behavior of the material given the input wavelength of 530 nm.[110] Pallets on both the GSMs and the standard arrays were completely transparent. Although these settings represented a simplified, idealized system, the selected feature properties were chosen to provide insight into expected real life results when using the devices and projected whether or not extended research into GSM usage was warranted.

Intensity values produced by the point light sources were generated at a plane parallel to the bottom surface of the simulated glass slide. These intensity values represented the light transmittance efficiency through the pallets directly beneath the point source. The irradiance values on the analysis plane generated for the GSMs were compared to those generated for standard micropallets. The results for this model are show in figure 4.4.1 along with an example of the visualized side coated pallet system.

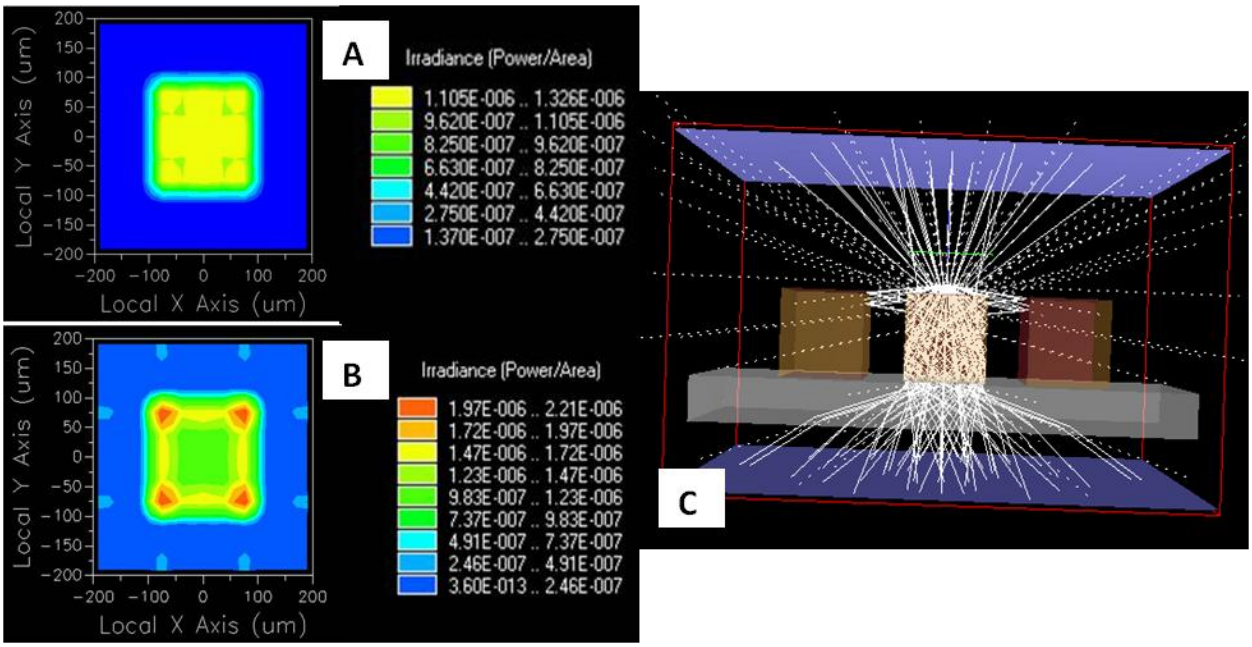

Figure 4.4.1: Irradiance of light captured beneath simulated micropallets
(A) Irradiance of region just below standard micropallets with transparent walls. Peak irradiance achieved was 1.32E-006 AU. (B) Gold sidecoated micropallets with reflective walls. Peak irradiance achieved was 2.21E-006. While less uniform, the GSM model achieved a higher peak irradiance than standard arrays. C) Visual representation of photon rays being projected downward from a point source located 20 µm above the center pallet structure. The reflective walls of the pallet keep all light captured within the pallet inside and underneath the pallet while the light moving towards the other pallets are reflected away from them. The pallet was modeled as a 40 (W) x 40 (L) x 50 (H) µm structure.

While the simulated irradiance of light on the plane below GSMs representing a microscope objective was less uniform than standard arrays, a higher peak magnitude was achieved. This result indicated that smaller signals that may be more realistic for biological samples would be better preserved through GSMs than standard pallets enabling a more robust system of detection. Stronger signal intensities would also allow for better differentiation of different colors on individual pallets as well allow for better tracking capability of cell position on the surface of the pallets. Another important point is the drastic difference in diffuse photons gathered at the bottom analysis plane. The blue regions on both images represent the lowest values of irradiance in each system. Standard arrays had a minimum value only one order of magnitude below the peak signal intensity. GSMs, on the other hand, showed seven orders of magnitude differences in signal intensity. The contrast produced by the reflective walls patterned over pallets would allow for simplified automation of pallet detection.

4.4.2 Light transmission and spread analysis

The average signal intensity at the top and bottom surfaces of GSM and standard arrays were analyzed and compared using a student paired t-test. While the intensities of the fluorescent signal collected at the top surface of the pallets were not significantly different among array types, transmission of the fluorescent signal through the pallets to their bottom surfaces differed. It was found that when imaging the bottom surface of GSMs, there was significantly higher average signal intensity when compared to standard arrays. GSM arrays exhibited an average signal transmission of 32.3% of the top surface signal while standard arrays exhibited 24.2% with a p-value of 3.89E-4 from 40 samples analyzed on each type of array. Furthermore, beads seeded to GSM arrays displayed significantly less signal spread from the seeded pallet, preventing false signal acquisition from surrounding pallets. The average signal spread distance for GSM arrays was measured to be 3.2 μm from the edges of pallets while spread for standard arrays ranged from 10.2 μm to 30.1 μm depending on distance of the seeded bead to the edge of the pallet. The two imaging improvements achieved by metal side coating micropallets have great implications for generating automated systems for micropallet analysis. Imaging the bottom surface of micropallet arrays creates the most visual contrast from pallet to surrounding borders and would best be utilized for forming scripts for detecting cell signal and ejecting corresponding pallets. Standard arrays imaged at this ideal height displayed fluorescent signal bleed into pallets without beads on their surface, making automated pallet selection difficult. Opaque metal side coatings on the arrays sequestered fluorescent signal to just within the corresponding pallet, enabling faster and more accurate cell detection. Signal intensity improvements at this height would allow for the detection of low cell expression levels and improve the utility of the technology.

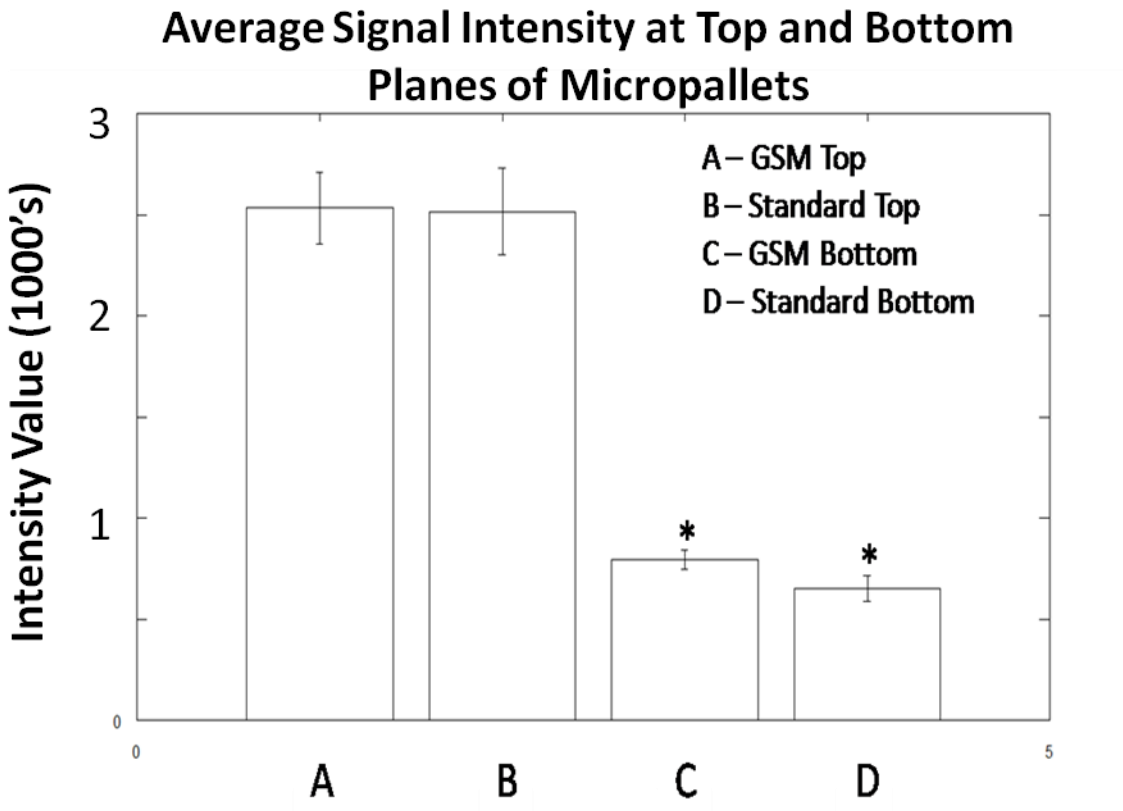

Figure 4.4.2: Average sample intensity at the top and bottom surfaces of micropallets
GSM refers to the gold side coated micropallets. The side coated pallets expressed significantly stronger intensity at their bottom surface when imaged by a confocal microscope compared to their uncoated counterparts. This difference is important because when targeting pallets for automated detection, it is the most simple to focus on the bottom plane of the arrays which best clarifies the perimeter of each pallet. As imaging is being conducted on the bottom surface, fluorescent expression of captured cell samples must be translated through to the bottoms of the pallets in order to have proper detection.

4.4.3 Cell viability on sidecoated micropallet arrays

Fixed cells fluoresced secondary to PI uptake through their compromised cellular membranes, a routinely used cell viability stain. Cells on both the GSMs and the standard arrays reflected the same level of healthy cell retention expressing fluorescent emissions from an average of 23 cells per 10,000 within a chamber, resulting in a 99.9% viability rate over a span of 24 hours. This level of viability was contingent upon the integrity of the exterior gold layer which were consistently maintained during cellular work.

Figure 4.4.3 is a representative image of cell viability testing.

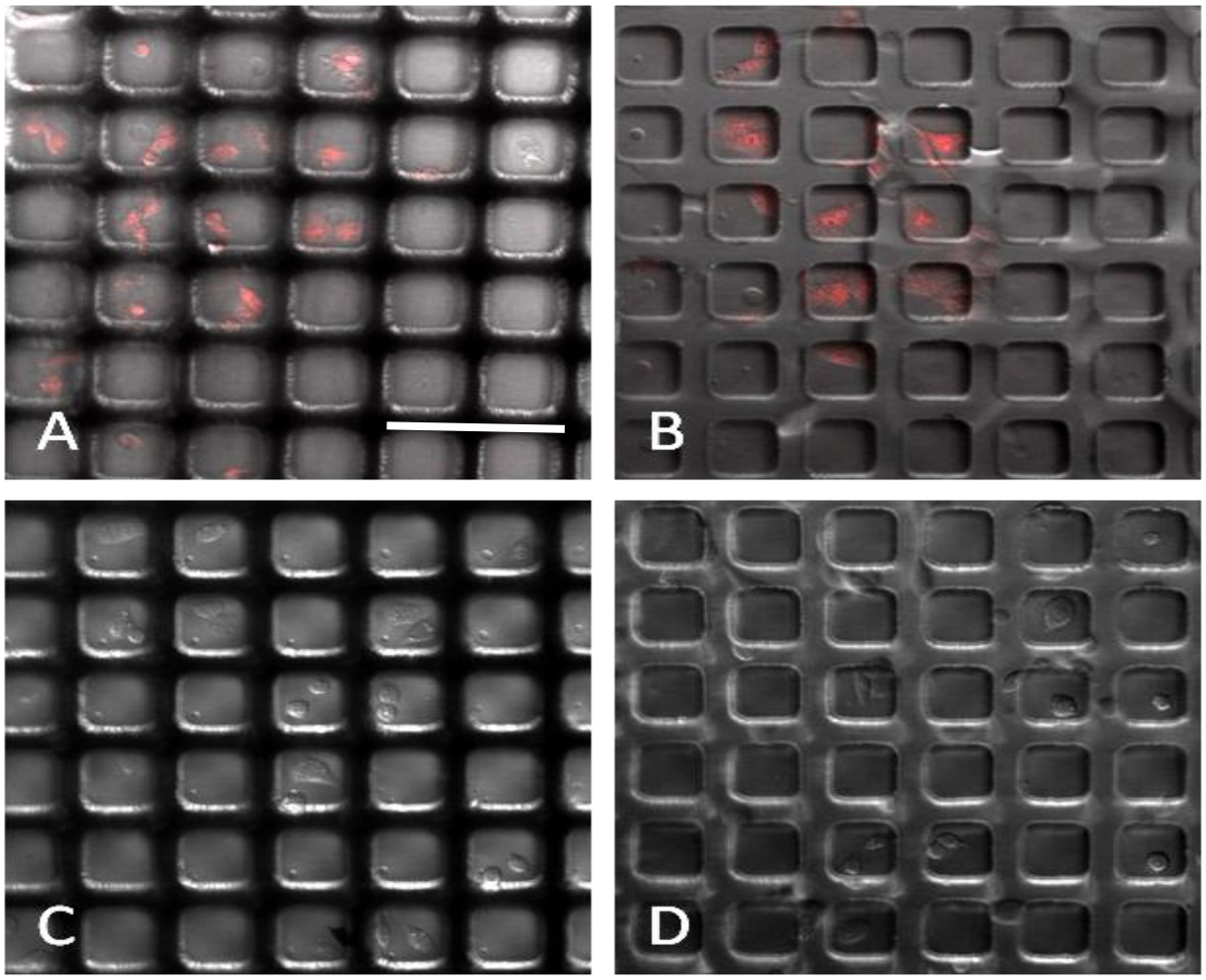

Figure 4.4.3: Propidium Iodide stain of cells captured to side coated micropallets
(A) Fixed 3T3 fibroblasts exhibiting fluorescent excitation of internalized propidium iodide (PI) plated on gold side coated micropallets. The scale bar is 110 µm. (B) Fixed 3T3 fibroblasts on standard micropallets. (C) Unfixed 3T3 fibroblasts showing no uptake of PI, signifying retained cell viability. (D) Unfixed 3T3 Fibroblasts on standard micropallet arrays exhibiting no PI uptake.

These early positive viability results created an important foundation for gaining confidence in the biological application of metal side coated micropallet arrays. Future work with the technology can be performed confidently as more relevant cell types and applications are tested. The images taken during the viability testing protocol also accentuated the contrast improvements achieved by the formation of the opaque nickel walls. Cellular forms and fluorescent signal were much clearer than those produced by standard micropallet arrays under the same visualization conditions as can be seen in the above figure.

4.5 Chapter 4 Conclusion

This chapter focused on exploring the prospect of utilizing a novel short wavelength enabled electroless nickel plating process to enhance micropallet array functionality. By experimenting with the UV electroless plating process, it was found that micropallet arrays adorned with nickel side wall coatings on every single micropallet could be fabricated by immersing whole arrays into electroless solution but keeping the top surfaces of the arrays blocked during plating. Up to this point, physical alteration to micropallet structures formed from 1002F photoresist had yet to be explored.

The nickel / gold side coating of micropallet arrays lead to increased transmission of light through pallets and decreased the amount of false signal generated by scattered light to the pallet proximity. These differences were especially notable when the pallets were imaged at their bottom surfaces which was significant due to that surface being ideal for potential automated sample detection software. Sidecoated arrays displayed adequate biocompatibility for cell sorting and also simplified sorting procedures by enabling magnetic collection of individual pallets upon their release. Microstructures made of 1002F photoresist with various shapes and sizes other than standard micropallet arrays could be sidecoated using the same methods established for the standard arrays. Larger and alternate microstructure shapes could expand the potential different types of cell sorting procedures which are otherwise impossible with the current micropallet form. Some images of different nickel sidecoated ships are included in Appendix C figure 6.3.1.

Future work with sidecoated micropallet arrays should first focus on improving on the robustness and repeatability of the side coating process. The methods described in this chapter yielded functional sidecoated micropallet arrays with every attempt, but oftentimes unusable regions of completely metal coated micropallets were formed in aggregate around the proximity of the micropallet arrays. Poor blocking of the top surfaces of the micropallet arrays during electroless plating was attributed to this issue. One method with the most potential for ideal pallet surface blocking is the formation and retention of sacrificial layers on the tops of micropallets during electroplating. Large scale surface blocking (such as the adhesive covering method used in this chapter) for the microscale micropallet array was not ideal

as uniform force distribution could not be checked during the procedure. Other large, physical barrier methods for blocking electroless plating on the tops of the micropallets should include a checking method to identify force distribution before immersing the micropallet arrays in electroless plating solution.

Chapter 5: Electronic Release Micropallet Array

5.1 Introduction

The micropallet array and its subsequent technological innovations have enabled scientists to manipulate single adherent cells and cell colonies while keeping them in contact with a growth substrate. Although the technology has been proven to be a useful tool, the many changes made to the system all rely on the same modality of utilizing a laser joined to a microscope for pallet selection and release. While this method is straightforward in practice, the specificity of the required technology limits the use of the arrays to users who readily have access to expensive imaging systems. These systems not only have prohibitive costs associated with their purchase and maintenance, but are also commonly used as shared resources among a vast number of labs resulting in undesirable scheduling conflicts which could hinder time sensitive biological studies. There is a need to translate the micropallet array for use with standard phase contrast microscope systems without paired laser systems that are more commonly found in research labs. As sample imaging on micropallet arrays is straightforward and can be done on most microscopes already, improvement efforts were directed to the release mechanism of the system to relieve the laser ejection requirements of the technology.

This chapter describes the ongoing work to make a micropallet array system with electronic release capabilities to circumvent classic laser release requirements. Micropallet arrays were fabricated on top of an x-y array of electrically conductive metal traces designed to electrolyze water and produce bubbles upon electrocution, enabling the selection of individual pallets placed over each point of trace intersection. The array of horizontal traces was separated from the vertical trace array by a transparent, biocompatible layer of UV patterned 1002F photoresist in order to prevent circuit shorting at unwanted locations. Although there are several possible ways to perform pallet ejection using such an array, as will be described later, the work that was accomplished for this study focused on the use of strategically patterned traces to produce microbubbles at specified locations by the electrolysis of water to generate gas

bubbles beneath pallets and eject them from the surface of the array. Regardless of what release mechanism was pursued, the most important constraints to the design of the system that were maintained included optically transparent pallets, consistent electric pallet release, and release dynamics that didn't damage captured cells.

5.2 Bubble Generation by the Electrolysis of Water

In order to make electrically addressable micropallet arrays, several potential current driven release dynamics were considered. Methods ranging from those with complicated moving components such as electrically triggered ejection cantilevers placed beneath pallets to a much more passive method of heat enabled sacrificial material decomposition were reviewed. Ultimately, several options were deemed feasible during brainstormed so selection came down to time availability to explore the options. The first method tested was the creation of bubble formation chambers beneath every individual pallet to force ejection via force generated by the expansion of gas bubbles.

The capability to produce bubbles by the electrolysis of water has been well documented for various applications.[111-113] Put simply, when two electrodes are placed separately in a shared volume of water and connected to an active power source to form disconnected cathodic and anodic elements, gas bubbles form at the electrode surfaces. The bubble generation phenomenon occurs due to the degradation of water (H_2O) to hydrogen gas (H_2) and oxygen gas (O_2) driven by the charge accumulation at the cathode and anode respectively as current passes from one electrode to the other through the water. The more conductive the shared liquid medium, the greater potential for bubble formation. The newly formed gasses create nano bubbles which quickly join with one another into larger bubbles which then float away from the electrodes. While the processes is relatively straightforward, pure water's low conductivity typically requires extreme electrical currents to produce bubbles. Oftentimes it is necessary to include electrolyte additions such as salts to increase the solution conductivity leading to a lower energy threshold for gas formation. Electrolysis bubble formation lent itself well to use with micropallet array technology because the formation of bubbles occurs in a predictable manner and the products of the reaction are

known to be biocompatible. Furthermore, media used for cell culture is typically highly conductive and so the inclusion of a electrolysis-ready solution does not infringe on healthy cell retention.

5.2.1 Location Specific Electrolysis Bubble Formation

Translation of electrolysis bubble generation to use as an ejection force for micropallet arrays required the sequestering of electrolysis events to just beneath individual pallets. The two major constraints to this consideration were the ability to form traces small enough to fit beneath cell colony sized pallets and also to be able to contain volumes of water into microwells so as to prevent liquid bridging from one electrode couple to another. Initial feasibility testing aimed to show that bubbles could be generated on command at user specified locations on a glass slide. The total number of electrode couples was kept low so as to not generate needless fabrication complexity for the proof of concept work.

The first set of devices fabricated for electrolysis bubble testing were created from gold coated glass slides strategically etched to form a series of square pads joined to traces forming electrode couples. 1 inch by 3 inch glass microscope slides (VWR, Radnor, PA) were washed in piranha etch solution (H_2SO_4 and NH_4OH at a 3:1 ratio), rinsed in water and dehydrated with nitrogen gas followed by a 30 minute bake in a 120˚ C oven . The slides were electron beam deposited (Vesco, Estero, FL) with 1000 Å titanium seed layers followed by the deposition of 2000 Å layers of gold. Gold adherence to the slides was confirmed using standard tape-lift tests. The gold coated slides were rinsed in isopropyl alcohol and dehydrated in a 120° C oven for 30 minutes. To pattern the gold coated slides into a desired electrode array configuration, photolithography assisted selective etching was performed. 5 µm thick Shipley photoresist was spin coated over the surface of the gold slides and baked at 60°C for 3 minutes to solidify the resist. A film transparency photomask bearing the positive design of the desired electrode array pattern was placed over the surface of the samples and secured between two quartz plates with clips. The samples were placed beneath a collimated UV light source (AB&M INC, Scotts Valley, CA) and irradiated at 1200 mJ/cm^2 to pattern the resist. After irradiation, the Shipley was developed in Microposit 351 developer (Dow Chemical, Torrance, CA) for one minute and rinsed with isopropyl alcohol, washing

away any resist that was exposed to the UV. The slides were hard baked at 90° C for 15 minutes to complete the photolithography process. Following the creation of patterned Shipley, the slides were etched to only leave the metal protected by the resist, creating the desired electrode configuration. The slides were first immersed into a gold etchant (Transene Company, Inc., Danvers, MA) for one minute and rinsed with diH_2O, leaving the titanium seed layer exposed at all regions not protected by the Shipley. The titanium was then etched in 2% hydrochloric acid (HCL) for 30 seconds or until all titanium was visibility dissolved from the slides. Following a rinse in diH_2O the slides were soaked in acetone for 30 minutes in order to dissolve the remaining resist. It was found that a manual surface abrasion using a cleaning swab was necessary to completely eliminate the photoresist from the slides and completely expose the gold below.

Initial electrode array designs included several junction points of traces coming from opposite sides of the glass slide and meeting in the middle. These junctions were designed to have the opposite traces to approach one another without making contact. The trace width was drawn to 50 µm, but the total surface area of each trace within a 200 µm junction area was altered by drawing different trace geometries to test changes in bubble formation based on shape. Two different pad configurations were tested. The first design had individual pads stemming from each trace while the second design had all traces on one side of the slide joining to one single universal pad with individual pads allocated to the traces coming from the opposite side. The second design represented a more realistic configuration for completed devices and was created to test whether adequate charge accumulation could be generated within a single trace junction to form bubbles even with current passing through several other traces sharing the same pad. Figure5.2.1 shows the mask designs of several different trace geometries as well as the completed gold traces using the mask.

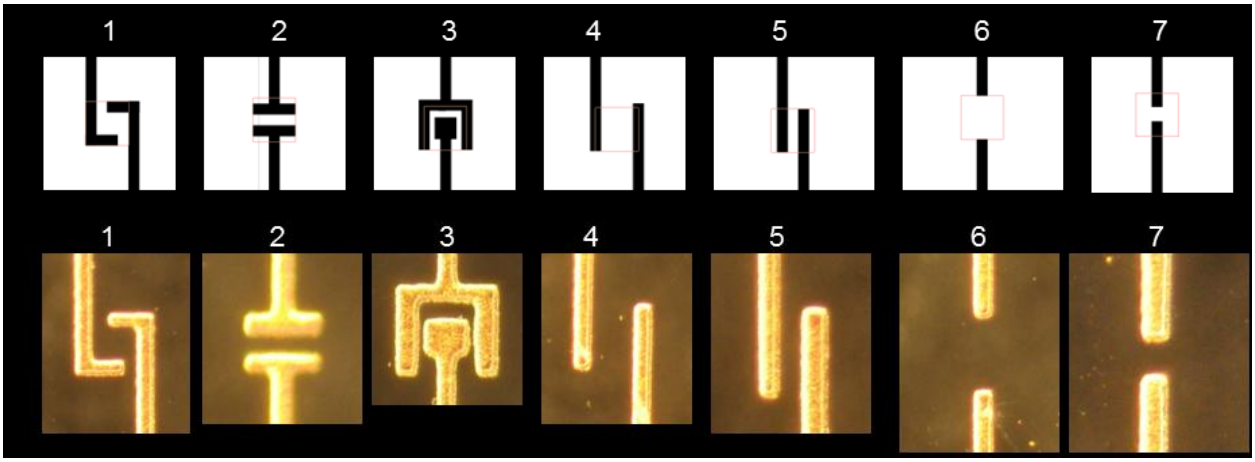

Figure 5.2.1: Gold trace junctions for electrolysis bubble formation
The top row shows mask designs used to pattern positive photoresist before gold etching. The thin red square included in each design is a theoretical 250 µm pallet that would be placed over the junction for ejection testing. The bottom row shows final traces corresponding to the mask designs above, fabricated from a gold coated glass slide. All traces were fabricated to be 50 µm in width. The different junction designs were tested for hydrolysis bubble formation capabilities.

Once the electrodes were fabricated, the next step was to sequester each couple with their own volumes of water. 8-well circular Labtek chamber slides (Nunc, Naperville, IL) were sawn into pairs to better fit the design of the electrode arrays. Individual wells were adhered with polydimethylsiloxane (PDMS) over each electrode junction in a manner to keep the gold pads extending from the electrodes exposed for user interfacing while sequestering each junction. The pads were then soldered to wires for simple power source interfacing with alligator clips. Figure 5.2.2 displays the experimental prototype and its setup for use. 1x phosphate buffered saline (PBS) was tested for bubble formation potential. PBS solution was selected as a model liquid for this study due to its known biocompatible and high electrical conductivity of around 15,000 µmhos/cm. The junction to be tested was then linked to an external power source and several voltage and current settings were tested for bubble formation potential.

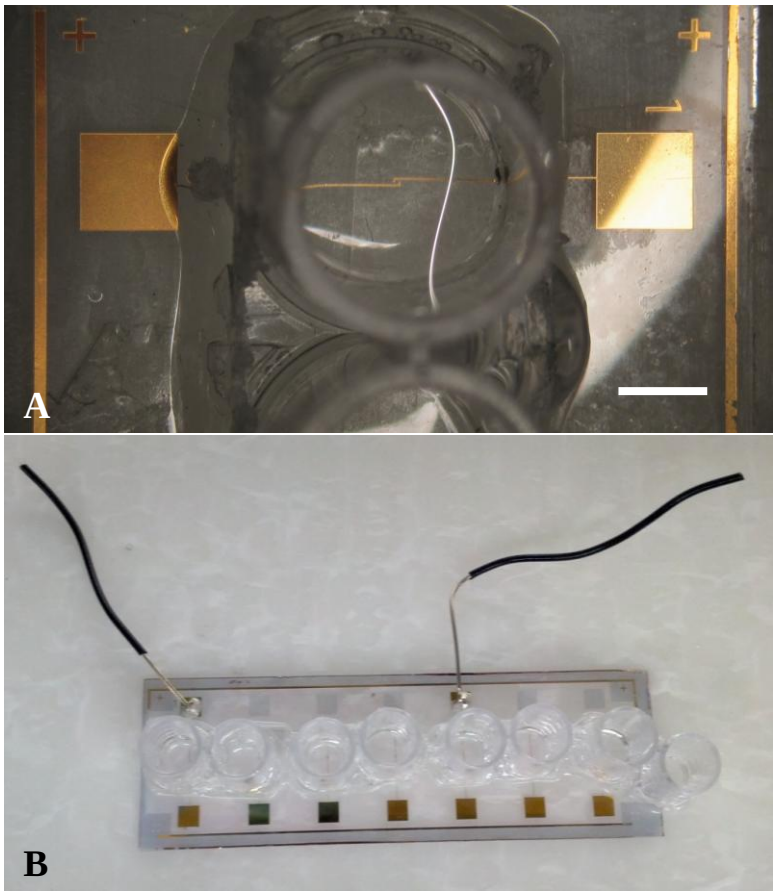

Figure 5.2.2: Electrolysis bubble formation testing prototype
Seven differently shaped junction trace designs were patterned from gold onto a slide with 14 corresponding pads for voltage application. A circular culture chamber array was adhered around each junction with PDMS to allow liquid retention over the traces without wetting the pads. A) Zoomed single testing junction. The scale bar is 5 mm. B) Single testing device with seven different junction designs being tested. Wires were soldered to the exposed pads to send current to the junctions from a power source. The glass slide dimensions are 25.4 mm by 76.2 mm.

Bubble formation occurred readily and repeatedly at the specified junction points. Formation on the gold electrode surfaces happened immediately upon turning the power source on and continued steadily until the power was shut off when using the correct settings. For the duration of these experiments, power source current output was set at 1.5 A and voltage was adjusted based on the device being tested. Variation in voltage was directly related to the variations in bubble formation rate with higher voltages resulting in faster bubble generation rate. The voltages used in this study ranged from 2 V to 6 V with 4 V being the average setting. Voltages below 2 V applied to the systems described in this chapter created microbubbles on the edges of traces, but formation was never rapid enough to aggregate

and combine bubbles to form combined large area bubbles sought for this work. Another characteristic of the bubble formation had to do with the relative proximity of the electrode to one another. Initial theorizing predicted that bubbles would only form at the specific junction point between the two electrodes because of the limited charge accumulation capability of the small scale traces. In practice gas was generated along the entire length of both of the traces at all areas submerged in the PBS. This result was most likely due to the highly conductive nature of the PBS which caused the entirety of the electrodes to be treated as a system instead of just the areas at a close proximity to one another. Adjusting to lower voltages results in less bubble formation at locations away from the junction but the result was never completely eliminated.

Judging from the preliminary results, it was concluded that in order to have site specific bubble formation there was a need to separate regions of the traces where bubbles were undesired from the liquid above using a physical barrier. There were many commonly utilized methods to pattern thin films over surfaces available that were capable of creating liquid tight seals. For initial testing, a method of patterning silicon nitride was utilized to cover regions where unwanted bubble formation could occur. Gold electrode coated glass slides, identical to those prepared previously, were washed in isopropyl alcohol, dehydrated at 120˚ C, and coated in a 5 µm layer of Shipley photoresist as described above. The Shipley was patterned using a film photomask resulting in the formation of structures on each of the square 200 µm by 200 µm electrode junction points as well as the pads. Once the Shipley was formed, the slides were coated in silicon nitride by chemical vapor deposition using an EasyTube 3000 system (firstnano, Central Islip, NY) to 500 nm in thickness. The resist was then developed, exposing the regions of the electrodes that were initially covered during the silicon nitride deposition step. In this way it was possible to only have the trace junction region exposed to the PBS solution above while covering the undesirable regions. Initial testing using the previous settings for bubble formation resulted in bubble formation only occurring at the exposed electrode junctions as expected. However, prolonged activation lead to delaminating of the silicon nitride from the glass surface and micro bubbles began forming beneath the film. Soon after initial delaminating, tearing occurred over all electrode regions beneath the

silicon nitride. Figure 5.2.3 displays the progression of a previously unused silicon nitride coated electrode junction to the eventual delaminating and unwanted bubble formation along the gold trace surfaces. This study proved that while conceptually the idea of only exposing the electrode junction to the fluid could result in location specific bubble formation with electrolysis, it was necessary to use a more robust insulating material to make a longer lasting cover layer.

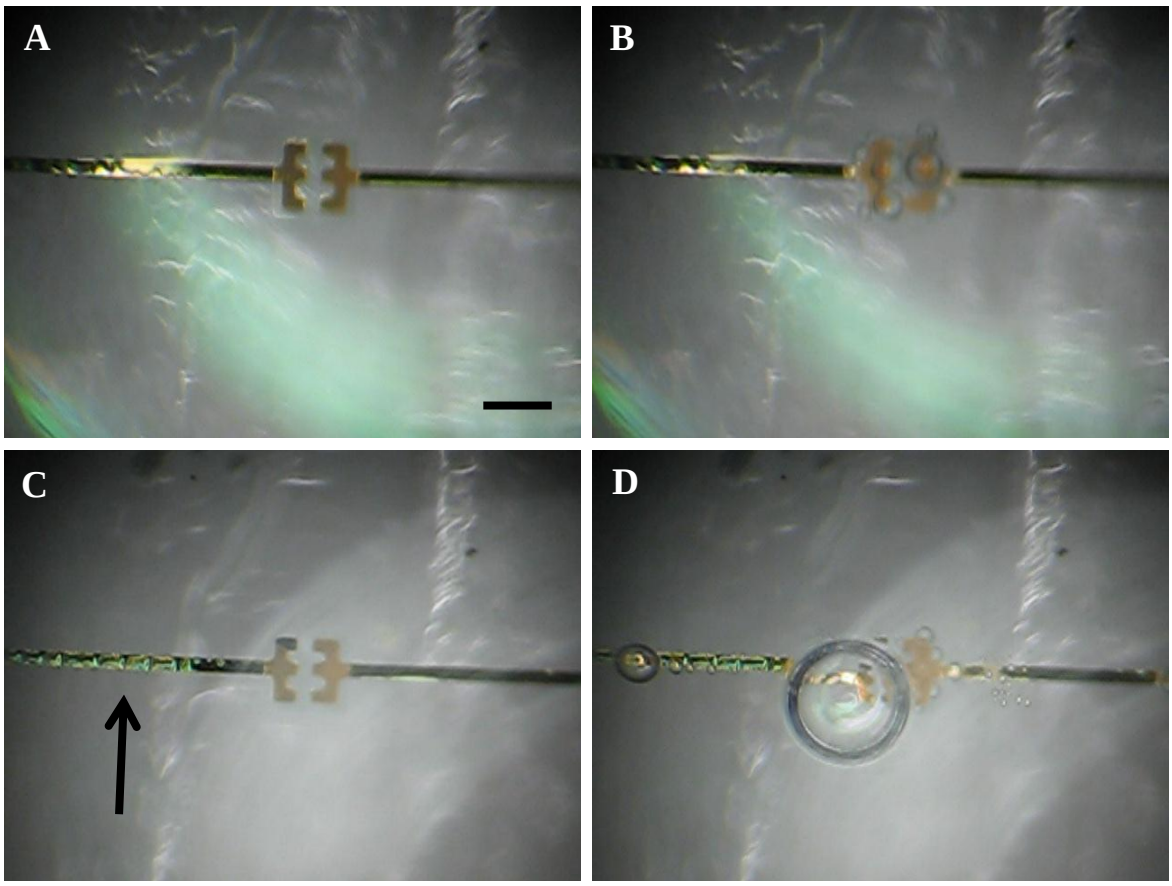

Figure 5.2.3: Electrolysis bubble formation at an exposed electrode junction
A single trace junction is exposed to conductive phosphate buffered saline (PBS) through an insulating silicon nitride layer. A) Test junction before application of voltage immersed in 1x PBS. The scale bar is 200 µm. B) Bubble formations during application of current. C) Delamination of silicon nitride layer caused by bubble formation as highlighted by an arrow. C) Second current application leading to bubble formation at the junction region as well as beneath the delaminated and torn silicon nitride.

A second attempt to cover trace regions on the slides was repeated using 50 µm thick patterned 1002Fphotoresist. The 1002F was patterned using the same methods as described in the previous chapters, but it is important to note that a negative version of the mask that was used for Shipley patterning had to be fabricated ahead of time due to 1002F being a negative photoresist while Shipley is a

positive type. The 1002F film layer proved to be a much better barrier material than the silicon nitride and held up to repeated on / off experimentations with no unwanted bubble formation occurring on the covered trace regions. The resist was also known to be biocompatible and was easy to work with due to vast prior experience fabricating with the material. Utilizing the new film, it was shown that the electrolysis of water could be repeatedly performed in order to generate micro bubbles at specified locations. At this time, it was concluded that the project could move forward into designing more complicated systems to be eventually integrated with actual micropallet arrays.

5.3 X-Y Electrolysis Bubble Junction Design

The primary constraint to the development of an electrically controlled micropallet system was the small feature size of standard single cell micropallet structures. The 50 μm by 50 μm pallet geometry incurred fabrication limitations due to the need for thousands of traces to be fitted side by side with no contact within a very limited space. While creating a tightly packed branching trace array is possible with precision metal etching or deposition techniques, the process would be complicated and not scalable due to manually intensive fabrication requirements. It was also unknown whether the small trace surface areas would be capable of carrying the charge required for bubble formation by electrolysis. These constraints, however, were by intending the design of the system to be for larger sized pallets such as those utilized for adherent cell colony sorting described in chapters 2 and 3. The additional space afforded by the colony pallets enabled both wider traces, which eased fabrication, and greater spacing from one trace to the next which increased robustness by allowing larger margins of error. Even with the alleviated space requirements, it was decided that the system would require an x-y overlapping trace array configuration, as opposed to a interwoven collection of tightly packed traces, in order to achieve single pallet release capability given the high number of individual structures that needed to be addresses.

5.3.1 Fabrication of X-Y Bubble Junction Devices

The process for creating the initial prototypes for x-y electrolysis bubble generation arrays was very similar to the development of the previous study for single plane electrodes as described at the

beginning of this chapter. In addition to the selective etching of gold to form traces and the patterning of spin coated 1002F photoresist, a third step of depositing nickel onto the 1002F to form a second set of traces was utilized. The 1002F layer was used as an intermediary in order to prevent shorting of the crossing traces to make specific x-y position stimulation possible. The two sets of traces will henceforth be referred to as bottom side traces (those underneath the 1002F) and top side traces (patterned on top of the 1002F). Gold coated glass slides were patterned using the same methods as the previous section, but with a new photomask design. Pads were fabricated on one side of the glass slide with 50 μm wide traces extending from the pads down the length of the slide. Each horizontal trace extension had four perpendicular branches protruding vertically that were 500 μm in length that were intended to form the electrolysis junctions with the traces to be fabricated on top of the 1002F. After patterning the bottom side traces, the slides were cleaned with isopropyl alcohol and dehydrated. 1002F photoresist was spin coated onto the slides to a thickness of 50 μm and patterned in a manner to expose the gold pads and 200 μm by 200 μm squares encompassing the vertical branches extending from the traces. The squares were aligned to contain the branches to a single side in order to maximize room for the top side electrodes to share the chamber without making contact with the other trace. The bottom side electrode and 1002F layer are shown in figure 5.3.1.

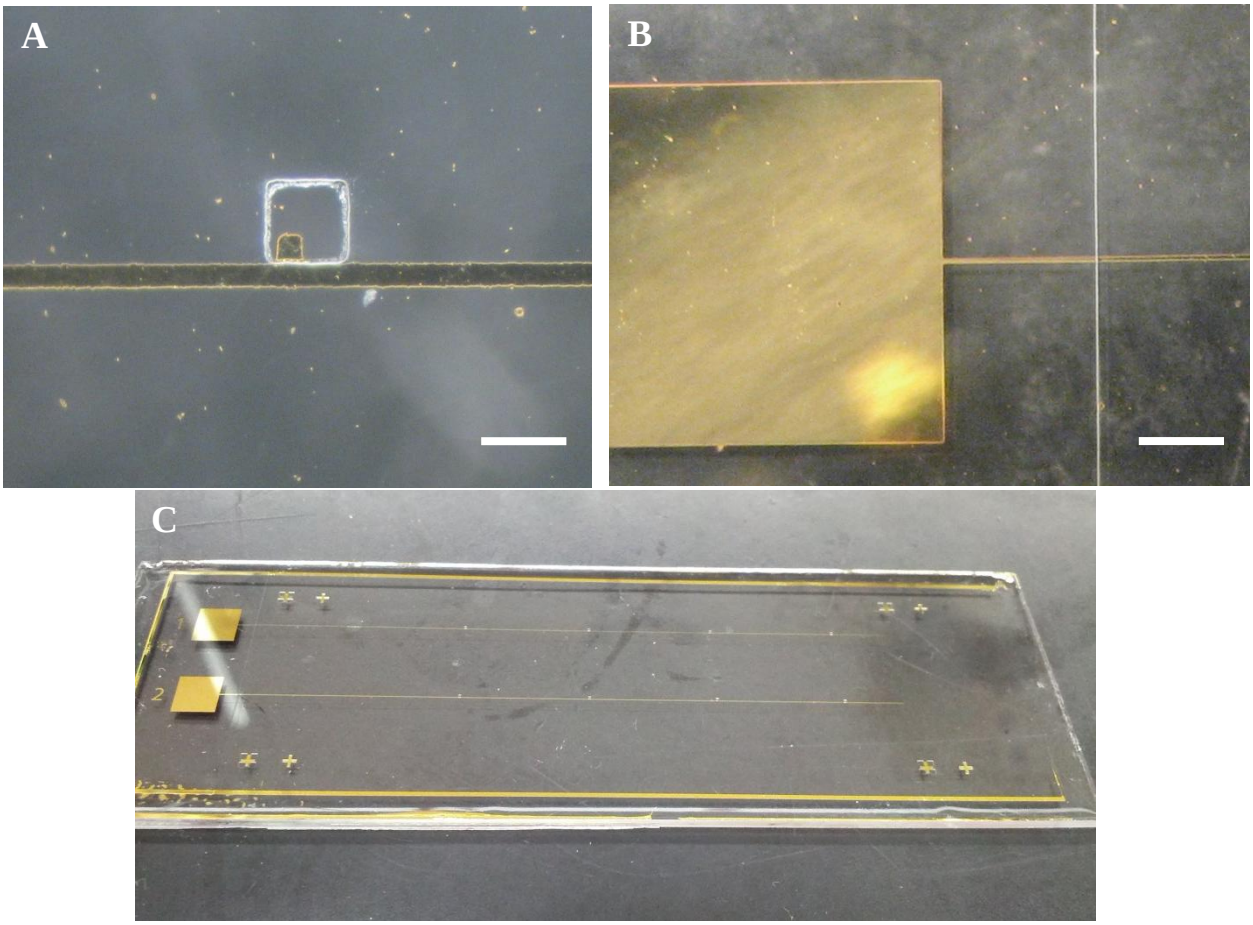

Figure 5.3.1: Patterned gold bottom side traces covered with 50 µm thick 1002F photoresist A) 50 µm wide trace with a branching structure designed to form a junction with top side traces. A 200 µm by 200 µm square hole was patterned in the 1002F layer to expose the junction. Scale bar is 200 µm. B) Large gold pad designed for user interaction. The 50 µm wide traces were too small to work with so they were designed to extend from larger pads 5 mm pads. The sharp white line on the right side of the image is the border of the 1002F layer. The pads were exposed to allow trace excitation. The scale bar is 1 mm. C) Complete image of glass side (25.4 mm by 76.2 mm) with bottom side traces and 1002F layer. The plus signs at each corner of the device are alignment markers.

The process to create the top side traces used a method of altering the wettability of surfaces using short wavelength ultraviolet (UV) irradiation in order to achieve patterned metal deposition by electroless plating. This process was brought over by collaborative partners from Kanto Gakuin University and Koto Electronics Co. in Japan. These organizations have documented the use of short wavelength UV for patterned metal deposition.[109] In short, many polymer materials can be roughened to nano scale depths using high powered short wavelength UV irradiation. The nano roughening of the polymer surface causes greater hydrophilicity than unaltered areas of the same sample. By using an

opaque photomask, short wavelength UV light could be sequestered to select regions in order to pattern hydrophilic regions on materials that otherwise exhibit hydrophobicity. The areas of the polymer that were roughened were then readily metal plated using electroless deposition, which is a wet procedure, while the unaltered surfaces were unable to be plated. For this project, a 1 inch by 3 inch quartz slide coated with a layer of opaque titanium was selectively etched to reflect the features of a film photomask bearing the top side electrode configuration. For the short wavelength process, materials with greater light transmission characteristics were required to be used in place of standard film masks to allow adequate passage of the UV light. The mask was aligned to the electrode arrays over the 1002F layer and placed into Koto's short wavelength UV lamp system. The lamp emitted 254 nm and 184.9 nm wavelength dispersed light within a metal enclosure. The stage holding the device was raised to 30 cm from the lamp and held for 3 minutes of exposure time. Only the regions of the device beneath the transparent portions of the titanium photomask were altered by the UV light. Being a liquid driven reaction, the electroless plating of metal to follow the UV irradiation required a hydrophilic sample surface in order to generate sufficient liquid to surface contact to enable electroless deposition. By limiting the amount of time the samples were immersed in the plating solutions, it was possible to only plate those regions most likely to be wetted which were in this case the UV treated areas. The two most commonly utilized electroless plating metals were copper and nickel. While both metals were not idea for biological usage, the nickel electroless plating solution was selected as it was known to be more stable and less cytotoxic than copper. Also, any metal plating done during this step could be further plated with gold to increase biocompatibility. This plating process had not previously been tested with 1002F photoresist, but initial plating tests using the previously established settings resulted in repeatable metal patterning on the resist. The top side trace mask was aligned in such a way as to have the vertically extending traces overlap with the opposite side of the square holes as the bottom side trace branches displayed in figure 5.3.1 (A). The mask design was intended to generate the side wall coating of the 1002F, as described in chapter 4, in order to bridge sections of the top side traces plated on the surface of the 1002F with the plated metal on the glass within each chamber. Because electrolysis bubble formation required there to be zero contact

between the two traces at a junction, alignment of each layer with respect to one another was vital to the success of the fabrication of the devices. Figure 5.3.2 includes a 3D CAD design drawn in Solidworks (Dassault Systemes, Velizy-Villacoublay, France) rendering of the device junction and the completed device.

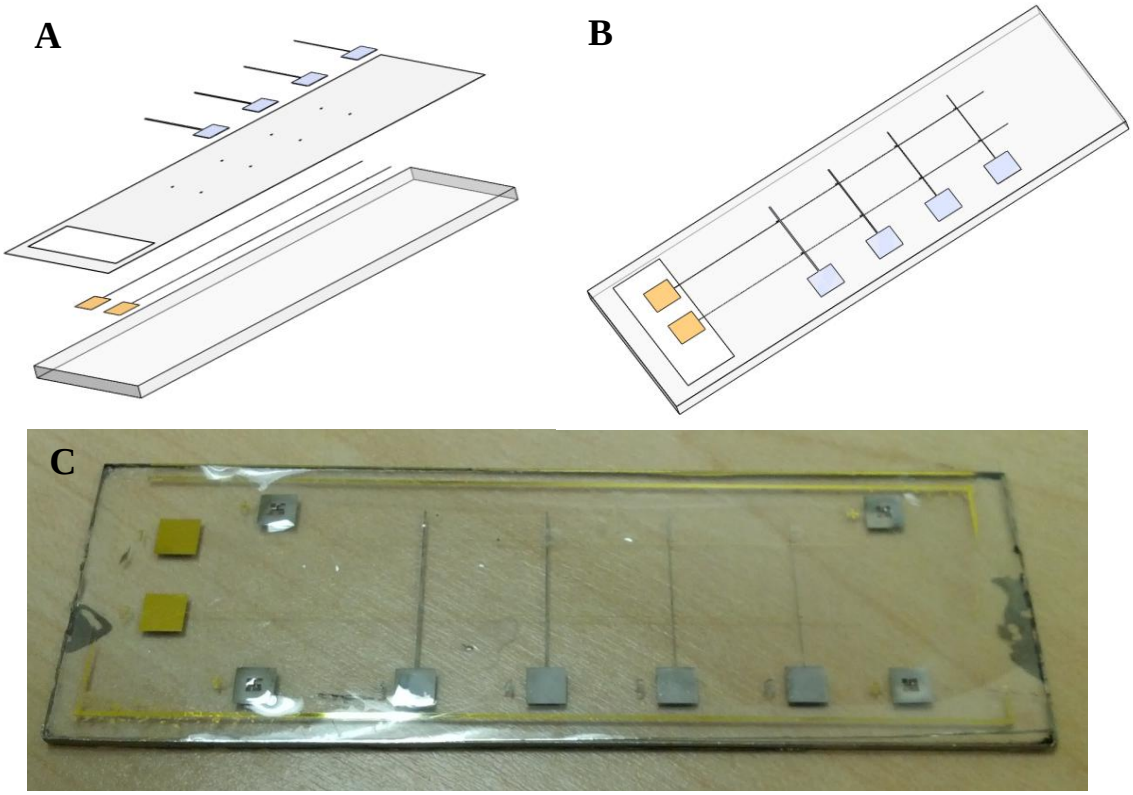

Figure 5.3.2: Three layer x-y trace bubble formation test device
The first layer included patterned gold horizontal traces extending from pads on the left side of the device. The second layer is a transparent 1002F insulating layer which had via holes patterned to form each junction point. The third and final layer was electrolessly plated vertical nickel traces extending from pads located at the bottom of the slide. The nickel was selectively plated onto the 1002F layer by utilizing a short wavelength UV surface preparation method. A) Solidworks rendering of exploded view of the device exposing each layer. B) Solidworks rendering of top view of device displaying intended alignment. C) Real completed x-y bubble formation test device. Alignment marks can be seen near the four corners of the slide. Some unintended nickel plating occurred near the edges of the slides but did not have an effect on performance. The glass slide is 25.4 mm by 76.2 mm.

Although the titanium mask was designed to produce traces at 50 µm in width, the electroless plating resulted in traces at around 60 µm consistently. This discrepancy in size most likely had to do with two features of the patterned electroless plating process. First, due to the dispersed light source, it was possible that UV light spread out further than the transparent regions of the titanium photomask and

slightly increased the hydrophilic area on the 1002F. Second, electroless plating of the sample could have created wider electrodes because plating always occurs in all directions, not just perpendicular to the growth plane as intended. The larger trace size did not have an impact on the function of the devices because there was no unwanted contact made with the second electrode of each pair. Unlike the previous electrolysis device samples, the finalized two layer devices were not fitted with LabTek chambers. Rather, efforts were made to fill the 200 µm by 200 µm chambers housing the electrode couples so that bubble formation would only form at the junction point only. This was accomplished by placing a drop of phosphate buffered saline (PBS) on a single junction point and then carefully using a Kimwipe (Kimberley-Clark Professional, Roswell GA) to absorb all excess liquid and just leaving behind the PBS in the chamber. The surface tension of the liquid made this procedure quite simple as the liquid preferentially held itself into the chamber while the rest of the liquid wicked away easily from 1002F surface. Once liquid was left within the chamber, it was possible to test bubble formation by passing current through the electrode pads to the traces.

5.3.2 Lock and Key Junction Design

The initial run of three layer trace prototypes did not trigger bubble generation when the junction chambers were filled with PBS. Before questioning the functionality of the electrode design and placement, proper electric conductance of the traces was verified by covering a 3 mm radius around an individual chamber with PBS and turning on the power source. With this configuration, bubble formation occurred on the gold bottom side trace branch in the chamber as well as the entirety of the wetted nickel top side trace. This result revealed that conduction was occurring properly through the traces, but a proper trace junction was not formed within the chamber. It was concluded that the electroless plating did not generate nickel on the side of the 1002F layer as originally intended. Without nickel bridging down into the trace junction chamber, electrolysis could not occur. A new mask design was formulated to solve this issue by including a second via hole next to every liquid chamber specifically made for bottom side to top side bridging through the 1002F layer. This design, deemed the "lock and key" array, patterned the

bottom side traces in such a way to create a trace junction directly on the glass by keeping the original gold trace branch the same and adding an additional small island of gold with its own branch within the vicinity of the other branch. Then the 1002F layer was patterned with the same junction chamber size along with another smaller 50 µm by 50 µm via hole above the newly added gold island. The top layer trace mask was designed to create traces running directly over the via hole and gold island instead of the junction chamber itself. With this design, alignment of the masks was much more straight forward because in addition to standard alignment marks, users could double check mask placement by matching the ‘keys’ or top vertical traces to the ‘locks’ or via holes leading to the bottom side traces. Trace placement directly over the via holes allowed for greater UV irradiation than previous mask iterations and allowing for adequate surface roughening of the 1002F sidewalls to enable electroless nickel plating to occur. Activation of the lock and key electrodes resulted in the successful formation of bubbles just within the bubble formation chambers. This result indicated proper sidewall formation and bridging of the lower gold electrode island with the top side electrodes through the 1002F via holes. Figure 5.3.3 includes a Solidworks rendition and actual images of a lock and key bubble formation junction.

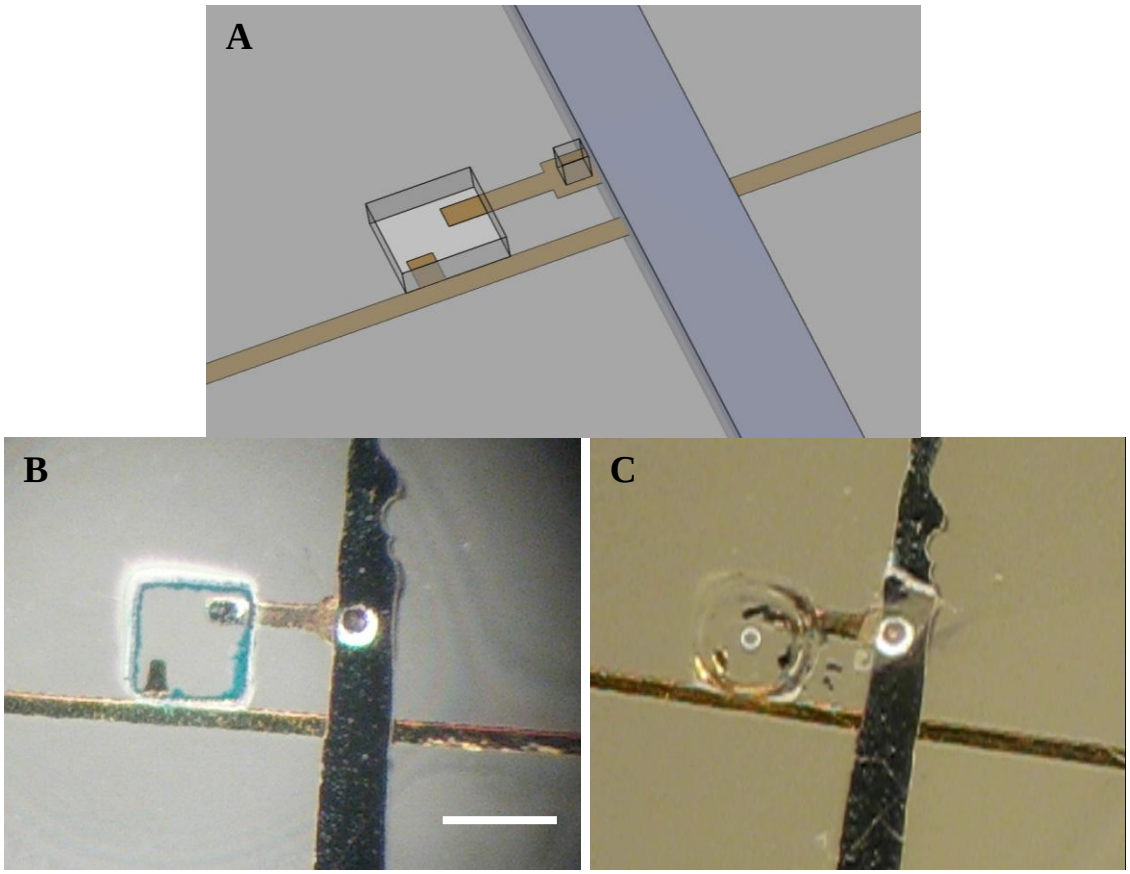

Figure 5.3.3: Lock and key bubble formation junction configuration
This junction configuration was superior to previous test designs both in production consistency as well as function. A) Solidworks rendering of intended features of lock and key junction. The bottom layer is 50 µm wide gold traces on glass. The second layer is a transparent 1002F layer with 50 µm thickness. The third layer is 75 µm wide nickel directly patterned onto the surface of the 1002F layer. The scale bar is 50 µm. B) Completed lock and key junction. The vertical nickel trace was directly patterned over a via hole in the 1002F leading to the bottom layer trace. Side plating of the via allowed contact between the first and third layer. C) Bubble being formed within junction. Upon excitation of the junction, small bubbles instantly began to form over the surface of each junction and combined to form large bubbles which filled the entirety of the chamber. It was believed that these large bubbles would be able to displace pallets placed over the chambers.

Previously established voltage and current settings translated to similar bubble creation performance on the x-y arrays as the originally tested prototype junction arrays. Differences in electrical resistivity of the gold traces and nickel traces did not have a noticeable effect on bubble size or formation rate. Further testing of the x-y arrays revealed several differences when using nickel electrodes versus the gold. Nickel traces proved to be more robust than gold traces upon repeated bubble formation trials. As mentioned earlier, the gold electrodes had a tendency to delaminate from their titanium seed layer below as bubble formation was repeated at junction sites. The delamination of the gold then led to a loss in

bubble formation repeatability as well as the consistency to form them just within junctions. The electroplated nickel boasted strong adherence to the 1002F photoresist and did not delaminate during bubble formation. A drawback of the nickel traces, however, was their inconsistent fabrication yield when compared to the gold electrodes. The electroless plating process oftentimes created nickel traces up to 50% wider than designed in the quartz photomasks and the process would result in varying quality levels. Minor cracks in nickel traces caused by substrate movement or improper handling after plating would lead to open circuits and thus prevent the ability to generate electrolysis of water on command from the external pads. Even with some of these drawbacks, the versatility of being able to directly pattern nickel traces with UV light was greatly desirable over the slow, expensive, and wasteful subtractive gold patterning process. For all further device design trials, all traces were be constructed using the short wavelength UV patterned electroless nickel plating process.

5.4 Short Wavelength UV Patterned Nickel X-Y Array Design

All preceding device designs described earlier in this chapter were created primarily to test whether bubbles could be formed by the electrolysis of water at specific locations based on the creation of independent trace junctions. The designs contained only a few junction points per device in order to best show site specificity when creating bubbles using shared traces that branched into each junctions. In order to create a bubble formation array to be used as a micropallet ejection substrate, however, it was necessary to fabricate devices containing tightly packed x-y junction points that would theoretically be aligned to an array of colony sized micropallets separated by 30 to 50 μm wide gaps in between adjacent structures. The resolution achieved during nickel trace patterning proved to be more than capable for meeting the spatial requirements for fitting individual traces next to one another with no contact within the junction chambers. The initial strategy in designing the micropallet ejection arrays was to limit the total number of ejection sites to one hundred points formed by ten “x” direction traces and ten “y” traces running perpendicularly to one another. As described in the previous section, the traces were separated by an insulating 1002F photoresist layer with strategically patterned via holes to create junction points

between the top side and bottom side traces. Typically, having only 100 individual micropallet structures available for cell sorting would not be viable as a useful cell sorting platform, but initial prototyping required simplification of trace design in order to preserve the ability for human control over pallet ejection. Manual control of the devices required adequately sized pads for wire soldering and thus the limited space on the surface of glass slides kept the total number of junctions to a minimum. Potential future work focusing on device adaptation to software enabled control would alleviate the spatial constraint issues by allowing the creation of miniscule pads that would interface with a microcontroller. This study resulted in the testing of two different device designs which both maintained the 100 junction point standard.

5.4.1 X-Y Array Design and Fabrication

The overall design of the first x-y array consisted of two sets of 10 different, 50 µm wide nickel traces spaced 50 µm from one another and separated by an insulating 1002F photoresist layer with via holes forming junction points between the top and bottom side traces as described above. To ease user control of the device, the small traces extended away from the junction region and branched out to a region containing 3 mm by 3 mm pads joined to individual traces. Unlike the prototype devices, it was decided that the bottom side traces and the top side traces would both be formed through the same short wavelength UV enabled electroless patterning process in order to remove the lengthy subtractive gold patterning resulting in a streamlined device manufacturing procedure. Cyclo olefin polymer was acquired from ZEONEX (Tokyo, Japan) after being selected as an ideal bottom substrate for device fabrication due to its low autofluorescence as well as the standardized capability to pattern metals on its surface using short wavelength UV.[109] The total process for device fabrication included several steps of UV light patterning via photomask alignment and subsequent material deposition. Two metal coated quartz photomasks were prepared for the bottom side trace and top side trace patterning steps via etching of the desired features into a 2000 Å Ti/Au metal layer. A third film mask was prepared in order to pattern the middle 1002F insulating layer with via holes to allow for top and bottom trace interfacing. In this case,

the mask did not have to be composed of quartz due to the longer wavelength UV used to pattern 1002F thus allowing for less demanding absorption requirements for the mask. Proper alignment of each layer was required with very limited tolerance due to the tight fitting nature of the design of the traces and junctions. To ease the fabrication process, alignment markers were included on unused portions of the device surface. The first mask included markings that matched only to those on the second layer and the third had another set of markings only corresponding to those on the first layer. The second layer was never directly aligned with any other layer as top and bottom alignment had the greatest significance for proper device functionality. While the masks were typically aligned by hand with an inspection scope in the clean room, the markings were designed to work with most commonly utilized alignment devices if a quicker fabrication was desired. Figure 5.4.1 shows an example of the standard alignment markers that were included on each mask design.

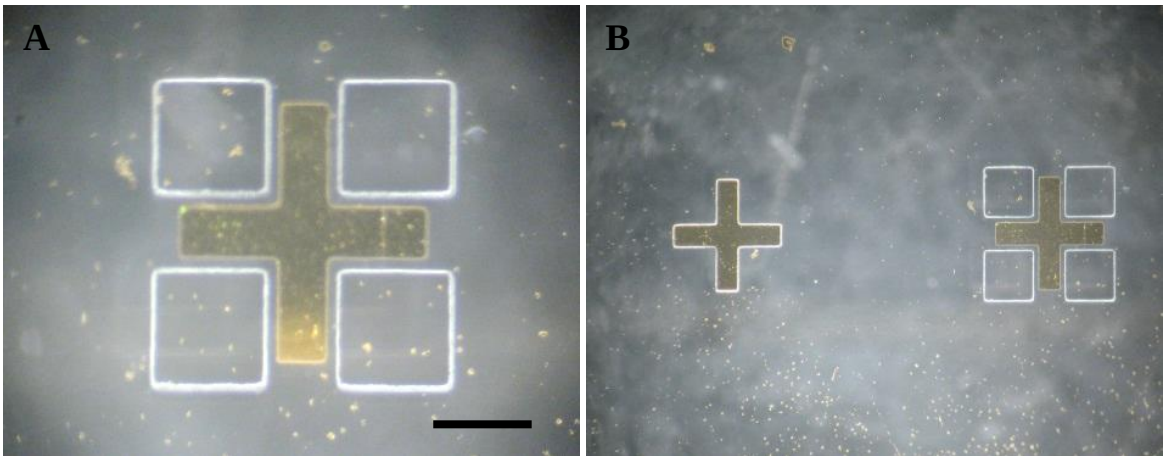

Figure 5.4.1: Alignment marker designs
A) Mark used to align separate layers during fabrication. For this example, the gold cross was formed on the bottom layer and the four holes in the 1002F photoresist layer surrounding the cross were formed on the second layer. The cross trace width was 50 µm and each square was 150 x 150 µm. This marker design was the same as that used for the x-y array device prototype. Each square was drawn to allow a space of 10 µm to the cross. Scale Bar is 100 µm. B) Alignment markers for different layers. The left cross was fabricated on the bottom layer to be aligned to the third electrode layer while the cross on the right was formed for first to second layer alignment.

5.4.2 X-Y Array First Prototype Design and Fabrication

The complete fabrication procedure of the x-y arrays was lengthy, but quite repeatable as it only required simple clean room processes including photolithography and electroless metal plating which are

both described in detail in this section. Step one of the processes involved the preparation of the cyclo olefin polymer (COP) for patterned electroless plating. COP is a transparent, biocompatible polymer material commonly utilized for phone liquid crystal display screens(cyclo olefin polymer patent).[114] While the material is inherently hydrophobic and thus not compatible with standard electroless metal plating methods, it has been shown that irradiating its surface with short wavelength UV light can generate hydrophilic regions on the exposed areas(UV modification paper).[115] Increased wettability of these areas was achieved by the oxidization of the surface terminal groups into functional groups. Due to hydrophilic regions being completely isolated to just UV irradiated regions, it was possible to generate patterned hydrophilic regions of COP sheets. To quickly test this capability, stencils bearing desired test patterns were created by cutting lines through glossy paper using an infrared CO_2 laser cutting system. COP was cut to an arbitrary size and the stencils were placed over their surface and secured with clips. Similar to standard photolithographic procedures, care was made to make sure to lay the stencil down as flush as possible with the surface of the COP in order to minimize unwanted irradiation of unexposed regions through the scattering of the UV light. This was especially important for short wavelength UV irradiation as the device emitting the light was designed to produce dispersed UV and thus had even greater potential of unwanted scattering than standard lights used for photolithography which are usually collimated. Following the standard procedures previously developed by KOTO, the COP film and stencil were placed into the short wavelength UV emitter and elevated to a distance of 3 cm from the lamps positioned at the top of the UV chamber. The sample was exposed to UV light for 3 minutes to produce a hydrophilic surface pattern corresponding to the openings in the stencil.

Once the process was confirmed with the test stencil, photomasks for the first and third layers of the bubble formation device were fabricated on 1 inch by 3 inch quartz microscope slides. In short, 5000 Å of titanium / gold was electron beam deposited onto the surface of cleaned quartz slides. Shipley photoresist was then spin coated onto the surface of the gold to a thickness of 5 µm. Once cured, the Shipley was exposed to UV light through a film photomask with the positive representation of the desired pattern. The Shipley was irradiated at 200 mJ/cm^2. After exposure, Shipley was immersed in developer

for one minute with constant stirring leaving behind only regions of the Shipley that were protected by the photomask. The Shipley was then hard baked for 1 minute at 90 °C. The finished photoresist layer covered all regions of the gold layer to be kept on the quartz while leaving all regions to be etched exposed. The gold layer that was not protected by the Shipley was etched from the surface of the slides in gold etchant solution for six minutes. The titanium seed layer was then etched by immersing the slides in 2% hydrofluoric acid for 30 seconds. Finally, the slides were immersed in acetone for one hour and wiped with a swab to remove the remaining Shipley resist. Using the completed gold coated quartz photomasks, COP was patterned with hydrophilic regions using the short wavelength UV irradiation method mentioned previously in this chapter. The patterned COP slides were then electroless plated with nickel using the same method as described in section 5.4. The first layer of the devices consisted of horizontal running traces with branching structures designed to interface with the third layer traces. Figure 5.4.2 displays the test "MIDAS" pattern that was formed for the initial COP patterning test using stencil masks. In order to view the hydrophilic region, deionized water (DI H_2O) was quickly rinsed over the surface of the COP. DI H_2O remained adhered only to the hydrophilic regions of the film making the altered regions visible. The first layer of the x-y array electroplated to the COP is shown as well.

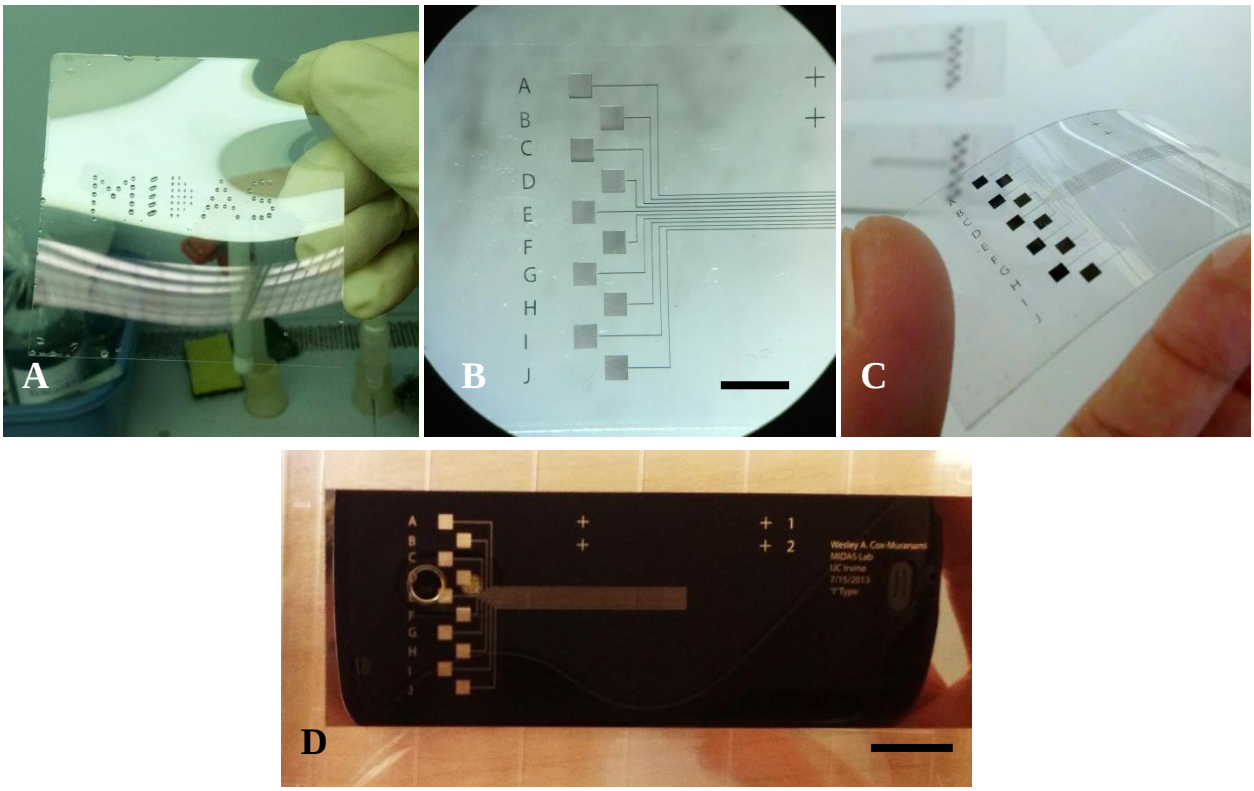

Figure 5.4.2: Hydrophilic alteration of cyclo olefin polymer (COP) and patterned nickel plating A) Short wavelength UV enabled hydrophilic patterning of COP visualized with diH_2O. Water was rinsed over the surface of the COP and only remained on the hydrophilic regions of the polymer. B) First layer of initial x-y array design created by electroless nickel plating on COP. Scale bar is 5 mm. C) Display of flexibility and transparent properties of COP. D) Titanium / gold coated quartz photomask used to pattern COP with hydrophilic regions. This mask was used to pattern the first layer electrodes. Scale bar is 10 mm.

The second layer of the x-y array devices consisted of an insulating layer of 1002F photoresist directly coated over the first layer traces and patterned to expose just the branching electrode junction points as visualized in figure 5.3.1 (A). The purpose of the second layer was to enable the overlapping of first and third layer electrode traces without them shorting with one another. While many types of materials could have theoretically been used as an insulator, 1002F was uniquely ideal for several reasons. The second layer of the device had to be transparent, biocompatible, and able to be plated with metal. The layer also had to be sufficiently thin to keep first and third layer traces close to one another for consistent electrolysis bubble formation using minimal current settings. 1002F photoresist has previously been shown to be optically transparent with low autofluorescence (1002F paper*).[79] It is also a biocompatible material and can readily be prepared for electrolysis nickel plating using short wavelength

UV as shown in chapter 3. Above all, the greatest utility that was afforded by selecting 1002F as the insulating layer was its capability to be patterned with sub millimeter features such as those required to create the first and third layer junction points. Coating COP with 1002F was not a completely straightforward procedure. As mentioned previously, COP is an inherently hydrophobic material that can only be properly wetted for electroless plating by using short wavelength UV irradiation. To pattern the first layer electrodes, only select regions were irradiated, leaving the rest of the COP surface hydrophobic. Spin coating 1002F onto the surface of unaltered COP resulted in inhomogeneous layer thickness and incomplete coverage of the COP substrates. To enable proper spin coating, the COP samples were exposed to the short wavelength UV once more with no photomask, making the entire surface of the substrate hydrophilic. 1002F was then spin coated onto the surface of the COP to 50 µm in thickness. Standard photolithographic procedures previously outlined for 1002F were then followed to form 100 holes exposing each of the branch structures jutting from the first layer traces. The region of 1002F coating over the first layer electrode pads was removed so as to not hinder wire connection to the pads. Figure 5.4.3 displays a COP slide with patterned bottom layer traces being prepared for spin coating.

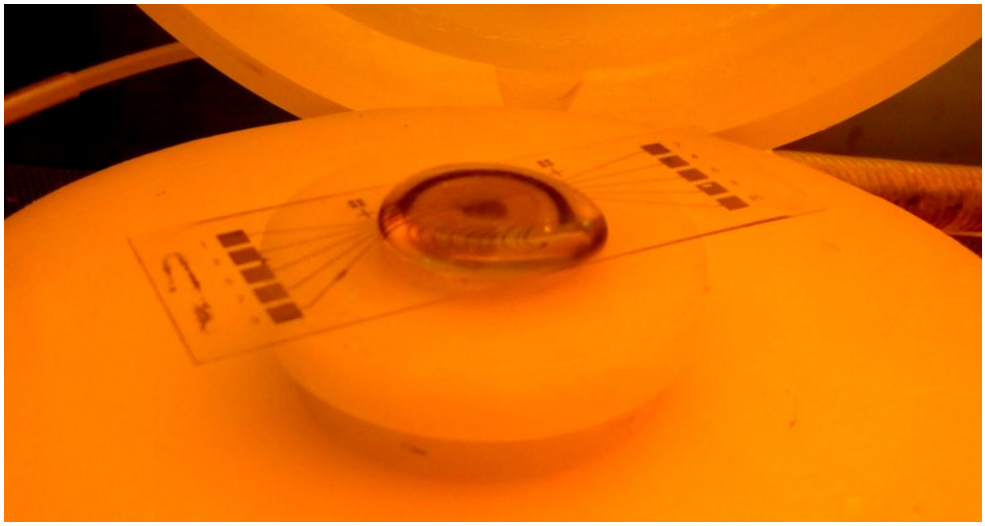

Figure 5.4.3: Cyclo olefin polymer with patterned bottom side traces being spin coated
Before being spin coated, the 25.4 mm by 76.2 mm cyclo olefin polymer (COP) slide that was previously plated with bottom side traces for bubble formation had to be completey exposed to short wavelength UV in order to make its surface hydrophilic. After irradiation, the COP could be spin coated with 1002F (visualized as the transparent liquid in the center of the slide). The image is yellow due to it having been taken inside of the photolithography room of the BION facility at the University of California, Irvine.

The final layer of the device was formed similarly to the first layer. The 1002F insulating layer was patterned with hydrophilic regions using the second quartz mask bearing the y-direction electrode design. Similar to the first layer, traces extending from larger excitation pads were formed to interface with the bottom side traces through the holes formed in the 1002F. The third layer traces did not have branching structures, however, and were aligned in a manner to run across the side of the 1002F holes opposite the branch from the first layer to expose the sidewalls of the holes to UV in order to enable side wall metal coating. The successful side coating of 1002F structures with short wavelength UV was discussed in chapter 3. Side wall coatings were expected to form connection of the third layer electrodes down towards the first layer to create tightly packed junctions without actually making contact between the two layers. After exposure, the 1002F surface was metal plated in the same way as the first layer with one exception. As a point of proper functionality, all bubble formation junctions needed to be sequestered from the open top surface of the arrays in order to prevent unwanted bubble formation on regions of the third layer electrodes exposed to the cell culture media. Cured 1002F was not as hydrophobic as COP and thus had to be plated for a shorter total amount of time in order to avoid unwanted metal deposition on undesirable areas. While the UV irradiation certainly made exposed regions much more hydrophilic and thus preferentially plated, the rest of the surface of the layer was not immune to electroless plating. With the temperature and voltage settings held constant, the total time of plating was cut to 75% of the time allotted for COP metal deposition. As a final note on fabrication, during the third layer plating, it was important to keep the first layer electrode pads out of the plating solution to avoid additional electroless plating on already patterned regions. A device completed using this first fabrication process can be seen in figure 5.4.4.

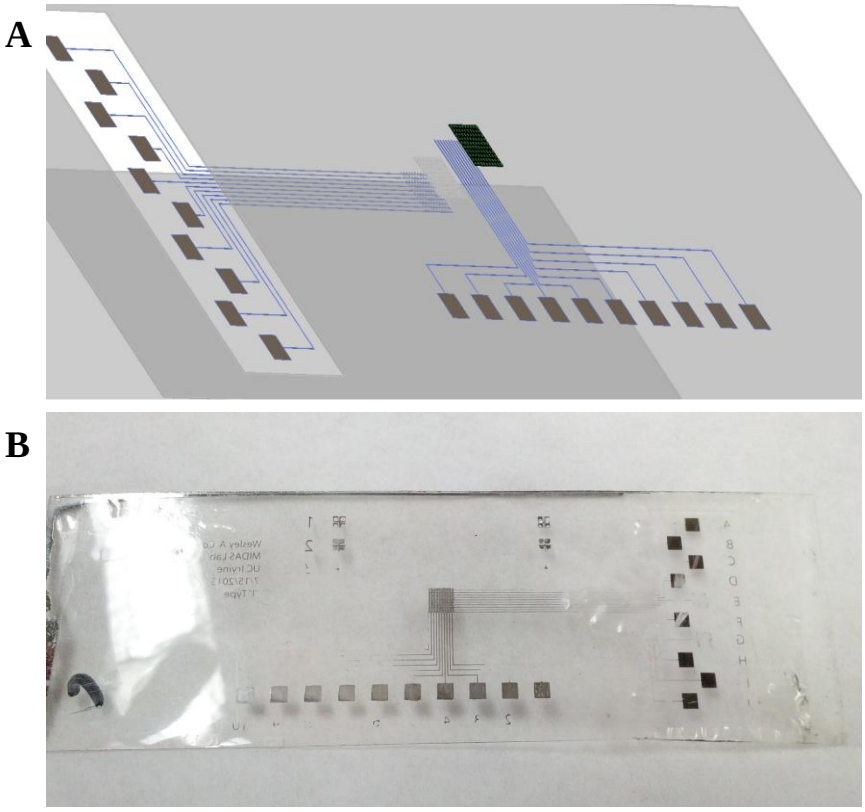

Figure 5.4.4: First X-Y bubble ejection array device prototype
A) Solidworks rendering of exploded view of device. The bottom layer is a selectively UV irradiated COP substrate. The second layer is patterned electroplated nickel traces. The third layer is a UV patterned 1002F insulating layer with holes forming junction points. The fourth layer is another patterned electroplated set of nickel traces. The fifth layer is patterned micropallets formed from 1002F photoresist. B) Real image of completed x-y ejection array. Some issues with nickel plating occurred due to traces being designed too thin at 50 µm. Design improvements are described further in this section. The device dimensions are 25.4 mm by 76.2 mm.

A number of issues arose from the initial run of device fabrication using the methods described above. Of the ten prototypes that were made, eight devices were non-functional as a result of either unwanted circuit shorting due to over plating or a complete lack of signal transmission due to poor trace plating quality. Shorting occurred within the pallet ejection region of the device and was caused by unwanted plating with the 1002F junction holes. Incomplete metal plating primarily occurred on the 1002F surface and not the COP which was most likely due to the 1002F tailored minimized plating time requirement. The two devices that appeared to be fabricated adequately were quite fragile and the thin traces began to peel while being handled before any tests could be conducted. Some junctions, however,

were able to be tested before the devices completely fell apart and bubbles were able to be formed using the traces still intact. Once again, the same successful voltage and current settings were utilized and the bubble formation output was not noticeably different from the initial prototypes. These early results indicated that further work towards creating better designs would potentially lead to functional bubble ejection arrays.

5.4.3 X-Y Array Second Design and Fabrication

The first x-y array device prototype revealed that there were still some limitations in consistent fabrication quality when using the short wavelength enabled electroless plating method described earlier in this chapter. Efforts focused on improving on batch throughput and consistency focused on alleviated precision requirements by forming wider traces that were spaced further apart from one another. The new traces were designed to be 100 µm wide with gaps of 500 µm separating each bottom side adjacent trace. The top side traces were spaced 250 µm apart. The 500 µm spaces on the first layer were achieved by splitting the ten total traces to five on each side of the COP substrate. Five traces were designed to extend from the left side of the device and five extended from the right side. Traces extending from opposite sides of the slides were zippered together in an alternating fashion. For example, trace number one extended from the left of the slide and trace number two extended from the right and so on. In this way, there was plenty of room to spread out the five user pads on each side of the device. The top side electrodes all extended vertically from the bottom of the device, but were spaced further apart than the initial prototype. Branch structures extending from the traces that formed the junction regions were designed at 50 µm wide. Wider trace design opened the UV irradiation area of the photomasks and thus lead to better surface alteration of the COP and 1002F surfaces for electroplating. The gap size increase between adjacent traces allowed longer plating times without the worry of over-depositing nickel onto the trace regions.

Another issue that had to be resolved was nickel plating which occurred within the bubble formation junctions during the electroplating of the top side electrodes. Previously, after the bottom side

electrodes were plated, the entire surface of the COP was irradiated with short wavelength UV in order to prepare the substrate for the 1002F layer. This step, however, altered the entirety of the COP including the regions that were to become the junction holes. When the top side electrodes were plated, the exposed regions of COP in the junction holes were plated as well which lead to shorting between the top and bottom electrodes, preventing the possibility of hydrolysis bubble formation. In order to prevent this from occurring moving forward, a new step was included in the device fabrication process.

After bottom side electrode plating, 5 μm thick Shipley photoresist was patterned in a way to form square blocks covering just the 100 junction region. The process was accomplished by using the same mask that was used to pattern the 1002F insulating layer with the junction holes themselves. The Shipley was patterned using the methods described in section 5.4.2. This was possible because Shipley is a positive resist while 1002F is a negative resist. As such, when Shipley was patterned with the mask intended for the 1002F, instead of creating holes within the Shipley layer the resist was patterned to form square structures covering just the junction regions after UV irradiation and development. Spin coating the COP substrate with Shipley did not require surface treatment ahead of time because there were very minimal requirements for the quality of the Shipley layer. The structures simply had to be formed thick enough to absorb UV and prevent alteration of the COP surface. When the COP was exposed to UV once more to prepare for 1002F patterning, the Shipley resist absorbed the short wavelength UV which prevented the junction regions from becoming hydrophilic. After exposure, the Shipley resist was washed away from the COP with an acetone soak followed by a DI H_2O rinse. Surface agitation to remove the Shipley was avoided in order to not scrape away the plated nickel. Figure 5.4.5 shows the unwanted nickel shorting which occurred on the first prototype devices and the Shipley blocks covering junction regions during fabrication.

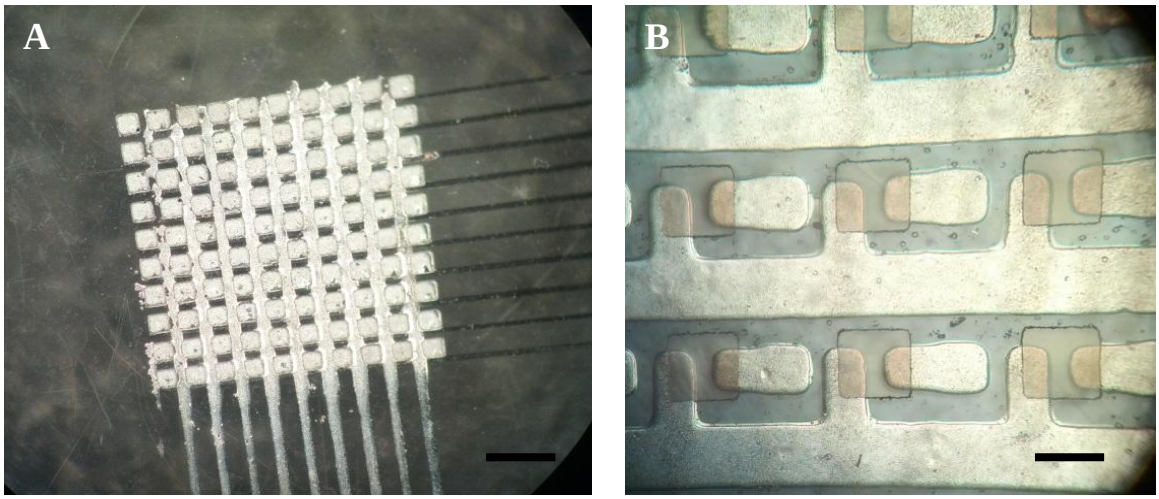

Figure 5.4.5: Nickel over-plating issue and corresponding resolution
A) Image of bubble ejection region of the first prototype device. Junction regions are the nickel plated squares. A properly fabricated device would not have these nickel squares which prevent proper hydrolysis bubble formation by shorting the top and bottom side electrodes. The scale bar is 1 mm. B) Fabrication solution to the nickel over-plating issue. 5 µm thick Shipley photoresist was patterned onto just the junction regions on the bottom side electrodes. The Shipley absorbed the short wavelength UV that would have otherwise enabled unwanted nickel plating. The Shipley was washed away with acetone before continuing fabrication. The scale bar is 200 µm.

The most dramatic change that was made to the initial prototype design was the inclusion of the lock and key junction formation scheme described in section 5.3.2. The second trace layout utilizing larger spacing allowed for greater design flexibility and thus enabled the integration of the better trace junction design. With the lock and key layout, it was no longer necessary to rely solely on the side coating of 1002F to generate top and bottom trace interfacing. Instead, the more robust electroforming techniques involving the filling of via holes was utilized. First, when patterning the bottom side traces, junction traces were also included within the first layer. A single "lock" trace was composed of a 150 µm by 150 µm square pad with a 100 µm horizontal extension. A single lock was placed at every junction region. The extensions were made perpendicular to the branching structures on the larger traces with a 50 µm gap separating the two. When patterning the 1002F insulating layer, a new 50 µm by 50 µm square via hole placed directly above the lock trace pad was patterned adjacent to each of the original junction via holes. The top side traces were designed to overlap the lock via holes to form the "keys" that connected the top layer traces to the corresponding bottom layer locks by filling the via with nickel. All electroplating

settings were kept identical to those used during the initial prototype fabrication. Figure 5.4.6 shows each completed stage of the fabrication process and a completed device.

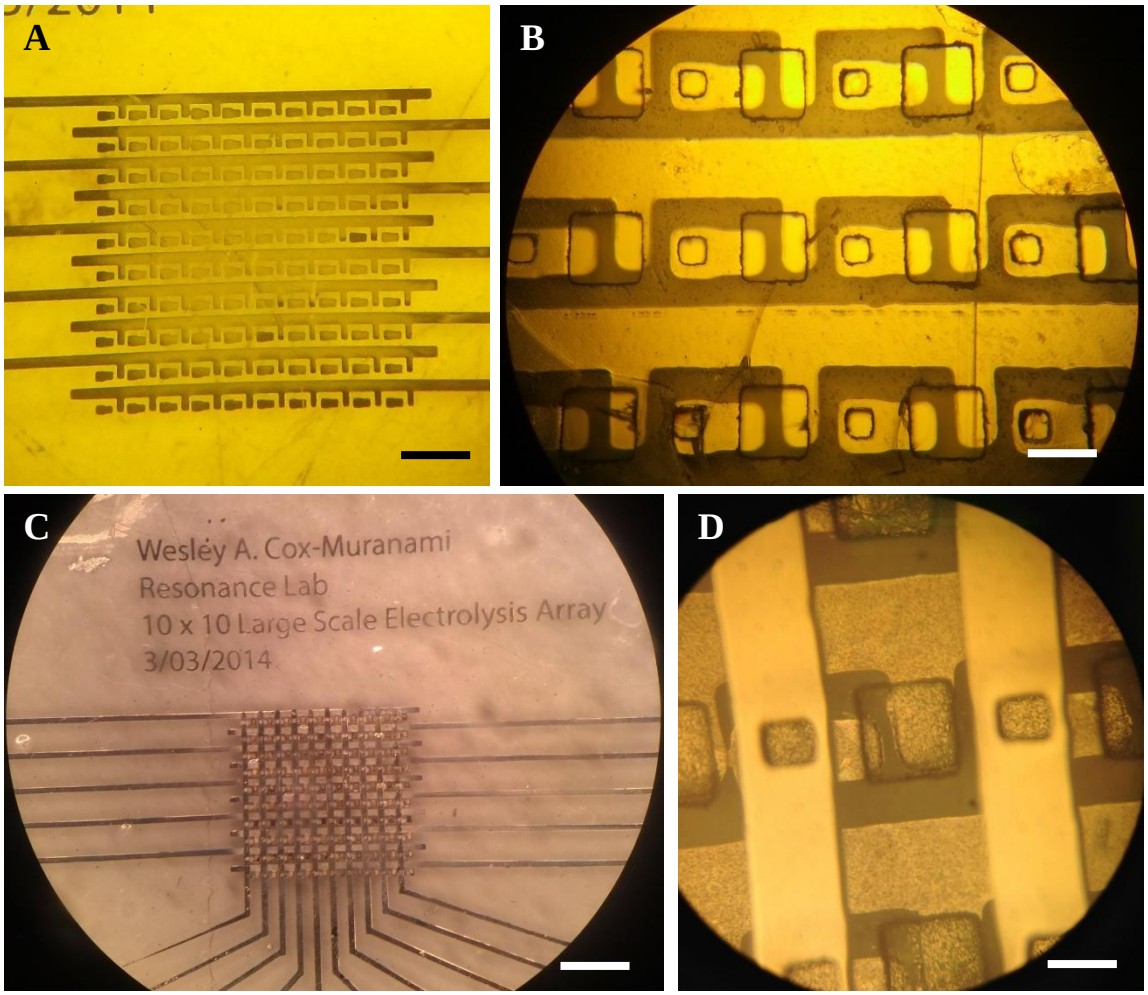

Figure 5.4.6: Second bubble ejection device prototype fabrication process
A) Nickel plated cyclo olefin polymer (COP) forming the first device layer. The "locks" of the lock and key junction design are visible as islands embedded within the 100 trace branches. Scale bar is 1 mm. B) The 1002F insulating layer was directly patterned on top of the first layer of the device following short wavelength UV irradiation. The layer was patterned with via holes forming both the junction holes as well as the key holes linking the bottom and top layers. Scale bar is 200 µm. C) Full view of pallet ejection region after top layer trace electroless plating. All traces were cleanly fabricated with proper alignment to form functional bubble formation junctions. The horizontal traces were separated from the vertical traces by an insulating 1002F photoresist layer. Scale bar is 2 mm. D) Zoomed image of individual completed bubble formation junction. Top layer traces can be observed passing directly over "key" via holes leading to the "lock" traces on the first layer. The junction hole formed within the 1002F reveals the bottom side traces through the insulating layer to allow interaction with contained liquids for hydrolysis bubble formation. Scale bar is 150 µm.

The overall robustness of the second device prototype fabrication process was much better than when making the first design. Out of the 15 total devices fabricated, 11 had at least 90 functional bubble

formation junctions. Three of the remaining devices had less that 40 percent functional junctions and the final device had no function. Circuit shorting was still the number one cause of non-functional junctions caused by trace over plating. Given the relatively high success rate, it was determined that even with the failed devices simple tweaks to the nickel plating times would solve any over plating issues hindering proper device function moving forward. When compared to the side coating junction formation utilized in the first prototypes, the lock and key trace configuration displayed an absolute improvement in both robustness and simplicity. The wider trace sizes better suited the short wavelength UV enabled electroless plating process and forming both of the junction traces on the same plane eased alignment requirements. To test bubble formation capability of the devise, 1x phosphate buffered saline (PBS) was flushed over the surface of the arrays. The arrays were then placed into a vacuum desiccator in order to extract air bubbles caught within each junction chamber. Once vacuumed, excess liquid was wicked from the surface of the arrays by absorbing the excess PBS not held within the chambers with a Kimwipes task wiper (Kimberly-Clark Professional, Roswell, GA). After the extra PBS was removed, it was possible to form hydrolysis bubbles just within each junction chamber. To do so, an external power source was linked directly to the user interface pads located on the perimeter of the arrays. Bubble formation occurred whether the cathode was selected as the horizontal or vertical trace as long as the anode was always selected as the perpendicular trace direction. Power source settings that most consistently generated bubbles on the device were 1.5 A for the current and 4 V for the voltage. While current was always held constant, it was found that using voltages exceeding 5 V results in the delamination and breakdown of the nickel traces which stop device functionality.

5.5 Micropallet Placement on Bubble Formation Arrays

The final step towards creating the hydrolysis bubble release arrays was the addition of micropallet structures over the ejection platform. Although micropallet formation has become an incredibly straight forward and well understood procedure, there have been few attempts at fabricating the structures on substrates other than flat glass microscope slides. The hydrolysis devices required pallets to

be made directly above the 200 µm by 200 µm junction holes. As a further complication, the device functionality required there to be liquid contained within the junction holes at the time of micropallet formation. The Bachman lab has previously had some success with forming large area micropallet structures on porous surfaces by utilizing a method of hot embossing dried 1002F resist. Unfortunately, due to the heat required for the embossing it was quite difficult to maintain moisture of such small volumes within the junctions while embossing. In order to create pallets on the surface of the devices, it was decided that a microstructure transfer process would be the most ideal.

5.5.1 Surface to surface micropallet transfer method

Two major requirements had to be met for a microstructure transfer process to work for this device. First, some kind of adhesive had to be used in order to have the micropallets stick to the bubble ejection array after transfer. Second, the micropallets had to be formed on some kind of sacrificial substrate that would release the structures on command in order to allow the transfer process to take place. When transferring, the sacrificial surface could not rely on harsh chemicals for release as such etchants could react with the nickel coating on the release arrays. There was also a fear that etchant based transfer of the structures could cause contamination of the ejection fluid which would then have the potential of poisoning the cell culture media during actual use of the devices. After researching several sacrificial layers for structural release, it was concluded that the best approach would be to use a water soluble dextran based layer. Dextran melted in diH_2O has previously been reported to work as a water soluble sacrificial layer which has the potential to be a substrates to be patterned on.[116] Furthermore, the dextran was shown to be immune to SU8 developer which enabled SU8 patterning over dextran without unwanted loss of the sacrificial layer. Dextran with a molecular weight of 70,000 g/mol was purchased from Sigma Aldrich and a solution containing 15% Dextran in diH_2O by mass was prepared by mixing the components until the dextran was completely incorporated at room temperature. The resist was spin coated onto clean glass microscope slides at a speed of 1000 RPM to a thickness of 1 µm and

dehydrated on a hot plate at 105° C. After dehydration, the dextran films appeared as hazy blotches primarily covering the mid sections of the glass. Different ratios of dextran to diH_2O with differing solution viscosities were tested on the glass slides but did not yield better coatings. This result indicated that the glass slides were not hydrophilic enough to form a uniform layer of the dextran over the entirety of the slide surfaces. To achieve uniform dextran resist layers, COP substrates exposed to short wavelength UV were utilized. Large sheets of the COP were exposed to short wavelength UV as described in section 5.4.2 and cut to 1 inch by 3 inch strips. The strips were then spin coated with the dextran resist and dehydrated. Unlike the glass slides, the COP strips exhibited relatively uniform dextran layers which were better suited for 1002F resist patterning when compared to the glass slides. Micropallet arrays composed of 250 µm by 250 µm square pallets with 50 µm gap spacing were formed over the surface of the dextran coated strips. The same methods as those described previously in this chapter were applicable to formation of the arrays on the COP. As anticipated, the dextran photoresist layer remained intact throughout the photopatterning process. The combination of COP with dextran and 1002F micropallets will henceforth be referred to as transfer chips. Figure 5.5.1 shows a transfer chip before and after exposure to diH_2O for 5 minutes.

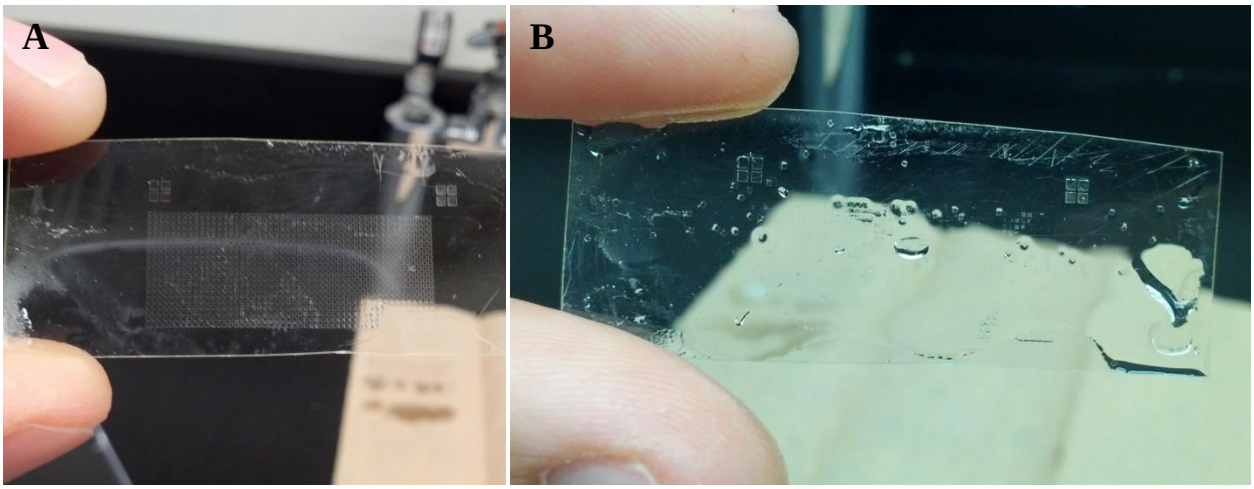

Figure 5.5.1: 1002F resist micropallet arrays patterned on thin dextran resist sacrificial layers
A) A "transfer chip" right after fabrication. Micropallet arrays composed of 250 µm by 250 µm square pallets with 50 µm gaps were formed on water soluble dextran thin films. The thin films were spin coated onto COP substrates that were pretreated with short wavelength UV. The transfer chips were completely stable until immersed in water at which point the dextran melted and released the pallets. B) Transfer chip after being immersed in diH_2O for 5 minutes. Most pallets from the array were released from the chip. Some pallets remained after water immersion due to the slightly splotchy nature of the dextran layer.

In order to transfer the micropallet arrays from the transfer chips to the bubble ejection device it was necessary to find a proper adhesive. For the transfer to work, the adhesive would have to cure at or near room temperature and be water resistant. Ideally, the adhesive would cure quickly to avoid unwanted shifting of the array during transfer as alignment was vital to the success of the device. The adhesive was also required to form a complete seal around the bubble formation chambers in order to prevent bubble leakage during ejection. Any leakage of the gas formed by electrolysis would release built up pressure and limit the force output of the chambers beneath the pallets. With these requirements in mind, it was decided that five minute epoxy type adhesives would work best. Specifically, Z-poxy quick set formula (Pacer, Ontario, CA) was selected for this step. The use of this particular epoxy had the added benefit of having the same cure as the time required to dissolve the dextran layer sufficiently. The epoxy was administered to the micropallets with a stamping procedure. Parts A and B of the epoxy were mixed at a one to one ratio and spread over the surface of a clean glass microscope slide. The slide was then scraped once with a razor blade in order to remove excess epoxy and create a thin uniform layer. A transfer chip was then lightly placed face down (pallets facing the epoxy) onto the glass slide and lifted off the surface

after the structures were dipped into the epoxy. Before structure transfer, the junction region of the bubble formation arrays were covered with a 1 mL droplet of 1x PBS and placed into a vacuum desiccator. The arrays were then vacuumed to extract air bubbles within the junction regions to fill them with the PBS. Then, the transfer chip was carefully aligned to a PBS filled bubble formation array device by matching alignment markers under an inspection scope. The chip was then held over the surface of the arrays which spread the remaining PBS over the entire surface of the transfer chip which effectively introduced the soluble dextran layer to water to start the transfer process. The transfer chips were held over the surface of the bubble formation array for seven minutes to allow excess time for both the curing of the adhesive as well as the dissolution of the dextran sacrificial layer. After seven minutes, the COP substrate of the transfer chip was carefully pulled away from the bubble formation array. As intended, the micropallets were left adhered to the surface of the bubble formation array with each individual pallet completely covering a corresponding junction region. Although the process itself worked consistently, one major issue that occurred was that too much adhesive was being carried by the transfer chips onto the junction arrays. Care had to be taken to avoid pressing the transfer chips too firmly against the glass slides coated in the adhesive in order to contain adhesive transfer to just the top surfaces of the micropallets and not their sides. Side transfer of the adhesive created unwanted adhesive webbing which joined adjacent pallets to one another and prevented proper device function. Figure 5.5.2 shows a completed device after micropallet transfer.

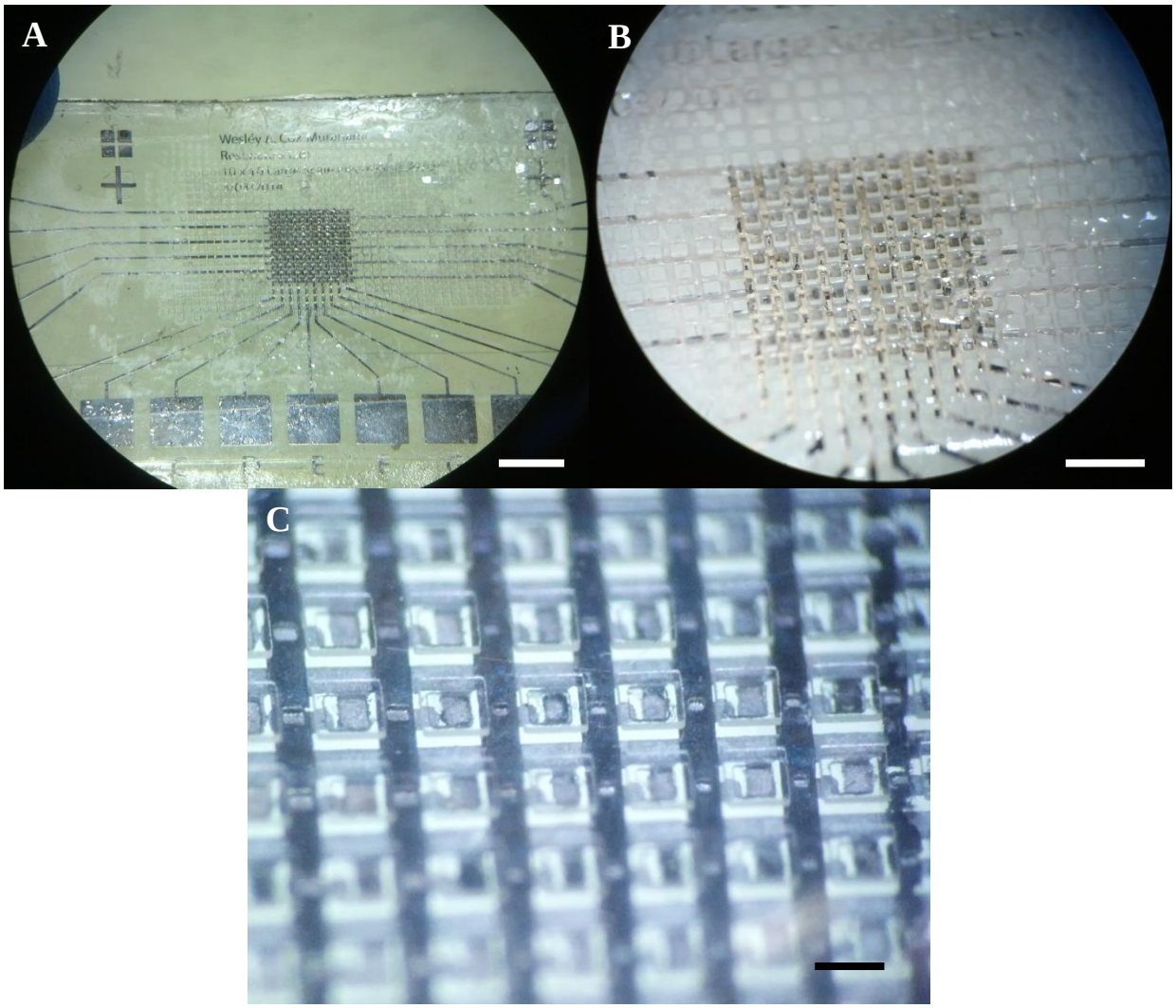

Figure 5.5.2: Micropallets transferred onto hydrolysis bubble formation arrays
A) Wide view of a completed device with stamp transferred micropallets. Extra pallets were formed surrounding the 10 by 10 bubble junction area to prevent bending the transfer chips while administering adhesive. The 100 bubble formation junctions are located in the middle section of the image. The scale bar is 4 mm. B) Zoomed in image of the bubble formation junction with surface adhered micropallets. Each pallet is 250 µm by 250 µm. Each junction region contained PBS sealed within the array by a pallet. The scale bar is 1 mm. C) Zoomed in image of pallets adhered over an array of bubble ejection junctions. Scale bar is 250 µm.

Pallet transfer utilizing the dextran sacrificial layers and five minute epoxy was successful in placing pallets over liquid filled junctions. Bubble formation was achieved up to three hours after the devices were fabricated when they were kept in air and 24 hours when kept in a high humidity environment. This result indicated that seals formed by the pallets were not completely stable and would

release over time, allowing evaporation of the PBS to occur. Bubble formation within a single chamber could be achieved for around 15 seconds before function of the junction ceases. For future optimization of this technology, it would be necessary to figure out ways of creating longer lasting bubble formation arrays, but for early prototype testing these devises were sufficient.

While bubble formation occurred as expected on the device, the final results were not ideal. When a specific junction point was activated by electrifying a single ‘x’ and a single ‘y’ electrode pad, electrolysis induced bubbles formed beneath the intended target pallet, but a successful pallet ejection did not take place. At first, once electrified, bubbles could be seen forming through the 1002F pallet but were stuck beneath the pallet. After an average of 3 seconds had transpired, a single edge of the pallet would lift up enough to allow the bubbles to escape. This partial ejection prevented the expected full release by preventing any further pressure build up and thus potential energy necessary to eject the entirety of the pallet. The same result occurred for every successive ejection trial on the remaining devices. These results indicated a fundamental issue with the concept of using a bubble release chamber method for pallet ejection. For normal pallets, plasma generation created by a targeted laser beam created an instantaneous shock wave which forces pallets to eject from their glass substrates. The gold absorptive layer enabled laser vapor bubble release system mentioned in chapter 2 and chapter 3 also used bubbles as a form of ejection, but did not require a buildup of pressure underneath the pallets. For this technology to succeed during future investigation, it will be necessary to target two specific aspects of the hydrolysis bubble release system. First, bubble formation should be made as explosive as possible. The current device design generates micro and nano bubbles which immediately join together to form larger area bubbles capable of displacing larger pallet objects when allowed to sufficiently build up pressure. Due to the gradual formation of the bubbles, the slow generation of force on the underside of the pallets only disrupts the weakest points of adhesion thus creating a partial release instead of a complete dislocation of the pallet. One method to make the bubble formation pressure greater at a faster rate would be to minimize the bubble formation chamber size while maintaining the same surface area for the bubble traces. In this way the same amount of bubbles will form given the same application current and time, but the bubble

pressure will maximize much faster within the chamber and may create a greater pushing force beneath a pallet. Stricter fabrication requirements will be necessary to fit traces closer together without overlap and trace fabrication methods may need to be revisited.

5.6 Chapter 5 Conclusion

A micropallet array with electronically controlled release capabilities was designed fabricated using electroplating enabled by short wavelength UV surface treatment. The ejection methodology of the devices utilized the creation of oxygen and hydrogen bubbles which formed when water was electrolyzed with two separate traces forming an anode and cathode. By patterning traces to run near each other only within tiny junction chambers with a conductive liquid, it was possible to selectively generate bubbles at specifically desired locations. The design included a two dimensional array of x-y perpendicular traces patterned onto a cyclo olefin polymer cut to 1 inch by 3 inches. The x and y traces were separated by an insulating 1002F photoresist layer which included via holes to create the bubble formation chambers. The final device prototype included 100 distinct chambers which could all be individually activated by an external power source. All chambers were filled with phosphate buffered saline and covered with an array of large micro pallets using a dextran sacrificial layer transfer method. The completed devices were capable of selective bubble formation beneath pallets, but the bubbles were unable to fully eject the pallet on a consistent basis. Also, due to the junction chambers being large in order to ease fabrication, the arrays were primarily designed for cell colony sorting and at this point the devices were not ideal for single cells. Future work with this technology should focus on the generation of forces strong enough to release the pallets by physical means, or look for alternate release methods such as those with electronically activated sacrificial layers patterned beneath the pallets.

Chapter 6: Appendices

6.1 Appendix A

This section covers additional material pertaining to chapter 2. The work described in this chapter was a result of a quick discussion with Dr. Mark Bachman at a cafe close to the University of California, Irvine. I spoke to Dr. Bachman about a new idea had regarding simplifying the release of large micropallet structures by using a gold thin film below them which would potentially absorb laser energy and heat up to release the pallets. At the time of this work, electroplating was being heavily utilized in our lab and interposer creation was also a hot topic. Dr. Bachman mentioned that it would be interesting if we could someone utilize the gold layer as a seed layer for metal formation in some way. It just so happened that at that time I was also pursuing the nickel side coated pallet project discussed in chapter 4 and realized the electroplated nickel could be used as a magnetic core formed within 1002F photoresist which was a procedure that was used for interposer formation. These ideas all came together and resulted in the creation of the first magnetic micropallet arrays which were then further refined as written in chapter 3 to become the "ferrocore" micropallet arrays.

6.1.1 Early idea for simplified cell colony pallet ejection

The introduction to chapter 2 discusses some early ideas that were presented during my qualifying exam before the project was started. Early brainstorming resulted in the conclusion that sacrificial layers would be ideal for easy large pallet ejection and was also an unexplored area of research with micropallet arrays. Figure 6.1.1 displays an idea tree discussing sacrificial layer design for micropallets.

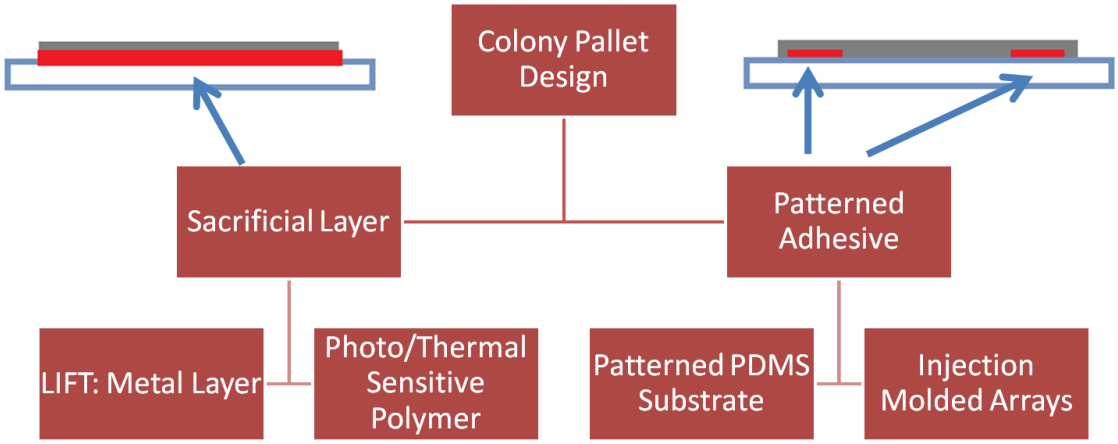

Figure 6.1.1: Idea tree including early thoughts regarding large pallet ejection
This figure was presented during a qualifying exam proposing the large area micropallet improvement project. Early on the idea of using sacrificial layers or patterned destructible adhesives were thought to have the greatest potential for success. The left discusses the use of targetable layer formation below micropallets to facilitate ejection. The right shows potential uses of patterned adhesives below micropallets to be targeted for release.

The concepts hinted in the diagram on the bottom row will be discussed from left to right. Lift: metal layer was the idea that ultimately resulted in the path that was selected for this project. It refers to the use of thin metal layers used as carriers for biological sample transfer from one surface to another with the use of lasers. Before experimentation, it was thought that this transfer process could be utilized with pallets on the surface of metal films. Photo/thermal sensitive polymer refers to the use of thin polymer sacrificial layers patterned underneath large pallets. (polyimide papers).[117-120] The polymers were to be transparent to allow cell visualization and also destructible by laser excitation. Patterned PDMS substrate was an interesting idea where PDMS would be used as a substrate for pallets. Due to PDMS being hydrophobic, pallets would not preferentially stick to the material surface and thus would require some kind of patterned adhesive to adhere. If pallet adherence was adhesive dependent, it was thought that a laser could be used to destroy the adhesives thus releasing the pallets from the PDMS surface. Finally injection molded arrays was an interesting idea with much potential where micropallet arrays were to be fabricated by injection molding and would have various shapes and features made into pallets that would otherwise be impractical and probably impossible by standard photolithographic fabrication. One idea was to fabricate pallets with pockets to be filled with laser destructible adhesives

that would release pallets upon laser irradiation. Any of the proposed ideas still have the potential to work and may be quite interesting to pursue.

6.1.2 Micropallet fabrication

Micropallet fabrication with ferromagnetic cores was surprisingly straightforward and successful. Even though the core elements and the mesh surrounding the pallets were electroformed at the same time, pallet ejection only resulted in the release of the cores. Although it would have been entirely conceivable that the cores would stay behind during pallet release and stay adhered to the gold films below, the friction force generated between the pallet structures and their interior cores was enough to carry the cores along with the pallets. The force generated by the magnetic probe was also typically not strong enough to cause the cores to leave the pallets either. There were, however, a couple rare instances where cores left the pallets during magnetic recovery, but these events did not occur enough to pose a concern. Figure 6.1.2 displays the various via core sizes that were tested in chapter 2.

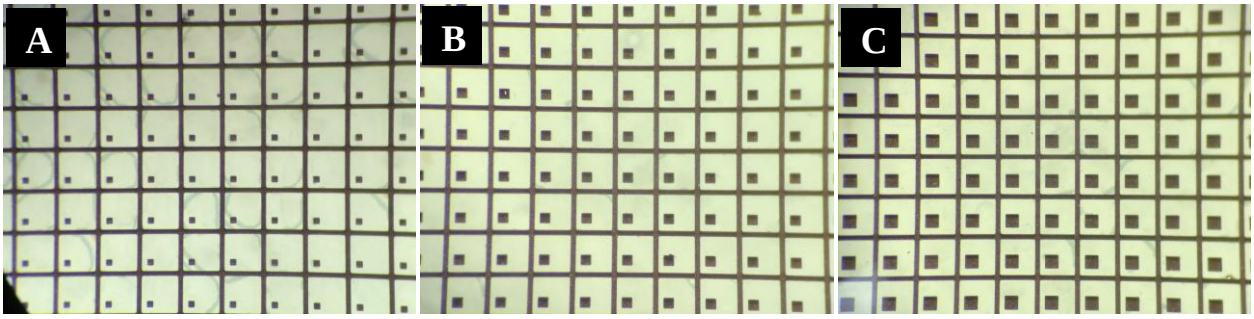

Figure 6.1.2: Micropallet arrays with different sizes of ferromagnetic cores
Micropallet arrays with three different sized ferromagnetic cores are shown. All pallets in the images have the dimensions of 270 µm (W) by 270 µm (L) and 50 µm (H). A) Micropallet with 50 µm by 50 µm ferromagnetic core. B) Pallet with 75 µm by 75 µm core. C) Pallet with 100 µm by 100 µm core.

6.1.3 Nickel and gold plating on magnetic micropallet arrays

It was shown in chapter 2 that in order to achieve high lives of biocompatibility with the magnetic micropallet arrays, it was necessary to coat the ferromagnetic nickel cores with thin gold layers. Figure 6.1.2 was included here to show the striking visual differences between nickel coated micropallet arrays and those with the addition of the biocompatible gold layer.

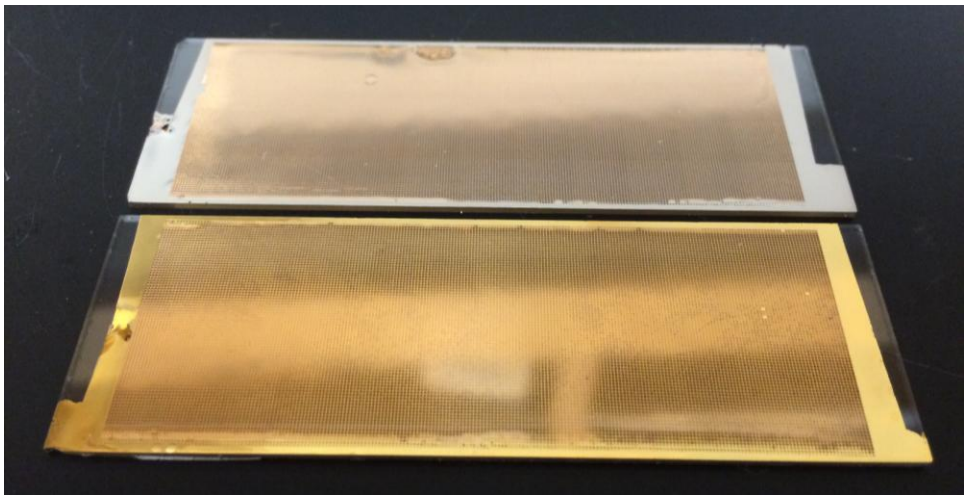

Figure 6.1.3: Nickel and gold coated magnetic micropallet arrays
This image compares the visual differences between nickel and gold coated micropallet arrays. Gold layers were formed over the ferromagnetic nickel structures of the arrays in order to increase the biocompatibility of the devices. An interesting note is that the regions covered in micropallets on the nickel only slide still appear to be bold in color because the transparent pallets reveal the gold then film beneath them. The areas on the sides of the glass slides with no metal coating never had gold thin film deposition on their surface as those areas were covered in tape that secured the slides to the e-beam device.

6.1.4 Overplating of ferromagnetic cores

Probably the most common and most detrimental issue that occurred with the fabrication of the magnetic micropallet arrays with the potential for overplating the metal structures. With such limited surface area to plate, the electroformation conditions had to be just right to properly replicate metal structures no taller than 30 μm within and around the pallets. Before the plating conditions were perfected and solidified, there were many instances in which electroplating resulted in structures either becoming flush or growing past the top surfaces of the pallets. In both instances the pallets would become impossible to eject by laser and cells were not properly sequestered on the arrays due to there being no physical gaps between adjacent structures. Even when ideal plating conditions were properly documented, alterations had to be made whenever new plating solutions were utilized. Figure 6.1.4 shows an example of metal overplating.

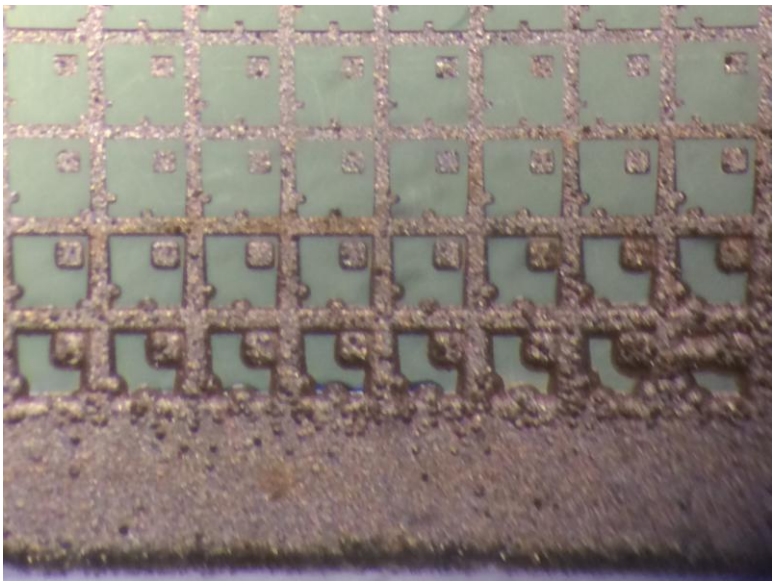

Figure 6.1.4: Overplating of metal structures in and around micropallets
The overplating of metal structures on the magnetic micropallet arrays would occur in instances where the current settings were set too high during fabrication and also if the plating time was too long. In either case, overplating was disastrous to the micropallets as it made it impossible to eject the pallets. Ideal structure height was found to be at or slightly below 30 μm.

6.1.5 Large bubble formation during pallet ejection

The laser ejection procedure utilized for magnetic micropallet ejection described in section 2.3.9 would typically result in many microbubbles forming below pallets and moving upward which would dislodge target micropallets. Sometimes these bubbles would combine with one another, forming one large bubble below the target pallet and would continue to expand as the gold was heated by the laser. These large bubbles still succeeded in ejecting the pallets, but the pallets would remain stuck to the bubble until being collected by the magnetic probe. This occurrence did not cause any issues, but was an interesting observation. Figure 6.1.5 shows a large bubble with a stuck pallet after ejection.

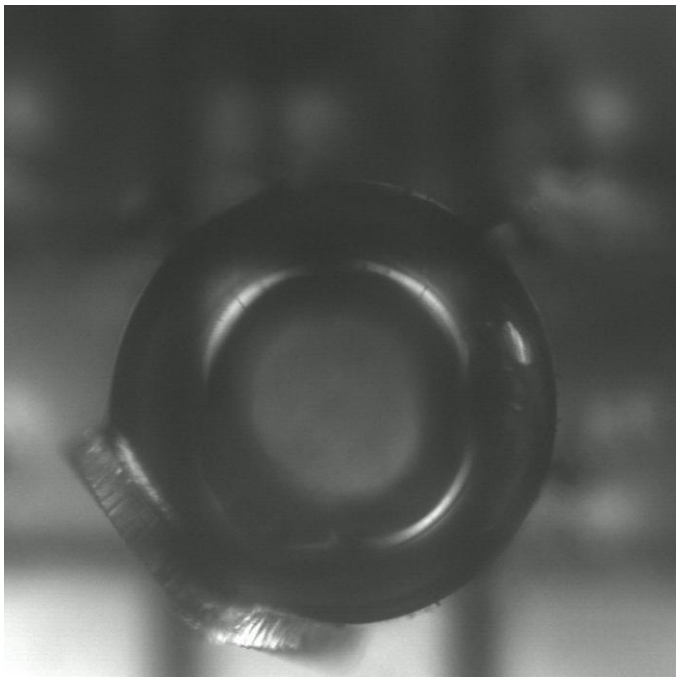

Figure 6.1.5: Rare large bubble formation by the heating of gold thin films below pallets
Large vapor bubble formation below targeted micropallets was a rare, but interesting occurrence. While these events did not have any negative impact on either cell viability or pallet collection and actually made pallet location following ejection simple as the ejected pallet would stay stuck to the bubble. This phenomenon may someday be harnessed in interesting ways, such as for microfluidic valve creation.

6.2 Appendix B

6.2.1 Magnetic control of Ferrocore micropallet in microfluidic channels

In addition to the cell colony sorting capabilities described in detail in chapter 3, Ferrocore micropallets allow for better device integration of the micropallet arrays by allowing direct transfer and control of ejected cells through microfluidic channels by magnetic probe. The magnetic response of the pallets were strong enough to allow a relatively distance magnetic probe to pull the pallet though a microfluidic channel fabricated from paper infused with cured PDMS. Figure 6.2.1 shows a successful control even of moving an ejected Ferrocore pallet through a channel and into a perpendicular fluidic well with a 90˚ entrance path.

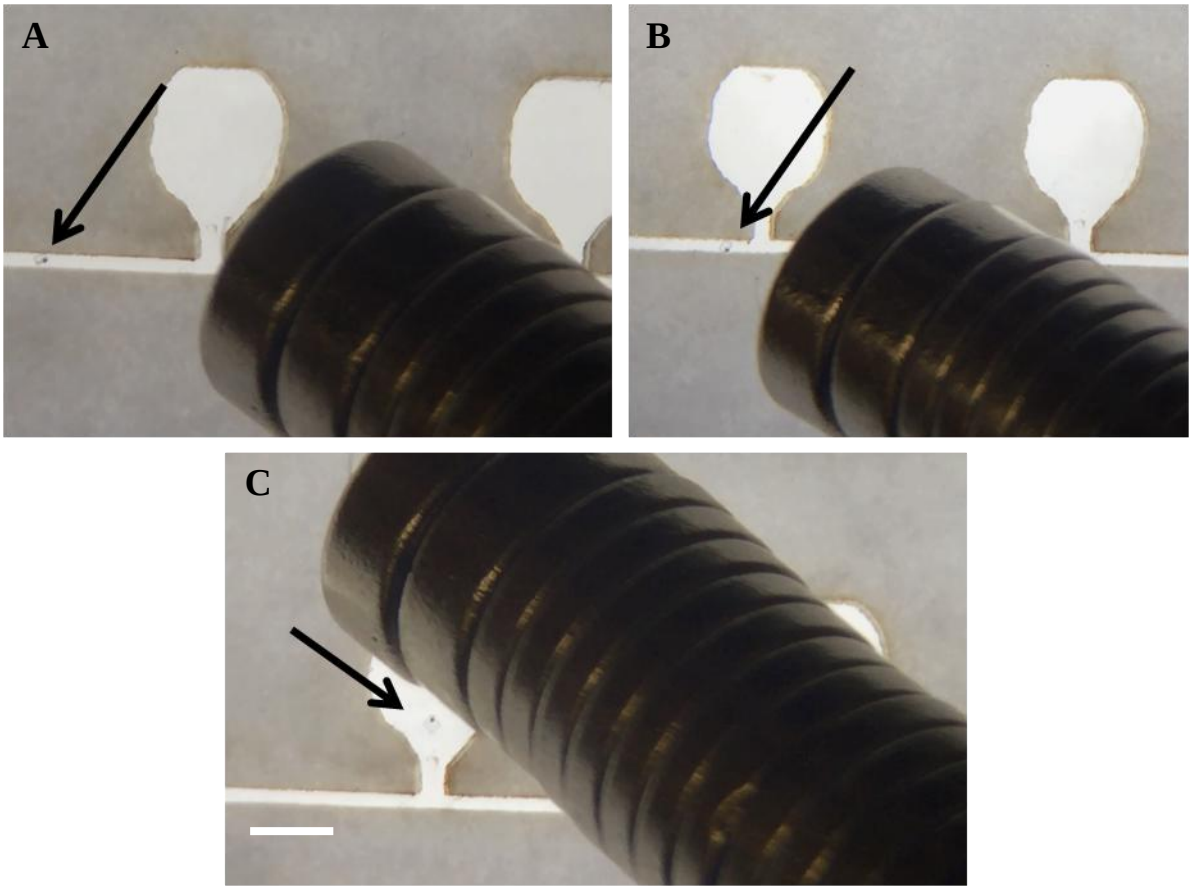

Figure 6.2.1: Magnetic control of Ferrocore micropallet after ejection from array
This series of images shows the control of a magnetic micropallet through a fluidic microchannel with an external magnet. A paper microfluidic system representative of more complex systems was sandwiched between a glass slide and an acrylic sheet with fluidic inlets drilled into it for channel access. A micropallet structure was collected from an array using laser excited vapor bubble ejection (as described in chapter 2) and transferred to the fluidic system by magnetic probe. The micropallet was then moved through the channel into a well without any other external forces besides the presence of the magnet shown as the large object over the fluidic channels. Images A, B, and C show the movement of the pallet from left to right to into a separated chamber. The black arrow in each image points to the pallet structure which is a little hard to see in the images due to it being primarily transparent. The scale bar in C is 1 mm.

6.3 Appendix C

6.3.1. Various nickel sidecoated microstructure shapes

The nickel sidecoating of micropallet arrays described in chapter 4 enhanced the imaging quality of the arrays and also enabled the magnetic collection of released pallets. The sidecoating process applied

to standard micropallet arrays could also be used to create sidecoatings on various microstructure shapes and sizes. Figure 6.3.1 displays examples of some of the shapes that were successfully coated.

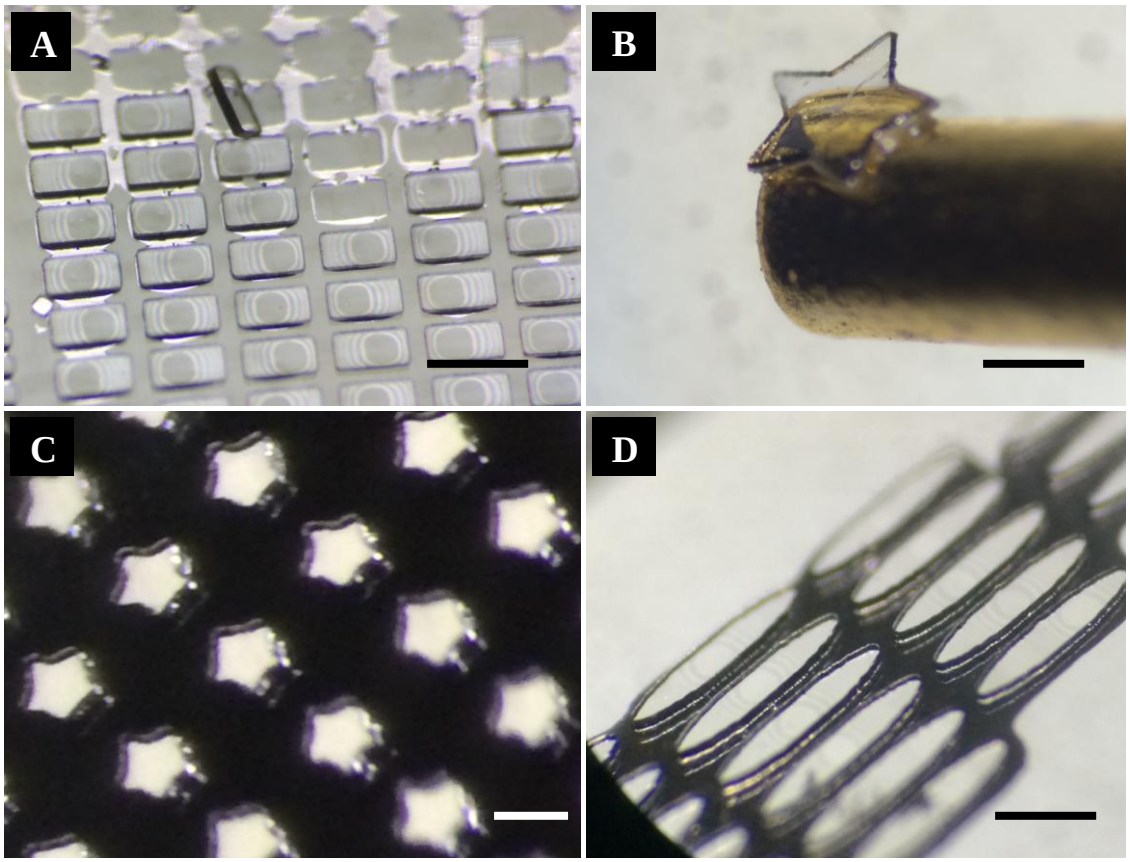

Figure 6.3.1: Various shapes fabricated from 1002F photoresist and nickel sidecoated Electroless nickel plating was performed on various shapes of microstructures in order to test the ability to form nickel sidewalls on non-square shapes. All tested shapes could successfully be sidecoated and further were magnetically collectable following removal from the glass substrate. A) Large, 400 µm by 400 µm square pallets. Scale bar is 500 µm. B) Array of small star structures. Scale bar is 50 µm. C) Large star structure captured with magnetic probe. Scale bar is 500 µm. D) Oblong ovals successfully sidecoated with nickel. Each oval is 800 µm long and 200 µm wide. Scale bar is 400 µm.

Literature Cited

1) A. Orfao, A. Ruiz-Arguelles. General concepts about cell sorting techniques *Clinical Biochemistry*, 1996, 29(1), 5-9.
2) S.M. Browne, M. Al-Rubeai. Selection methods for high-producing mammalian cell lines. *Trends in Biotechnology*, 2007, 25(9), 425-432.
3) L.M. Barnes, A.J. Dickson. Mammalian cell factories for efficient and stable protein expression. *Current Opinion in Biotechnology*, 2006, 17, 381-386.
4) S.C.G. Brezinsky, G.G. Chiang,, A. Szilvasi, S. Mohan, R.I. Shapiro, A. MacLean, W. Sisk, G. Thill. A simple method for enriching populations of transfected CHO cells for cells of higher specific productivity. *Journal of Immunological Methods*, 2003, 277, 141-155.
5) H.J. Tanke, M. van der Keur. Selection of defined cell types by flow-cytometric cell sorting. *Trends Biotechnol.*, 1993, 11(2), 55-62.
6) M. Girotti, G. Banting. TGN38-green fluorescent protein hybrid proteins expressed in stably transfected eukaryotic cells provide a tool for the real-time, in vivo study of membrane traffic pathways and suggest a possible role for ratTGN38. *J Cell Sci.*, 1996, 109(12), 2915-2926.
7) G. Seth, S. Charaniya, K.F. Wlaschin, W. Hu. In pursuit of a super producer - alternative paths to high producing recombinant mammalian cells. *Current Opinion in Biotechnology*, 2007, 18(5), 557-564.
8) F.L. Battye, A. Light, D.M. Tarlinton. Single cell sorting and cloning. *Journal of Immunological Methods*, 2000, 243, 25-32.
9) R.L. Rietze, H. Valcanis, G.F. Brooker, T. Thomas, A.K. Voss, P.F. Bartlett. Purification of a pluripotent neural stem cell from the adult mouse brain. *Nature*, 2001, 412, 736-739
10) J. McNeish. Embryonic stem cells in drug discovery. *Nature Reviews*, 2004, 3, 70-80.
11) L. Ricci-Vitiani, D.G. Lombardi, E. Pilozzi, M. Biffoni, M. Todaro, C. Peschle, R. De Maria. Identification and expansion of human colon-cancer-initiating cells. *Nature*, 2007, 445(4), 111-115.
12) B.R. Kao, B. McColl, J. Vadolas. Generation of BAC Reporter Cell Lines for Drug Discovery. *Methods Mol. Biol.*, 2015, 1227, 323-343.
13) D. Mattanovich, N. Borth. Applications of cell sorting in biotechnology. *Microbial Cell Factories*, 2006, 5(12).
14) L.A. Herzenberg, D. parks, B. Sahaf, O. Perez, M. Roederer, L.A. Herzenberg. The history and future of the fluorescence activated cell sorter and flow cytometry: a view from Stanford. *Clinical Chemistry*, 2002, 48:10, 1819-1827.
15) W.A. Bonner, H.R. Hulett, R.G. Sweet, L.A. Herzenberg. Fluorescence Activated Cell Sorting. *Review of Scientific Instruments*, 1972, 43(3), 404-409.
16) B.P. Cormack, R.H. Valdivia, S. Falkow. FACS-optimized mutants of the green fluorescent protein (GFP). *Gene*, 1996, 173, 33-38.
17) H. Lin, S. Chiou, C. Kao, Y. Shyr, C. Hsu, Y. Tarng, L. Ho, C. Kwok, H. Ku. Characterization of pancreatic stem cells derived from adult human pancreas ducts by fluorescence activated cell sorting. *World J. Gastroenterol.*, 2006, 12(28), 4529-4535.
18) I. Verms, C. haanen, C. Reutelingsperger. Flow cytometry of apoptotic cell death. *J. Immunol. Methods*, 2000, 243(1-2), 167-190.
19) L.A. Sklar, M.B. Carter, B.S. Edwards. Flow cytometry for drug discovery, receptor pharmacology and high throughput screening. *Curr. Opin. Pharmocol.*, 2007, 7(5), 527-534.
20) S.F. Ibrahim, G. Engh. High-speed cell sorting: fundamentals and recent advances. *Current Opinion in Biotechnology*, 2003, 14, 5-12.
21) S. Basu, H.M. Cambell, B.N. Dittel, A. Ray. Purification of specific cell population by fluorescence activated cell sorting (FACS). *J. Vis. Exp.*, 2010, (41), e1546.

22) C.S. Owen, N.L. Sykes. Magnetic labeling and cell sorting. *Journal of Immunological Methods,* 1984, 73, 41-48.
23) S. Miltenyi, W. Muller, W. Wichel, A. Radbruch. High gradient magnetic cell separation with MACS. *Cytometry,* 1990, 11, 231-238.
24) J.D. Adams, U. Kim, H.T. Soh. Multitarget magnetic activated cell sorter. *PNAS,* 2008, 105(47), 18165-18170.
25) K. Schriebl, G. Satianegara, A. Hwang, H.L. Tan, W.J. Fong, H.H. Yang, A. Jungbauer, A. Choo. Selective removal of undifferentiated human embryonic stem cells using magnetic activated cell sorting followed by a cytotoxic antibody. *Tissue Engineering: Part A,* 2012, 18(9), 899-909.
26) X. Tong, Y. Xiong, M. Zborowsky, S.S. Farag, J.J. Chalmers. A novel high throughput immunomagnetic cell sorting system for potential clinical scale depletion of T cells for allogeneic stem cell transplantation. *Experimental Hematology,* 2007, 35, 1613-1622.
27) Q. Li, X. Zhang, Y. Peng, H. Chai, Y. Xu, J. Wei, X. Ren, X. Wang, W. Liu, M. Chen, D. Huang. Comparison of sorting efficiency and influence on cell function between the sterile flow cytometry and immunomagnetic bead purification method. *Preparative Biochemistry and Biotechnology*, 2013, 43(2), 197-206.
28) M.J. Tomlinson, S. Tomlinson, X.B. Yang, J. Kirkham. Cell separation: terminology and practical considerations. *Journal of Tissue Engineering*, 2012, Review.
29) M. Geens, H. Van de Velde, G. De Block, E. Goossens, A. Van Steirteghem, H. Tournaye. The efficiency of magnetic-activated cell sorting and fluorescence-activated cell sorting in the decontamination of testicular cell suspensions in cancer patients. *Human Reproduction,* 2007, 22(3), 733-742.
30) M. Li, J. Xu, M. Romero-Gonzalez, S.A. Banwart, W.E. Huang. Single cell Raman spectroscopy for cell sorting and imaging. *Current Opinion in Biotechnology*, 2012, 23, 56-63.
31) M. Li, D.G. Boardman, A. Ward, W.E. Huang. Single-cell Raman sorting. *Methods Mol. Biol.*, 2014, 1096, 147-153.
32) C.C. Co, C. Ho, G. Kumar. Motility-based cell sorting by planar cell chromotography. *Anal. Chem.*, 2012, 84, 10160-10164.
33) H. Kim, J. Doh, D.J. Irvine, R.E. Cohen, P.T. Hammond. Large area two-dimensional b cell arrays for sensing and cell-sorting applications. *Biomacromolecules*, 2004, 5, 822-827.
34) G. Vona, A. Sabile, M. Louha, V. Sitruk, S. Romana, K. Schultze, F. Capron, D. Franco, M. Pazzagli, M. Vekemans, B. Lacour, C. Brechot, P. Paterlini-Brechot. Isolation by size of epithelial tumor cells. *American Journal of Pathology*, 2000, 156(1), 57-63.
35) S. Zheng, H. Lin, J. Liu, M. Balic, R. Datar, R.J. Cote, Y. Tai. Membrane microfilter device for selective capture, electrolysis and genomic analysis of human circulating tumor cells. *Journal of Chromatography A*, 2007, 1162, 154-161.
36) O.V. Podgorny. Live cell isolation by laser microdissection with gravity transfer. *J. Biomed. Opt.*, 2013, 18(5), 05502.
37) Z. Sun, H. Su, B. Long, E. Sinclair, S.W. Hetts, R.T. Higashida, C.F. Dowd, V.V. Halbach, D.L. Cooke. Endothelial cell high-enrichment from endovascular biopsy sample by laser capture microdissection and fluorescence activated cell sorting. *Journal of Biotechnology*, 2014, 192, 34-39.
38) O.V. Podgorny, N.F. Polina, V.V. Babenko, I.Y. Karpova, E.S. Kostryukova, V.M. Govorun, V.N. Lazarev. Isolation of single Chlamydia-infected cells using laser microdissection. *Journal of Microbiological Methods*, 2015, 109, 123-128.
39) J. Autebert, B. Coudert, F. Bidard, J. Pierga, S. Descroix, L. Malaquin, J. Viovy. Microfluidic: An innovative tool for efficient cell sorting. *Methods*, 2012, 57, 297-307.
40) H.A. Stone, A.D. Stroock, A. Ajdari. Engineering flows in small devices: microfluidics toward a lab-on-a-chip. *Annu. Rev. Fluid Mech.*, 2004, 36, 381-411.
41) A.B. Fuchs, A. Romani, D.Freida, G. Medoro, M. Abonnenc, L. Altomare, I. Chartier, D. Guergour, C. Villiers, P.N. Marche, M. Tartagni, R. Guerrieri, F. Chatelain, N. Manaresi.

Electronic sorting and recovery of single live cells from microlitre sized samples. *Lab Chip,* 2006, 6, 121-126.
42) J. El-Ali, P.K. Sorger, K.F. Jensen. Cells on chips. *Nature,* 2006, 442, 403-411.
43) A.Y. Fu, C. Spence, A. Scherer, F.H. Arnold, S.R. Quake. A Microfabricated fluorescence-activated cell sorter. *Nature Biotechnology,* 1999, 17, 1109-1111.
44) H. Tsutsui, C. Ho. Cell separation by non-intertial force fields in microfluidic systems. *Mechanics Research Communications,* 2009, 36, 92-13.
45) N. Pamme, C. Wilhelm. Continuous sorting of magnetic cells via on-chip free-flow magnetophoresis. *Lab Chip,* 2006, 6, 974-980.
46) M.D. Vahey, J. Voldman. An equilibrium method for continuous-flow cell sorting using dielectrophoresis. *Anal Chem.,* 2008, 80, 3135-3143.
47) M.P. MacDonald, G.C. Spalding, K. Dholakia. Microfluidic sorting in an optical lattice. *Nature,* 2003, 426, 421-424.
48) T.D. Perroud, J.N. Kaiser, J.C. Sy, T.W. Lane, C.S. Branda, A.K. Singh, K.D. Patel. Microfluidic-based cell sorting of Francisella tularensis infected macrophages using optical forces. *Anal. Chem.,* 2008, 80, 6365-6372.
49) B.M. Taff, J. Voldman. A scalable addressable positive-dielectrophoretic cell-sorting array. *Anal. Chem.,* 2005, 77, 7976-7983.
50) J. Baret, O.J. Miller, V. Taly, M. Ryckelynck, A. El-Harrack, L. Frenz, C. Rick, M.L. Samuels, J.B. Hutchison, J.J. Agresti, D.R. Link, D.A. Weitz, A.D. Griffiths. Fluorescence-activated droplet sorting (FADS): efficient microfluidic cell sorting based on enzymatic activity. *Lab Chip,* 2009, 9, 1850-1858.
51) J. Luo, E.L. Nelson, G.P. Li, M. Bachman. Microfluidic dielectrophoretic sorter using gel vertical electrodes. *Biomicrofluidics,* 2014, 8, 034105.
52) M. Abdelgawad, A.R. Wheeler. The digital revolution: A new paradigm for microfluidics. *Adv. Mater.,* 2009, 21, 920-925.
53) R.B. Fair. Digital microfluidics: is a true lab-on-a-chip possible? *Microfluid Nanofluid,* 2007, 3, 245-281.
54) A.H.C. Ng, M.D. Chamberlain, H. Situ, V. Lee, A. R. Wheeler. Digital microfluidic immunocytochemistry in single cells. *Nature Communications,* 2015, 6, 7513.
55) M.H. Stewart, M. Bossee, K. Chadwick, P. Menendez, S.C. Bendall, M. Bhatia. Clonal isolation of hESCs reveals heterogeneity within the pluripotent stem cell compartment. *Nature Methods,* 2006, 3(10), 807-815.
56) J.R. Smith, R. Pochampally, A. Perry, S. Hsu, D.J. Prockop. Isolation of a highly clonogenic and multipotential subfraction of adult stem cells from bone marrow stroma. *Stem Cells,* 2004, 22, 823-831.
57) S.M. Phadnis, N.O. Loewke, I.K. Dimov, S. Pai, C.E. Amwake, O. Solgaard, T.M. Baer, B. Chen, R.A. Reijo Pera. Dynamic and social behaviors of human pluripotent stem cells. *Scientific Reports,* 2015, 5, 14209.
58) M. Greaves, C.C. Maley. Clonal evolution in cancer. *Nature,* 2012, 481, 306-313.
59) K. Ishizawa, Z.A. Rasheed, R. Karisch, Q. Wang, J. Kowalski, E. Susky, K. Pereira, C. Karamboulas, N. Moghal, N.V. Rajeshkumar, M. Hidalgo, M. Tsao L. Ailles, T. Waddell, A. Maitra, B.G. Neel, W. Matsui. Tumor-initiating cells are rare in many human tumors. *Cell Stem Cell,* 2010, 7(3), 279-282.
60) M.A.C. Huergo, M.A. Pasquale, P.H. Gonzalez, A.E. Bolzan, A.J. Arvia. Growth dynamics of cancer cell colonies and their comparison with noncancerous cells. *Physical Review E,* 2012, 85, 011918.
61) A. Puliafito, L. Hufnagel, P. Neveau, S. Streichan, A. Sigal, D.K. Fygenson, B.L. Shraiman. Collective and single cell behavior in epithelial contact inhibition. *PNAS,* 2012, 109(3), 739-744.
62) P.G. Wylie, W.P. Bowen. Determination of cell colony formation in a high-content screening assay. *Clin. Lab Med.* 2007, 27(1), 193-199.

63) K. Buch, T. Peters, T. Nawroth, M. Sanger, H. Schmidberger, P. Langguth. Determination of cell survival after irradiation via clonogenic assay versus multiple MTT assay - a comparitive study. *Radiation Oncology,* 2012, 7, 1-6.
64) N.A.P. Franken, H.M. Rodermond, J. Stap, J. Haveman, C. van Bree. Clonogenic assay of cell *in vitro*. *Nature Protocols,* 2006, 1(5), 2315-2319.
65) A. Alvarez, G.A. Barisone, E. Diaz. Focus formation: a cell-based assay to determine the oncogenic potential of a gene. *J. Vis. Ep.,* 2014, 94.
66) W. Kang, E. Shin. Colormetric focus-forming assay with automated focus counting by image analysis for quantification of infectious hepatitis C virions. *PLoS ONE,* 2012, 7(8), e43960.
67) J. Kupper, M. Muller. Improved protocols for the isolation and *in-situ* cryopreservation of cell colonies. *Cytotechnology,* 1996, 21, 225-229.
68) S. Jaupt, J. Grutzner, B.H. Rath, H. Mohlig, O. Brustle. Automated selection and collection of pluripotent stem cell colonies using the CellCelector. *Nature Methods,* 2009, 6, i-iv.
69) V. Espina, J.D. Wulfkuhle, V.S. Calvert, A. VanMeter, W. Zhou, G. Coukos, D.H. Geho, E.F. Petricoin III, L.A. Liotta. Laser-capture microdissection. *Nature Protocols,* 2006, 1(2), 586-603.
70) O.V. Podgorny. Live cell isolation by laser microdissection with gravity transfer. *Journal of Biomedical Optics.* 2013, 18(5), 055002.
71) Z. Komyei, S. Beke, T. Mihalffy, M. Jelitai, K.J. Kovacs, Z. Szabo, B. Szabo. Cell sorting in a Petri dish controlled by computer vision. *Scientific Reports,* 2013, 3, 1088.
72) Y. Wang, G. Young, P.C. Aoto, J. Pai, M. Bachman, G.P. Li, C.E. Sims, N.L. Allbritton. Broadening cell selection criteria with micropallet arrays of adherent cells. *Cytometry Part A,* 2007, 71A, 866-874.
73) Y. Wang, G. Young, M. Bachman, C.E. Sims, G.P. Li, N.L. Allbritton. Collection and expansion of single cells and colonies released from a micropallet array. *Anal. Chem.,* 2007, 79, 2359-2366.
74) G.T. Salazar, Y. Wang, G. Young, M. Bachman, C.E. Sims, G.P. Li, N.L Allbritton. Micropallet arrays for the separation of single, adherent cells. *Anal. Chem.,* 2007, 79, 682-687.
75) C.E. Sims, M. Bachman, G.P. Li, N.L. Allbritton. Choosing one from the many: selection and sorting strategies for single adherent cells. *Anal. Bioanal. Chem.,* 2007, 387, 5-8.
76) G.T. Salazar, Y. Wang, C.E. Sims, M. Bachman, G.P. Li, N.L. Allbritton. Characterization of the laser-based release of micropallets from arrays. *J. Biomed. Opt.,* 2008, 13(3), 034007.
77) P.A. Quinto-Su, G.T. Salazar, C.E. Sims, N.L. Allbritton, V. Venugopalan. Mechanisms of pulsed laser microbeam release of SU-8 polymer "micropallets" for the collection and separation of adherent cells. *Anal. Chem.,* 2008, 80, 4675-4679.
78) K.L. Berkowski, K.N. Plunkett, Q. Yu, J.S. Moore. Introduction to photolithography: preparation of microscale polymer silhouettes. *Journal of Chemical Education,* 2005, 82(9), 1365-1369.
79) J. Pai, Y. Wang, G.T. Salazar, C.E. Sims, M. Bachman, G.P. Li, N.L. Allbritton. A photoresist with low fluorescence for bioanalytical applications. *Anal. Chem.,* 2007, 79(22), 8774-8780.
80) Y. Wang, M. Bchman, C.E. Sims, G.P. Li, N.L. Allbritton. Stability of virtual air walls on micropallet arrays. *Anal. Chem.,* 2007, 79, 7104-7109.
81) Y. Wang, G.T. Salazar, J. Pai, H. Shadpour, C.E. Sims, N.L. Allbritton. Micropallet arrays with poly(ethylene glycol) walls. *Lab Chip,* 2008, 8(5), 734-740.
82) N.M. Gunn M. Bachman, G.P. Li, E.L. Nelson. Fabrication and biological evaluation of uniform extracellular matrix coatings on discontinuous photolithography generated micropallet arrays. *Journal of Biomedical Materials Research A,* 2010, 95A, 401-412.
83) H. Shadpour, C.E. Sims, N.L. Allbritton. Enrichment and expansion of cells using antibody-coated micropallet arrays. *Cytometry Part A,* 2009, 75A, 609-618.
84) N.M. Gunn, R. Chang, T. Westerhof, G.P. Li, M. Bachman, E.L. Nelson. Ferromagnetic micropallets for magnetic capture of single adherent cells. *Langmuir,* 2010, 26(22), 17703-17711.
85) P.C. Gach, C.E. Sims, N.L. Allbritton. Transparent magnetic photoresists for bioanalytical applications. *Biomaterials,* 2010, 31, 8810-8817.

86) J. Pai, W. Xu, C.E. Sims, N.L. Allbritton. Microtable arrays for culture and isolation of cell colonies. *Anal. Bioanal. Chem.,* 2010, 398(6), 2595-2604.
87) W. Xu, A. Herman, C. Phillips, J. Pai, C.E. Sims, N.L. Allbritton. Selection and separation of viable cells based on a cell-lethal assay. *Anal. Chem.,* 2011, 83(1), 278-283.
88) J. Pai, K. Kluckman, D.O. Cowley, D.M. Bortner, C.E. Sims, N.L. Allbritton. Efficient division and sampling of cell colonies using microcup arrays. *Analyst*, 2013, 138, 220-228.
89) S. Guo, Y. Wang, N. Allbritton, X. Jiang. Ultrasound-induced release of micropallets with cells. *Applied Physics Letters*, 2012, 101. 163703.
90) B.Hopp, T. Smausz, N. Kresz, N. Barna, Z. Bor, L. Kolozsvari, D.B. Chrisey, A. Szabo, A. Nogradi. Survival and proliferative ability of various living cell types after laser-induced forward transfer. *Tissue engineering*, 2005, 11(11/12), 1817-1823.
91) B. Hopp, T. Smausz, Z. Antal, N. Kresz, Z. Bor, D. Chrisey. Absorbing film assisted laser induced forward transfer of fungi (Trichoderma conidia). *Journal of Applied Physics*, 2004, 96(6), 3478 - 3481.
92) M. Colina, P. Serra, J.M. Fernandez-Pradas, L. Sevilla, J.L. Morenza. DNA deposition through laser induced forward transfer. *Biosens. Bioelectron*. 2005, 20(8), 1638-1642.
93) Gon, D. Prasad, P. Paul. Complex garment systems to survive in outer space. *Journal of Textile and Apparel*, 2011,7(2).
94) M. Kitz, S. Preisser, A. Wetterwald, M. Jaeger, G.N. Thalmann, M. Frenz. Vapor bubble generation around gold nano-particles and its application to damaging of cells. *Biomed. Opt. Express*, 2011, 2(2), 291-304.
95) L. Hou, M. Yorulmaz, N.R. Verhart, M. Orrit. Explosive formation and dynamics of vapor nanobubbles around a continuously heated gold nanosphere. *New J. Phys*., 2015, 17.
96) W. Strober. Trypan blue exclusion test of cell viability. *Current protocols in Immunology*, 1997, 21:3B:A.3b.1 - A.3B.2.
97) T. Ishii, Y. Okahata, T. Sato. Mechanism of cell transfection with plasmid/chitosan complexes. *Biochimica et Biophysica Acta,* 2001, 1514, 51-64.
98) T.K. Kim, J.H. Eberwine. Mammalian cell transfection: the present and the future. *Anal. Bioanal. Chem.,* 2010, 397, 3173-3178.
99) R. Jove, H. Hanafusa. Cell transformation by the viral src oncogene. *Ann. Rev. Cell Biol.,* 1987, 3, 31-56.
100) X. Xie, A.M. Xu, S. Leal-Ortiz, Y. Cao, C.C. Garner, N.A. Melosh. Nanostraw-electroporation system for highly efficient intracellular delivery and transfection. *American Chemical Society,* 2013, 7(5), 4351-4358.
101) C.T.A. Brown, D.J. Stevenson, X. Tsampoula, C. McDougall, A.A. Lagatsky, W. Sibbett, F.J. Gunn-Moore, K. Dholakia. Enhanced operation of femtosecond lasers and applications in cell transfection. *J. Biophoton.,* 2008, 1(3), 183-199.
102) V.P. Torchilin, T.S. Levchenko, R. Rammohan, N. Volodina, B. Papahadjopoulos-Sternberg, G.G.M. D'souza. Cell transfection *in vitro* and *in vivo* with nontoxic TAT peptide-liposome-DNA complexes. *PNAS*, 2003, 100(4), 1972-1977.
103) H. Shadpour, C.E. Sims, R.J. Thresher, N.L. Allbritton. Sorting and expansion of murine embryonic stem cells using micropallet arrays. *Cytometry Part A*, 2009, 75A, 121-129.
104) H. Shadpour, N.L. Allbritton. In-situ roughening of polymeric microstructures. *ACS Appl. Mater. Interfaces*, 2010, 2(4), 1086-1093.
105) M.P. Sanna, E. Sanna, M. De Las Heras, A. Leoni, A.M. Nieddu, S. Pirino, J.M. Sharp, M. Palmarini. Association of Jaagsiekte sheep retrovirus with pulmonary carcinoma in sardinian moufflon. *J. Comp. Path.,* 2001, 125, 145-152.
106) A. Hofacre, H. Fan. Jaagsiekte sheep retrovirus biology and oncogenesis. *Viruses.,* 2010, 2, 2618-2648.

107) K. McGee-Estrada, M. Palmarini, H. Fan. HNF-3β is a critical factor for the expression of the Jaagsiekte sheep retrovirus long terminal repeat in type II pneumocytes but not in Clara cells. *Virology*, 2002, 292, 87-97.
108) Lodish H, Berk A, Zipursky SL, et al. Molecular Cell Biology. 4th edition. New York: W. H. Freeman; 2000. Section 24.1, Tumor Cells and the Onset of Cancer. Available from: http://www.ncbi.nlm.nih.gov/books/NBK21590/
109) K. Inoue et al., "Effect of UV irradiation on electroless Cu-Ni-P plating on cycloolefin polymer," Transaction of the Institute of Metal Finishing 87(1), 51-54 (2008).
110) W.W. Coblentz, R. Stair. Reflecting power of beryllium, chromium, and several other metals. J. Res. Natl. Bur. Stand. 1929, 2, 343-354.
111) V.B. Svetovoy, R.G.P. Sanders, M.C. Elwenspoek. Transient nanobubbles in short-time electrolysis. J. Phys.: Condens. Matter, 2013, 25, 184002.
112) H. Lee, J. Kim, H. Lim, E. Cho, N. Huh, C. Ko, J. Park, J. Choi, S. Lee. Electrochemical cell lysis device for DNA extraction. Lab Chip, 2010, 10, 626-633.
113) D. Carlo, C. Ionescu-Zanetti, Y. Zhang, P. Hung, L.P. Lee. On-Chip cell lysis by local hydroxide generation. Lab Chip, 2005, 5, 171-178.
114) B. Lee, U. Si, S. Park, et al. U.S. Patent No. US 2014/0212648 A1 (31 July, 2014)
115) Y. Kiim, Y. Saniguchi, K. Murase, Y. Taguchi, H. Sugimura. Vacuum ultraviolet-induced surface modification of cyclo-olefin polymer substrates for photochemical activation bonding. Applied Surface Science. 2009, 255(6), 3648-3654.
116) V. Linder, B.D. Gates, D. Ryan, B.A. Parviz, G.M. Whitesides. Water-soluble sacrificial layers for surface micromachining. Small, 2005, 1(7), 730-736.
117) S. Metz, S. Jiguet, A. Bertsch, Ph. Renaud. Polyimide and SU-8 microfluidic devices manufactured by heat-depolymerizable sacrificial material technique. Lab Chip, 2004, 4, 114-120.
118) C.K. Harnett, G.W. Coates, H.G. Craighead. Heat-depolymerizable polycarbonates as electron beam patternable sacrificial layers for nanofluidics. J. Vac. Sci. Technol. B, 2001, 19(6), 2842-2845.
119) L. Gu, Y. Qin, Y. Gao, X. Wang, F. Wang. Hydrophilic CO_2-based biodegradable polycarbonates: synthesis and rapid thermo-responsive behavior. Journal of Polymer Science, Part A: Polymer Chemistry, 2013, 51(13), 2834-2840.
120) H.A. Reed, C.E. White, V. Rao, S.A. Bidstrup Allen, C.L. Henderson, P.A. Kohl. Fabrication of microchannels using polycarbonates as sacrificial materials. J. Micromech. Microeng., 2001, 11, 733-737.